

STRUCTURAL PROGNOSIS FOR THE EFFECTIVE MANAGEMENT OF NATION'S CULTURAL HERITAGE



Project Director

Sez Atamturktur

Clemson University, Glenn Department of Civil Engineering
110 Lowry Hall, S Palmetto Blvd, Clemson, SC 29634
(864) 656-3003 sez@clemson.edu

Team Members

Civil Engineering

Saurabh Prabhu, Ph.D. Candidate

Elizabeth Wheeler, Ph.D. Student

Greg Roche, Ph.D. Student

Xiaoyu Hu, Ph.D. Student

Ashley Haydock, M.S. Graduate

Tun Li, M.S. Graduate

Computer Science and Engineering

Jacob Sorber, Assistant Professor

Josiah Hester, Ph.D. Candidate

Keerthan Jaic, Ph.D. Student

Kyle McGuigan, Undergraduate Student

prepared for

US Department of the Interior

National Park Service

National Center for Preservation Technology and Training

6th September 2014

ABSTRACT

In recent years, a significant amount of research has been directed towards the development of prognostic methodologies to forecast the future health state of an engineering system assisting condition based maintenance. These prognostic methods, having furthered the maintenance practices for mechanical systems, have yet to be applied to historic masonry structures, many of which stand in an aged and degraded state. Implementation of prognostic methodologies to historic masonry structures can advance the planning of successful conservation and restoration efforts, ultimately extending the service life of these heritage structures.

This multi-disciplinary research project, which builds upon the findings of the ongoing NCPTT-funded project on Structural Health Monitoring (SHM) to determine the health of the nation's historic structures, aims to develop Life-Cycle Assessment charts for Preservation and Rehabilitation (LCA-PR) of historic structures. Quantifiable parameters will be developed through the LCA-PR charts to evaluate not only the structural state of the heritage building, but also the effect of rehabilitation campaigns. Through this project, the PI will bring a novel idea to the preservation and management of historic masonry structures and address the NCPTT's priority to "develop appropriate technologies to preserve houses of worship."

TABLE OF CONTENTS

	Page
TITLE PAGE	i
ABSTRACT	ii
LIST OF FIGURES	v
LIST OF TABLES	ix
 CHAPTER	
I. INTRODUCTION	1
Motivation.....	1
Background.....	1
Summary of Main Contributions	3
Organization of the Report.....	5
II. A REVIEW ON PROGNOSTIC EVALUATION OF HISTORIC MASONRY STRUCTURES	7
Introduction.....	7
Masonry Degradation and Assessment.....	9
Prognostic Approaches	17
Prognostic Algorithms	19
Challenges and Future Direction in Prognostics as Applied to Historic Masonry Construction.....	26
Conclusion	29
III. ADAPTIVELY WEIGHTED SUPPORT VECTOR REGRESSION: PROGNOSTIC APPLICATION TO A HISTORIC MASONRY COASTAL FORTIFICATION	31
Introduction.....	31
Background on Prognostic Evaluation of Historic Masonry	32
Methodology	33
Case Study	41
Conclusion	47
IV. AN EMPIRICSL ASSESSMENT OF LOAD CARRYING CAPACITY	

	OF A SCALED MASONRY DOME: SIMULATIONS VALIDATED WITH NON-DESTRUCTIVE AND DESTRUCTIVE MEASUREMENTS	49
	Introduction	49
	Scaled Dome Model	52
	Finite Element Model Development	53
	Correlation of the FE Model with Non-Destructive Tests: Linear Properties	59
	Test Analysis Correlation with Destructive Tests: Nonlinear Properties of the FE Model	67
	Simulation of Damage via Experimentally Informed FE Models	70
	Conclusion	79
V.	DEVELOPMENT AND DEPLOYMENT OF WIRELESS SENSOR NETWORK FOR LONG TERM MONITORING OF HISTORIC MASONRY MONUMENTS	81
	Introduction	81
	Fort Sumter National Monument	83
	Background	83
	Wireless Sensor System	84
	Remote Data Transferring and Online Monitoring	91
	Fort Sumter Deployment	92
	Conclusion	94
VI.	CONCLUSIONS	96
VII.	REFERENCES	99

LIST OF FIGURES

Figure	Page
1.1 SHM campaign methodology for health monitoring.....	2
1.2 SHM can enable us to construct life-cycle charts for structural Sustainability and resiliency of a structural system.....	4
1.3 Flowchart of report contributions	5
2.1 Estimation of the RUL (printed with permission from Atamturktur et al. 2013b)	8
2.2 Tests applied to civil structures (reprinted with permission from D.M. McCann & M.C. Forde, 2001).....	11
2.3 Nodal layout of artificial neural network (printed with permission from Nagy et al. 2002).	22
2.4 Establishing of the margin and support vectors (printed with permission from Atamturktur et al. 2013b).....	24
3.1 Support vectors and margin bounds.....	35
3.2 Quadratic loss function for a linear SVR.....	36
3.3 Trade-off between flatness and goodness of fit varying from (left) more extreme λ values to (right) more compromising λ values	38
3.4 Magnitude of λ required to fit a given trend as noise is added	39
3.5 Dataset divisions for preliminary and forecasting stages of adaptively weighted SVR	40
3.6 Current aerial view of Fort Sumter (Courtesy: National Park Service).....	42
3.7 FE model of Fort Sumter casemate used in case study.....	43
3.8 Initial model configuration on level surface (left) and settlement configuration (right).....	44
3.9 Locations Point 1 and Point 2 of monitored strains during settlement (circled).....	45

List of Figures (Continued)

Figure	Page
3.10 Settlement induced strains obtained from FE model of Point 1 (left) and Point 2 (right) with added noise	45
3.11 Comparison of adaptively weighted SVR to non-weighted SVR using Point 1 data with increasing noise: (a) predicted response, (b) prediction error, and (c) λ value used for prediction model.....	46
3.12 Comparison of adaptively weighted SVR to non-weighted SVR using Point 2 data with increasing noise: (a) predicted response, (b) prediction error, and (c) λ value used for prediction model.....	47
4.1 The scaled dome constructed with ACC tile and fast-setting gypsum cement	53
4.2 FE model of the dome.....	54
4.3 Asymptotic convergence of the six natural frequencies as mesh is refined	55
4.4 Simplified stress-strain curve for concrete in ANSYS	57
4.5 (Left) Excitation points, (Right) Measurement points.....	61
4.6 Typical response history measurements: (Left) hammer impact, (Right) vibration response.....	62
4.7 Reciprocity check.....	63
4.8 Linearity check (Top) the driving point FRF for the crown of the dome, (Bottom) the corresponding coherence function.....	64
4.9 Experimental setup for the destructive testing, (Ramage (2006), with permission).....	69
4.10 Test and simulation correlation.....	70

List of Figures (Continued)

Figure	Page
4.11 (Top) Spherical masonry domes without hoop tension carrying mechanism: aerial and plan view of cracks (reproduced with permission, (Heyman, 1995)); (Bottom) Spherical masonry domes with a tension ring: aerial and plan view of cracks.	71
4.12 1 st principal stress distribution above the tensile stress capacity (>0.14 MPA (20 psi))	72
4.13 Cracks introduced in the FE model.....	73
4.14 Natural frequencies of the five health conditions	74
4.15 Comparison of load-carrying of damaged and undamaged models.....	74
4.16 (Left) Span-to-height ratio of 0.21; (Right) Span-to-height ratio of 0.35 representing the dome studied herein.	78
4.17 The semi-empirical formulation	78
5.1 Wireless network topologies.....	84
5.2 Key components of the wireless sensor nodes.....	85
5.3 Key functional components of the base station	86
5.4 Wireless sensor system	87
5.5 Shaker table experimental setup	89
5.6 Time history plot for wired (blue) and wireless (red) sensors for ambient testing	89
5.7 Time history plot for wired (blue) and wireless (red) sensors for shaker table testing	90

List of Figures (Continued)

Figure		Page
5.8	Time history plot for wired (blue) and wireless (red) sensors for impact testing	91
5.9	Sample of Remote Data Transferring	92
5.10	Roof plan of fort sumter highlighting the case mates on which the SHM system is deployed	93
5.11	Collected Data from Sensor 3 at Fort Sumter for (a) 30 second window and (b) 5 second window	94

LIST OF TABLES

Table	Page
3.1 Pseudocode for adaptively weighted SVR.....	40
3.2 Total prediction error for adaptively weighted SVR and non-weighted SVR.....	47
4.1 Geometric properties of the dome.....	52
4.2 FE Model input parameters before and after calibration	59
4.3 Variables of the digital signal-processing.....	62
4.4 Comparison of the predicted and measured natural frequencies and corresponding mode shapes	66
4.5 Modal analysis solutions, natural frequencies (Hz).....	73
4.6 Comparison of the simulated mechanical behavior of the dome.....	75
5.1 Wired sensors specifications.....	88
5.2 Comparison of sensor statistics.....	91

CHAPTER ONE

INTRODUCTION

1.1. Motivation

The National Register of Historic Places lists 3290 Gothic style buildings in the United States, with 593 of those being houses of worship (National Park Service 2010). The need to maintain the nation's aging and deteriorating heritage structures with constrained budgets poses a great challenge to infrastructure managers. Therefore, it is essential to equip infrastructure managers with science-based techniques, rather than purely qualitative guidelines for prescribing maintenance and rehabilitation schemes. It is envisioned that science-based monitoring and assessment techniques, such as Life-Cycle Assessment charts for Preservation and Rehabilitation (LCA-PR) charts, described in this report, not only provide quantitative, scientifically defensible and real time measures on the integrity of the structure, but also evaluate the benefits of the preservation and rehabilitation campaigns. Quantitative information about the structural degradation can aid in the development of the most cost-effective, long-term infrastructure management plans that reduce both energy and material consumption, thusly yielding sustainable maintenance schemes for the nation's cultural heritage.

1.2 Background

Structural Health Monitoring is an established diagnostic technique that can detect, quantify, localize and classify structural damage based on changes in structural response (Farrar and Worden 2007). Generally speaking, SHM is based on the structural dynamics concepts that a structure's vibration response is related to its mass, damping, and stiffness properties. Changes in the structure, whether due to damage or rehabilitation efforts, will result in changes to these

properties, and thus an altered vibration response. SHM often relies on in-situ vibration measurements to detect these changes in system properties and relate them to the structure's overall state (Carden and Fanning 2004; Doebling, et al. 1996; Sohn, et al. 2004). SHM implementation consists of three main stages: data collection, feature extraction, and statistical discrimination. Figure 1.1 outlines the SHM process. In this process, a negative discrepancy between the damaged structure's response (ω) and the healthy reference point (ω_R) indicates the structure has been degraded or damaged, while a positive discrepancy indicates an improvement in the structural functionality due to repair or recovery campaigns. This calculation can then be used to provide data to alert infrastructure managers of the health of a system (Dalton et al., 2012).



Figure 1.1: SHM campaign methodology for health monitoring

Data collection can be periodic or continuous and is achieved by placing sensors at strategic locations within the structure (Prabhu and Atamturktur, 2012). The next step in the SHM process is to identify damage-sensitive response features and extract these features from the collection of data. The utilization of real time, long-term monitoring technique of SHM is one of the components of the LCA-PR framework.

* Note: "th" represents threshold. This failure threshold is a conservative limit on damages level, beyond which the system is inadequate for its intended use.

Life Cycle Assessment (LCA), on the other hand, was originally developed to quantify the environmental impact that a product has over its entire lifespan. It is understood as “a cradle-to-grave investigation and evaluation of the environmental, social, and economic impacts of a given product during the production, use, and disposal phases of its life”. LCA helps to determine the environmental and social tradeoffs between alternative designs or alterations in a product or system in an effort to improve sustainability. The concepts originally developed for LCA are adapted in the context of SHM in this study to develop the LCA-PR framework, further details of which are provided in the following section.

1.3 Summary of Main Contributions

As part of this report, Structural Life Cycle Analysis (S-LCA) charts, which can measure the structural sustainability of a structure in regards to its measured versus designed performance, are developed (Dalton et al., 2012). Figure 1.2 shows a conceptual view of the proposed S-LCA. The rate at which the decrease in structural functionality occurs depends upon the structural sustainability of the built system. Structural Sustainability is a measure of the degradation rate and inversely relates to the slope of the S-LCA curve. Figure 1.2 represents the lifespan for a structure that has been recently constructed. For an existing structure, a reference point of structural functionality must be determined according to the current structural condition.

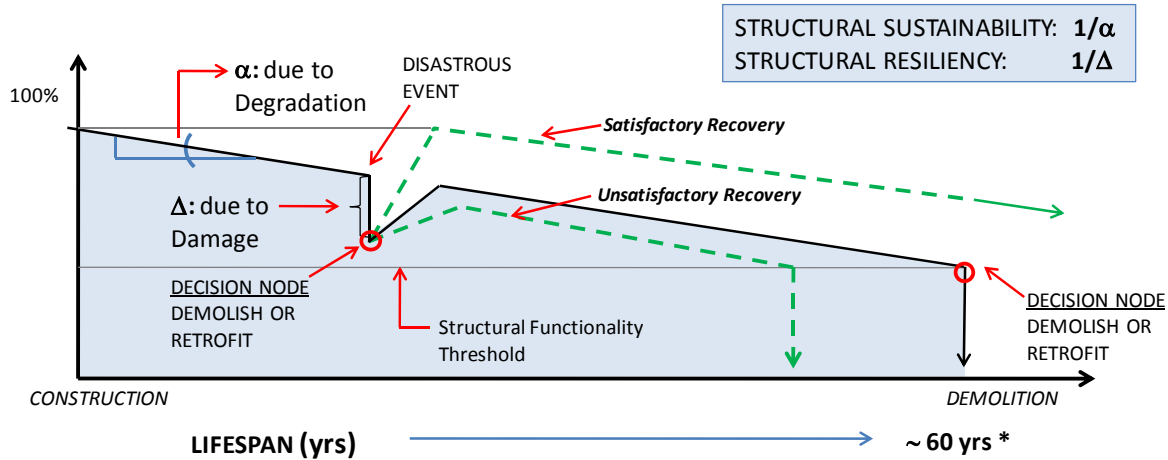


Figure 1.2: SHM can enable us to construct Life-Cycle charts for Structural Sustainability and Resiliency of a structural system.

Based on the S-LCA curve and the goal of preservation to ensure that historic structures survive for posterity, the new LCA-PR framework addresses and incorporates three scenarios: (1) gradual structural degradation from environmental and operational conditions, (2) rapid structural damage from disasters and (3) rapid structural improvement due to preservation or rehabilitation campaigns. While rapid degradation or improvement in structural integrity can only be evaluated after the occurrence of an event, the gradual structural degradation naturally allows for prognosis of future behavior. In this report, to predict the long term, gradual degradation of a structural system, prognostic methodologies are implemented into the LCA-PR framework. Such prognosis is accomplished by training Support Vector Regression (SVR) models with the data collected through sensors placed on the structure. In this prognostic approach, as more data is collected, the trained SVR model is refined and prediction accuracy is improved. Figure 1.3 schematically outlines the LCA-PR framework.

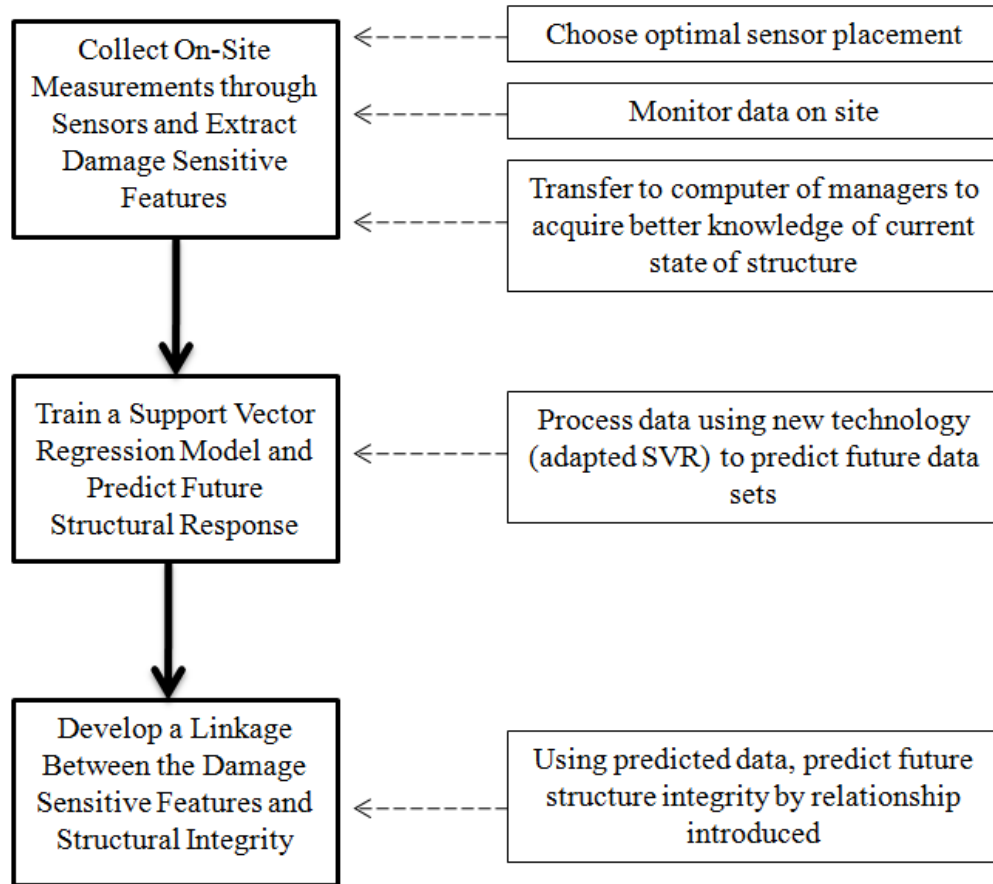


Figure 1.3: Flowchart of Report Contributions

1.4 Organization of the Report

Chapter Two of this report presents a review of not only the established literature on prognostic evaluation but also the available inspection techniques for masonry construction with an objective to relate these two disassociated areas of knowledge, thus laying the foundation for prognostic evaluation of historic masonry. The findings obtained in Chapter Two were submitted to The Masonry Society and have been conditionally accepted.

Among the available techniques for prognostic evaluation, SVR shows particular potential for applicability to historic masonry structures as it is capable of handling the nonlinear responses of masonry assemblies due to the complexity of their materials and geometry. Chapter Three of this report presents the proposed adaptively weighted SVR approach. In this chapter,

the theoretical background for SVR as well as the algorithmic development for adaptive weighting is both presented. Furthermore, the application of this proposed approach is demonstrated on the settlement induced damage of a coastal fortification, Fort Sumter in Charleston.

Chapter Four focuses on the establishment of a semi-empirical relationship to estimate the reduction in the load carrying capacity due to damage by exploiting the experimentally detected deviations in the natural frequencies for a tile dome. A finite element model developed to analyze the dome is calibrated against both non-destructive vibration measurements and destructive load-displacement measurements up to failure. The model is then executed to simulate incremental development of cracks. The first natural frequency and remaining load carrying capacity of the dome are monitored to define the desired empirical relationship, which is ultimately generalized for spherical domes with varying span-to-rise ratios.

Chapter Five presents the experimental campaign for a wireless sensor network developed at Clemson University. The system was validated at Clemson before being deployed at Fort Sumter. The components of the wireless system are explained in detail and the findings of the testing performed are discussed.

CHAPTER TWO

A REVIEW ON PROGNOSTIC EVALUATION OF HISTORIC MASONRY STRUCTURES

2.1. Introduction

Historic masonry structures are degraded by a multitude of physical, chemical and biological processes which subvert the material and structural characteristics of those monuments. At critical levels, the degradation caused by these processes may lead to structural failure and the loss of culturally-significant monuments. Examples throughout the last century include the 1902 collapse of St. Mark's Campanile in Venice, Italy, the 1989 collapse of the Civic Tower of Pavia, Italy, the 1990 collapse of the Church of Kerksken, Belgium, the 1992 collapse of a bell tower at the church of St. Maria Magdalena in Goch, Germany, the 1996 collapse of the Noto Cathedral in Sicily Italy and the 2006 partial collapse of the Maagdentoren Tower in Zichem, Belgium. While such failures are typically sudden events, the processes of material and structural decline which precede these catastrophic events tend to be gradual, often going unaddressed for extensive periods.

With on-site monitoring techniques opening new doors to the analysis of large-scale historic masonry structures, engineers may benefit from *prognostic approaches*. This new technology allows engineers to predict system performance and configure suitable maintenance and rehabilitation efforts, ultimately resulting in prolonged structural reliability and the preservation of significant cultural heritage.

The goal of prognosis is to project the remaining useful life (RUL) of a system. Prognosis is accomplished by analyzing a system's performance with the goal of making accurate projections about future system performance (as demonstrated in Figure 1). The RUL which is

forecasted from performance data does not predict a system's ultimate failure but rather reflects a convergence between the continued degradation of a system and the threshold selected to define the system's functional inadequacy. With detailed RUL forecasts, condition-based maintenance (CBM) routines can be initialized to reflect a system's current and future needs, as opposed to time-based maintenance schemes, which take place at predefined intervals without knowledge of the condition of the system. CBM can help avoid secondary damage stemming from exceedingly infrequent care, and can simultaneously limit the expenditure of resources (Jardine et al. 2006).

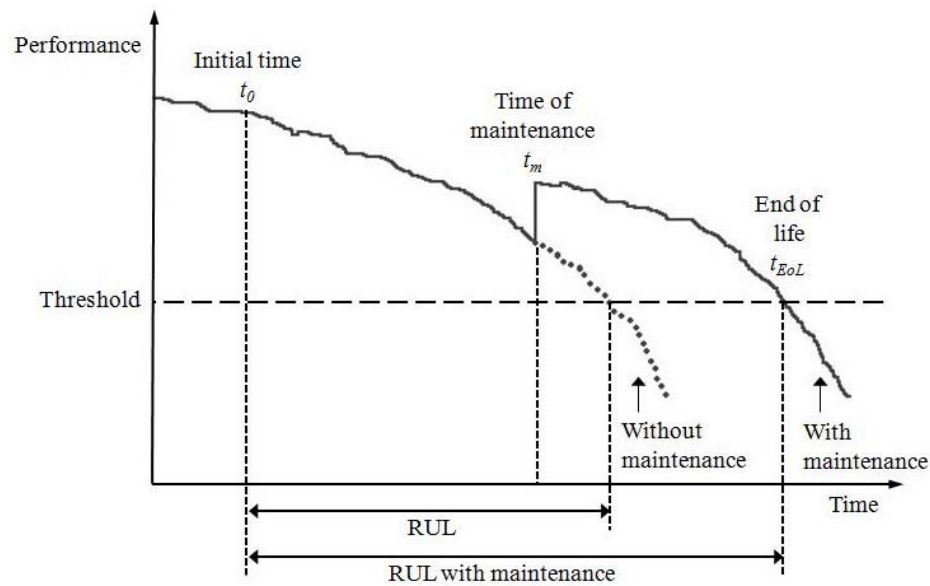


Figure 2.1: Estimation of the RUL (printed with permission from Atamturktur et al. 2013b)

The success of CBM routines is however based on the accuracy and timeliness of the RUL prediction (Saxena et al. 2010). This prediction is dependent upon a variety of factors including system's initial design and construction, its current health and the operational, loading and environmental conditions it endures. While easily conceptualized, these quantities are often imprecisely known and thus, the challenge becomes predicting not only the RUL of a highly

complex system but also establishing a satisfactory level of confidence in the predictions. It is therefore necessary that an evaluation of the developing field of prognostics be conducted with critical attention given to its potential inclusion within efforts aimed at maintaining historic masonry structures. The cause of such a review stems from the potential benefits prognostic methods stand to offer the care-takers of historic masonry, namely a more intimate knowledge of these historic structures from which the most appropriate and effective maintenance routines might be derived.

The organization of the manuscript begins with a discussion in Section 2 of factors contributing to the degradation of masonry structures that are amenable for incorporation into a prognostic framework through the use of appropriate inspection methods. In Sections 3 and 4, the authors introduce common prognostic approaches and review various established prognostic algorithms. An overview of the future direction and challenges in applying prognostic techniques to historic masonry monuments follows in Section 5. Finally, concluding remarks are provided in Section 6.

2.2. Masonry Degradation and Assessment

In the following two subsections are discussed a variety of chemical, biological and physical factors which routinely lead to the decline of historic masonry structures. In the last two subsections, common inspection techniques for historic masonry structures are overviewed for their potential implementation within a prognostic framework.

2.2.1. Masonry Degradation by Chemical & Biological Processes

Chemical and biological processes attack the composition and durability of masonry materials. In many of these processes, water is a key factor which can both initialize and sustain the processes of weathering, ice formation, freeze/thaw cycling, capillary flow, and biological

growth (Grimm 1982; Collepari 1990). Additionally, water from the surrounding environment provides a vehicle for the transportation of potentially hazardous particles and is involved in many of the subsequent chemical reactions that take place. Symptoms of water intrusion relevant to structural assessment may include plant growth, reduced freeze-thaw resistance, material expansion and contraction and chemical attack (Groot et al. 2004). The effects of this water-induced degradation typically appear in the form of cracks, which alter the mechanical properties of the masonry materials (Grimm et al. 1988).

In a process called biodegradation, agents such as mold, algae, bacteria and other plant life can act to degrade the mechanical properties of masonry materials (Mack et al. 2000). This mechanical deterioration can occur by way of the physical presence of these biological organisms and their byproducts which act to separate grains in the stone and mortar creating stresses that slowly break the material apart at the micro-scale. In the macro-scale, historic masonry buildings may fall under the attack of larger plant systems (Mishra et al. 1995). In addition to causing material cracking, extensive plant growth can increase fire hazards and help spread and sustain areas of heavy moisture.

Additionally, stone masonry can be chemically affected by the well-known alkali-silica (or alkali-aggregate) reaction, which occurs at the mortar joint between alkalis present in the mortar and minerals within the stone. Furthermore, both stone and brick masonry are commonly subjected to the ill-effects of gypsum, a binder routinely used in historic masonry mortars, in which the presence of sulfate can cause degradation (West 1996; Duran et al. 2010).

A prognostic framework for evaluating the effects of these chemical and biological processes must be grounded in knowledge of the rate at which the structural performance of historic masonry materials declines in time and how this degradation will ultimately affect the

integrity of these structures. Such information is currently not available in the literature for the chemical and biological processes discussed in this section. For instance, material deterioration caused by the presence of moisture, which can result in structural degradation, requires sufficient time to progress and short-term fluctuations make directly linking the in-situ moisture content of masonry to its structural health difficult. Therefore, while radar and thermography tests can determine the moisture content of masonry materials, this knowledge yields little information regarding the resulting structural integrity (Avdelidis et al. 2004; Binda et al. 2009). For a prognostic framework to be applied, it is necessary to determine a link between the severity of sustained damage, the mechanical properties of the damaged material and the integrity of the overall structure.

2.2.2. Material Degradation by Physical Processes

Aside from overloading caused by short term events, which can occur by way of sudden foundation settlement, earthquakes, or war-time bombardment, historic masonry structures are also subjected to a variety of physical processes that slowly degrade the building materials. Wind, snow and ice, wave action, external vibration and the repeated fluctuation of ambient temperatures can all contribute to the reduction of a material's integrity, increasing the probability of crack formation and the eventual large-scale deterioration of important structural components.

In urbanized areas, historic masonry structures can also be affected by vibrational disturbance arising from nearby vehicle traffic. These urban vibrations, typically between 5 and 25Hz, are created by large vehicles as they pass over irregularities in road surfaces (Hunaidi 2000). In many cities, the distance between heavily trafficked streets and historic masonry structures is not sufficient to shield these structures from resulting vibration. Examples of

reported masonry degradation stemming from traffic vibration are given in the vault cracking of the St Thomas Church in Prague, damaged frescos in Rome's Villa Farnesina and in the Palace of Art in Budapest where foundation settlement has been attributed to nearby heavy traffic (Rainer 1982).

Furthermore, many medieval masonry structures throughout Europe are reported to lean towards adjacent roadways as traffic-induced vibration has induced uneven settlement (Rainer 1982). These sustained vibrations can worsen the already common problem of foundation settlement amongst historic masonry, which stems from the large weight of the structures coupled with the inadequate and often deteriorating soil bearing capacities (Chiorino et al. 2011). As masonry is primarily designed to carry loads in compression, the tensile stresses resulting from differential support settlement can induce cracking, which in severe cases can lead to structural discontinuities and inelastic hinges (Atamturktur et al. 2011).

Moreover, research has indicated that creep, a material process involving the gradual plastic deformation of a structural element under sustained load, may play a role in the sudden collapse of masonry systems (Henriques et al. 2003; Binda et al. 2000). Evaluation of materials gathered from the recent collapses of the Civic Tower of Pavia and the Tower of Maagdentrion confirmed that strain rates in masonry increase over time through unique phases which might offer engineers a means of monitoring these culturally significant monuments (Anzani et al. 2008).

Additionally, where considerable ambient temperature fluctuations are present, they have been linked to masonry degradation. In the summer months, increased exposure to direct sunlight elevates daytime surface temperatures while later exposures to nighttime air can present differences up to 50°C. In winter, the relatively low temperatures of the stone surfaces can result

in significant tensile stresses within the material. These temperature variations cause strains in the mortar, masonry units and bond region causing cracks in the masonry assembly (Twelmeier et al. 2006). When water is also involved and the masonry is saturated, structures in colder climates also endure the effects of repeated freeze-thaw cycles which can impart significant damage over time. This damage expedites the deterioration of the mortar, once again causing cracking in the masonry assembly (Hopps et al. 2012).

Each of these processes of physical degradation act to slowly degrade the mechanical properties of masonry materials and thus, the prevalence and severity of such processes must be monitored over the life of the structure. A vital question that remains to be answered is how this physical degradation (of a component or the entire structural system) can lead to a decline in structural integrity (perhaps quantified by remaining load carrying capacity). Experimentally substantiated computer models can be employed while estimating the degradations in load carrying capacity due to damage (see for instance, Atamturktur et al. 2013). Such estimates can ultimately transition real-time observations obtained through non-destructive measurements to information regarding the integrity of the structure and lead to better-planned maintenance campaigns.

2.2.3. Common Forms of Masonry Inspection & Assessment

In the case of historic masonry, the process of structural assessment typically begins with manual inspection, which is often laborious and limited to generating qualitative and subjective descriptions (Ozaeta et al. 2012; Atamturktur et al. 2013a). To obtain quantitative information, semi-invasive techniques such as flat-jack tests are commonly deployed to measure the local stresses and strains in a material (Binda and Tiraboschi 1999). These semi-invasive methods are commonly applied to historic masonry and are more desirable than those which involve drilling

or cutting material coupons for laboratory evaluation of the material's composition and overall condition. Of course, the risk of increasing both aesthetic and structural damage makes even semi-invasive techniques unappealing on the most culturally-significant sites (Schuller et al. 1995). If nothing else, semi-invasive tests are often limited to hidden areas of a structure leading to concern over how engineers might assess the more exposed facades of historic masonry which must be delicately treated and carefully preserved.

Providing a potential solution are non-destructive testing methods (NDT) which represent less intrusive alternatives for evaluating masonry structural elements. A wide array of useful comparisons of available NDT methods can be found in the literature (McCann & Forde 2001; Popovics 2003; Harvey & Schuller 2010). While each evaluation technique typically offers some advantage, experience and application tend to govern the selection of NDTs. Factors including relative cost, test complexity, necessary experience or training, structure size and evaluation parameters of interest help separate NDTs. Figure 2 offers a comparison of commonly deployed NDTs

Inspection Method	Parameter Measure	Advantage	Disadvantage	Cost
Visual	Surface condition	Quick; modest skills required	Superficial	Low
Proof load testing	Load carrying capacity	Definitive	Very slow and possibly dangerous	Very high
Coring	Mechanical properties of core samples	Yield accurate values of mechanical properties	Measurement only at test point; scars the structure	Moderately high
Vibration testing	Mode shapes and/or signature	Gives some indirect measure of current condition	Difficult to quantify data; heavily damped masonry yields little response	High

Impact testing	Mode shapes and/or signature	Gives some indirect measure of current condition	Difficult to quantify data; heavily damped masonry yields little response	Moderate
Ultrasonic NDT	Wave velocities through structure	Relatively quick	Only works on individual masonry blocks due to signal attenuation; no information on major elements	Moderate
Sonic	Wave velocity; tomographic cross-sections	Moderately quick; gives useful information on major elements	Requires skill to interpret data	Moderately high
Conductivity	Relative conductivity	Quick; gives relative conductivities over a large area to a maximum depth of 1.5m	Limited depth penetration of 1.5m; complements radar	Low
Radar	Electromagnetic wave velocity	Quick; good penetration; yields good image of internal structure	Poor penetration through clay infill; requires skill to interpret data	Moderately high

Figure 2.2: Tests applied to civil structures (reprinted with permission from D.M.

McCann & M.C. Forde, 2001)

One of the most commonly deployed NDTs is surface penetrating radar (Solla et al. 2012; Labropoulos & Moropoulou 2013). This approach analyzes the local uniformity of a material and can determine the location of voids (Orban & Gutermann 2009). Other NDTs such as the acoustic impact method (Anzani et al. 2010), the impact-echo method (Sadri 2003), the ultrasonic wave propagation method (Na et al. 2002) and sonic tomography make use of mechanical compression waves. Additionally, infrared thermography is another popular technique which has shown an ability to detect delamination, internal voids and local material uniformity despite its sometimes limited penetration depth (Avdelidis & Moropoulou, 2004; Cotic et al. 2013).

Overall expense and complexity represent the drawbacks of most NDTs as these methods typically make use of advanced technology and commonly require expert analysis of the results. Furthermore, the aforementioned NDT methods are typically local in nature, meaning that they measure localized properties of the system. Similar to their more invasive counterparts, these

NDT methods require *a priori* knowledge of damage as their application typically covers only a specified area resulting in costly, repetitive testing if applied extensively (Bosiljkov et al. 2010). One way in which the need for preliminary knowledge can be eliminated is through the use of techniques which monitor a structure's global properties. One such example of a global NDT method is vibration testing, which has only begun to be adapted to historic masonry (Atamturktur et al. 2012).

2.2.4. Vibration-Based Structural Health Monitoring Techniques

The assessment of civil structures has begun to advance with the implementation of structural health monitoring (SHM), particularly that of dynamic or vibration-based analysis (Aguilar et al. 2009). Vibration-based SHM primarily involves dynamic testing whereby sensors are strategically placed to observe the response of a structural system to ambient or imposed vibrational excitation. Data is collected before being interpreted by computer algorithms which allow engineers to determine dynamic features, such as the structure's natural frequencies and modal response. As the structure's response to external loading changes, up-to-date measurements are compared with original (or idealized) states to form an assessment of the structure's overall condition or *health* (Beck et al. 1994; Doebling et al. 1998). A great deal of existing literature is devoted to the research, technology and application of vibration-based SHM in the field of large civil infrastructure such as buildings, bridges and dams (Lynch 2006; Chang et al. 2003; Farrar et al. 2007; Brownjohn 2006). Some of the practical challenges of adapting SHM include continuous data transfer from the site, optimal placement of sensors (Prabhu et al. 2012), degrading effects of ambient vibrations, determination and identification of the most damage sensitive features (Prabhu et al. 2011; Aguilar et al. 2009) and selection of an appropriate algorithm for data interpretation.

Vibration-based SHM techniques are appropriate for application within a prognostic framework for historic masonry structures (De Stefano 2009; Samaras et al. 2012; Atamturktur et al. 2012; Atamturktur et al. 2013). However, there is a mismatch in what is being measured on site (dynamic characteristics of a structure, primarily related to stiffness) and what an engineer needs to know (load carrying capacity of a structure, primarily related to strength). Therefore, engineers must first directly link the measured changes in vibration response to changes in the system's structural integrity and ultimately to RUL predictions (Atamturktur et al. 2012). Furthermore, relating variations in global system response to various forms of localized damage and to the location and severity of such damage remains a current challenge in SHM. These issues depend on the unique material and geometric properties of structure under observation as well as the damage type of interest.

Finally, structural failure of a masonry construction tends to be sudden and often unexpected. Prognostics on a most fundamental level must be able to utilize SHM to not simply predict failure but do so in sufficient time that appropriately schedule maintenance might provide an alternative outcome (Carrar et al. 2007).

2.3. Prognostic Approaches

Prognostic frameworks fall within two families: *model-based* and *data-driven*. Model-based approaches consider the entirety of a physical system through the use of a numerical model and attempt to produce RUL forecasts based on simulations (Atamturktur et al. 2012). Model-based approaches benefit from the incorporation of a physical understanding of the system and thus have potential to significantly outperform their data-driven counterparts, particularly when varying load conditions are presented (Luo et al. 2003). While powerful, model-based techniques are most commonly developed for relatively small components where

minute material and mechanical failures represent substantial threats to system reliability (Gu et al. 2008). In the case of larger structures, the demands of creating such models are extensive. In those instances significant time must be invested into model development and calibration while the often complex physical laws of the system must be diligently scrutinized.

By comparison, data-driven methods are more adaptable in that they specialize in the rapid creation of prognostic models even where the systems governing physics, present condition, environment and future loads are imprecisely known. Thus, most forms of engineering prognosis concerned with the study of large-scale structures are data-driven. Over the last two decades, advances in sensor technology have increased engineers' ability to measure and record complex systems, however data interpretation remains a primary challenge. Stemming from the field of data-mining, the goal of data-driven prognostics is to reveal and extract empirical relationships existing within given data sets. Distinctive signatures from the data, known as *features*, are analyzed using prognostic algorithms which listen for changes throughout the system's lifetime. The challenge of interpreting data requires engineers to establish criterion for damage detection and to balance it with a model's insensitivity to small, irrelevant, short-term changes, also known as *noise*. Failure to exhibit such insensitivity to noise can lead to predictions that are skewed and inaccurate. Often termed *over-fitting*, this issue arises when a learning algorithm or model is highly influenced by noisy data with unwanted and misleading outliers. If interpreted correctly however, patterns within data can lead to RUL predictions under the assumption that a data set's features remain consistent unless the condition of the system has changed (Luo et al. 2008).

By their nature, data-driven methods have the inherent disadvantage of untoward reliance upon the quantity and quality of the system's operational data. Thus, insufficient historical or

operational data can limit the training and fidelity of data-driven techniques used to obtain health estimates and determine trend thresholds used for RUL predictions (Pecht et al. 2010). Furthermore, classification involving the nature of degradation, particularly amongst complex systems, also provides a distinct challenge (Sohn et al. 2003). A complementary introduction to and comparison of several data-driven approaches is provided in the literature (Schwabacher 2005; Goebel et al. 2008; Si et al. 2011) and subsequently discussed at length in section 4 where the adaptation of various data mining algorithms to prognostics are discussed.

2.4. Prognostic Algorithms

This section presents a brief description of widely implemented prognostic algorithms as well as a review of the challenges facing their deployment in both historic masonry and prognostic applications.

2.4.1. Common Concepts within Data-Mining

Data-mining algorithms are routinely deployed upon engineering problems involving classification and regression; terms that relate to health monitoring within diagnostics and prognostics, respectively. In classification problems, the algorithm is tasked with establishing the boundary between clusters within a separable data set (Basak et al. 2007; Ji et al. 2010). Accurately-trained models resulting from such classifier algorithms can be used in diagnostics to interpret data as representing damaged and undamaged states.

By its nature data-driven prognosis is a regression problem demanding the creation of a model capable of forecasting RUL given sufficient historical data. Thus, many advanced classifier algorithms have been evolved for suitability in regression analysis (Witten et al. 2005). Within this process, data occupying a space of n -dimensions (where n corresponds to the number of features used to describe a system's health) is analyzed for patterns in the time domain. In a

process known as *training*, the algorithm makes use of a subset of the available data to refine a series of competing model hypotheses while using subsequent data points to calibrate the model's predictive accuracy. In this way machine learning in prognostic applications falls under the heading of *supervised learning*, meaning that the algorithm's model is calibrated with output describing a known health state (i.e. a damaged or undamaged).

2.4.2. An Overview of Available Algorithms

Decision trees, statistical learning algorithms and instance based learning are examples of more basic machine learning techniques which can be pulled from the world of data mining. These approaches offer three advantages: an ability to operate on relatively small data sets, an ability to handle a large number of data parameters and an easily understood system of output classification. However, the basic structure of these approaches limits their accuracy. Amongst these algorithms, over-fitting, a model's unwanted sensitivity to irrelevant fluctuations in data, is of particular concern as the presence of regularly fluctuating ambient loads is expected to cause such noise. While attempts to 'smooth' the data can be applied during the collection phase, an algorithm's ability to avoid over-fitting remains of great significance (Atamturktur et al. 2013).

More advanced approaches can be called upon. Two forms of machine learning that have gained significant popularity over the last several decades are *Neural Networks* (NNs) and *Support Vector Machines* (SVMs). These improved forms of machine learning are comparatively robust in nature and trade away the quick-but-unreliable traits of simpler algorithms for several improvements: increased accuracy on larger data sets, an ability to handle highly interdependent data features and a higher level of noise tolerance. Compared to their predecessors, both NNs and SVMs represent advances in machine learning algorithms in their ability to handle more

complex data sets with less bias, a characteristic that can lead to predictions of greater accuracy and reliability (Burgess, 1998).

In some cases, it may prove ideal to combine such algorithms with model-based techniques within a *fusion* approach in an effort to create a ‘best of both worlds’ scenario where the strengths of one method offset the weaknesses of the other. This combined approach may be the most ideal prognostic approach to culturally-significant historic masonry monuments when sufficient data is available to support the development of a physics-based damage model. Nevertheless, the question still remains as to the selection of a particular algorithm for prognosis. Thus, in the following subsections a review is given of current algorithms involved in an array of prognostic applications.

2.4.2.1. Neural Networks

NNs create a computational structure which simulates the interconnected neurons within the brains of animals. In much the same way, the computational ‘network’ can interpret and learn from the information with which it is supplied. Within a NN, neurons are replaced by nodal points which have associated mathematical functions. As data is input into the system and distributed throughout the nodes the role of the mathematical functions is to weigh the data values accumulating at a particular node and to pass on a meaningful value, such as a weighted average. These functions, which are often algebraic equations, typically start with random coefficients which are tuned through back-calculation involving training data which has already been mapped accurately. With careful selection of neuron population, NNs can rapidly produce accurate numerical representations describing data sets in practice. A more detailed description of the conceptual and technical workings of NNs is available in the literature (Dougherty, 1995).

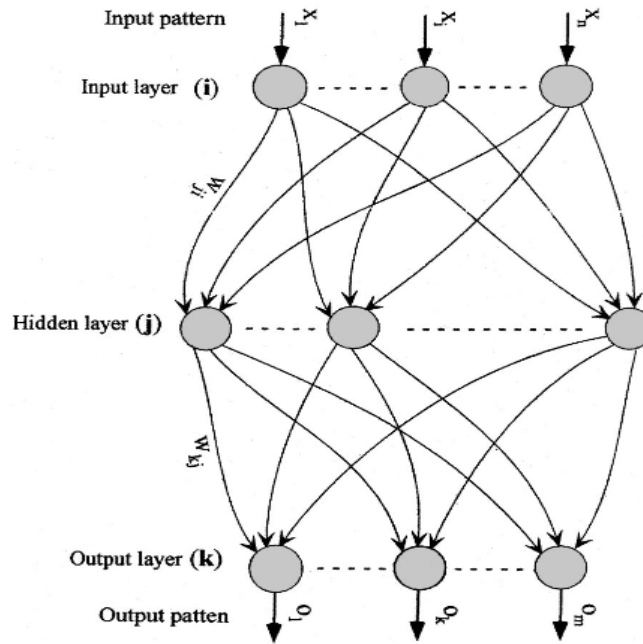


Figure 2.3: Nodal layout of artificial neural network (printed with permission from Nagy et al. 2002).

Within civil engineering, NNs have been applied within nearly every field including construction schedule simulations (Arafa and Alqedra 2011), seismic hazard mapping (Chen et al. 2010), structure response monitoring for vehicle identification (Windrow et al. 1994) and modal response of historic buildings (Bartoli et al. 2012). NNs have also been widely implemented for detection of damage within the context of structural health monitoring. For instance, DeLautour and Omenzetter (2009) adapted a NN for damage detection of a 3-storey ASCE Phase II Experimental Benchmark Structure. Their method hinged on the inclusion of data describing the undamaged structure, which authors suggested should be gathered from an analytical model. In a similar application, the residual strength in a damaged concrete member under stress was linked to ultrasonic wave propagation measurements using an NN (Shah et al.

2012). The authors recommended their method be used along with nonlinear ultrasonic testing. NNs were also used to model the relationship between structural properties to environmental factors. For instance, Ko and Ni (2005) found that an NN was capable of accurately modeling the relationship between the modal frequencies of a bridge and the surrounding ambient temperature.

Perhaps more relevant for prognosis, NNs have also been adapted to study creep-deformation. Creep-deformation is relatively new topic of discussion among historic masonry experts and has in fact become a primary suspect within recent masonry collapses. Additionally, this long-term process has been shown to be suitable for monitoring. In El Shafie et al. (2009), it was shown that the ability of NNs to model long-term creep deformations greatly outperforms traditional methods of curve-fitting. The ability of NNs to accurately predict creep-deformation could prove helpful within a prognostic framework, particularly if additional research confirms that such processes indeed contribute significantly to large-scale collapse.

Research on the prognostic capabilities of NNs is presently limited to isolated applications outside of civil engineering. For example, Wang and Vachtsevanos (2000) studied the predictive capabilities of dynamic wavelet neural networks, while incorporating stability analysis, uncertainty management and performance assessment using a defective (cracked) bearing through which they demonstrated the NNs potential for prediction. The authors proposed future research be conducted on a neuro-fuzzy version of their algorithm incorporating Dempster-Shafer theory to assist in the control of uncertainty. Shao and Nezu (2000) proposed a similar approach to predicting bearing life using a novel progression-based method for predicting RUL. The authors displayed a NN capable of accurate predictions describing the state of the damage mechanism within a bearing while including environmental effects. If such techniques

can be adapted to large-scale systems, such as those in historic masonry, the benefits could shape and guide maintenance efforts to avoid catastrophic events such as collapse.

2.4.2.2. Support Vector Machines

SVMs, another form of classifier, balance model complexity with fitting error according to the structural risk-minimization principle (Vapnik 1998). In doing so, SVMs seek to establish the boundary between two data clusters most efficiently by maximizing the *margin* (Figure 1), a term given to the distance separating those points in different data clusters which find themselves nearest each other. This concept makes SVMs relatively powerful algorithms capable of increased accuracy in many classification applications. Like NNs, SVMs are proven highly successful in applications involving non-linear classification. Given a nonlinear data set, an SVM can apply kernel functions which map the nonlinear data into higher-dimensional space where similar methods to those performed on linearly-separable data sets can be applied successfully.

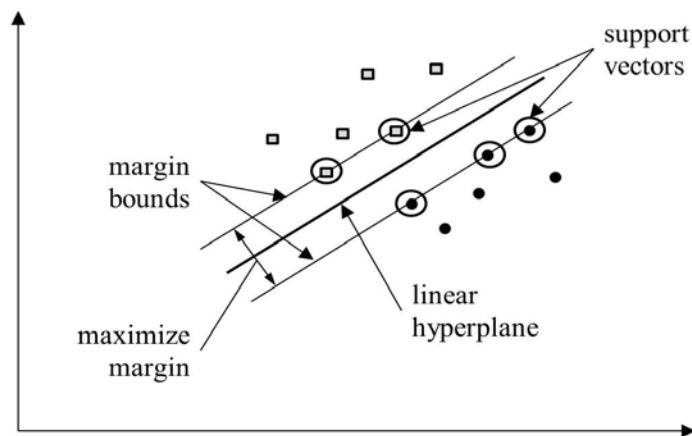


Figure 2.4: Establishing of the margin and support vectors (printed with permission from Atamturktur et al. 2013b).

When used for regression, SVMs produce models demonstrating high levels of accuracy using multi-dimensional or continuous data while avoiding the sensitivity to irrelevant features and extraneous noise that can plague neural networks (Kotsiantis 2007). Stepping beyond the limited abilities of NNs in regards to generalization, support vector regression (SVR) can allow a predetermined degree of generalizability, or *flatness*, in the model to achieve optimization without over-fitting (Xu 2012). Thus, by combining high levels of accuracy with improved capability for generalization and an ability to handle very high non-linearity, SVMs outperform a number of competing machine learning algorithms (Thissen et al. 2003).

Ko and Ni (2005) compared the performance of the NN model with those of linear and nonlinear regression models as well as a SVM model. The NN and SVM models showed increased predictive ability with the SVM model displaying a heavy reliance upon the selection of optimally-determined coefficients. To mitigate this heavy reliance, Atamturktur et al. (2013) used adaptively weighted SVR to support prognostic efforts on an historic masonry coastal fortification in Charleston, South Carolina. In an attempt to limit over-fitting, this method sought to minimize the effects of extraneous noise on model complexity thereby producing a model with increased generalizability, or *flatness*. This was accomplished by the inclusion of a user-defined weighting factor relating model accuracy and flatness which was iteratively adjusted to fit new input data.

An additional concern rises, as it did with much of the research conducted on NNs in prognosis, over the fact that SVMs lack probabilistic outputs. A relevance vector machine attempts to address this problem by using a Bayesian framework. A relevance vector machine uses probabilistic kernels to reject the effects of outliers and the varying number of data points at different time steps. This method requires fewer kernel functions while giving comparable

results for generalization compared to support vector machines. In a case study for estimating the RUL of batteries, a combined relevance vector machine and particle filter method gave more accurate and precise RUL predictions in the form of probability density functions compared with the autoregressive integrated moving average and extended Kalman filter methods (Saha et al. 2009).

2.5. Challenges and Future Direction in Prognostics as Applied to Historic Masonry Construction

Challenges arise in a variety of forms when one attempts to build a prognostic framework for historic masonry structures. Beginning with the structures themselves, future research must provide the crucial insights into how chemical, biological and physical degradation affect the mechanical properties of the material commonly seen through historic masonry construction. The techniques involved in structural health monitoring, namely those of dynamic analysis, may provide the critical means of establishing a framework for continuous health monitoring. But without critical review of what material degradation means for a masonry monuments structural condition, no link can be established between that structure's present condition and its future health.

Assessing the current approach to prognosis identifies the presence of uncertainties as another major issue impeding the application of prognostics to historic masonry structures. In model-based approaches, uncertainties arise from assumptions made during model creation. Masonry materials tend to be very complex and often behaves non-linearly as a result of the properties of the constituent materials (i.e. brick/stone, mortar, grout, and accessory materials) and even more so when accumulated degradation and damage is present (Atamturktur and Laman 2012). These properties must be acknowledged to accurately model a masonry structure

and assess its damage state (Capozucca 2011). Additionally, uncertainties in model input data are caused by variability in material properties, construction inconsistency, and the required estimation of the initial state of the system. In data-driven approaches, uncertainties exist within measurements due to the inability of practical systems to perfectly detect the global structural response, the dependency of the measured structural response to input force levels, the nonlinearity introduced by existing structural damage (i.e. opening and closing of existing cracks) during non-destructive evaluation as well as the loss of information in data reduction. Within either prognostic approach, the accuracy of the prognostic method is affected by how well these relevant uncertainties are addressed (Saxena et al. 2010).

Limitations in resources make it impracticable to fully detect every form of damage in an historic masonry structure. Non-destructive and semi-invasive inspection techniques, which are more suitable for the analysis of historically significant structures, are unable to provide equivalent knowledge of the strength and performance of a structure obtained from destructive testing (De Stefano et al. 2006; Atamturktur et al. 2012). Therefore, further research is required which can link the changes in the non-destructively measured quantities to the integrity of the structural system.

Moreover, the selected response features must be sensitive to the damage types of interest. However, sensitivity of these features to damage depends on each unique structure as well as the type and severity of damage present. As no one particular response feature is sensitive to all damage types, collection and assimilation of multiple response features increases the likelihood of encompassing various damage types in an assessment of the overall health state of the masonry structure. Furthermore, past research has shown that the sensitivity of response

features may also vary with damage level (Prabhu et al. 2012); thus future studies should evaluate the sensitivity of response features for variable damage levels.

Additionally, response features that are insensitive to extraneous noise due to natural variability in environmental and/or operational conditions are desirable. Many response features, especially those that are indicative of the dynamic behavior of a structure, are influenced by operational or environmental conditions, such as wind, temperature, and excitation level. Although it is a customary to incorporate temperature and wind measurements in the diagnostic processes applied to civil infrastructure systems, for historic masonry structures the effect of moisture absorption on the structure's stiffness and mass and consequently its dynamic response must also be considered (Ramos 2007).

An entirely separate, but potentially more challenging issue is that monitored features must provide a global assessment of the structural system instead of indicating localized behavior. The difficulty of exciting the structure uniformly through controlled excitation devices makes obtaining global vibration responses challenging. An additional challenge brought forth due to the flexibility of masonry structural joints, appears in the fact that the behavior of connections between masonry structural components relies on the frictional and mechanical properties of the materials and thus tends to be load dependent. Practical difficulties in global response identification such as optimal sensor and excitation location (Prabhu et al. 2012) must also be resolved.

An alternative to global assessment is *distributed prognostics*, an evolution of current prognostic architectures influenced by the emergence of smart sensors. The application of these smart sensors may relieve large, computationally-powerful central computing hubs of the burden created by continuous assessment. Within distributed prognostics, the task of data analysis in

health monitoring can be passed from the central hub to the smart sensors which themselves generate prognostic forecasts for the sub-systems which they monitor. Because large structures, particular historic masonry, are often large in size and complex in behavior, it may be more cost effective to analyze different parts of the system separately with these new sensors. Through the use of sub-models, the accuracy of local predictions can be enhanced with more traditional prognostic methods building upon this information. (Daigle et al. 2011).

Information provided by the selected response features must be straightforwardly linked to the structural integrity of the historic masonry structure. As the relationship between health quantities, such as a structure's remaining load carrying capacity, and commonly implemented response features in diagnostic evaluations are currently unknown, future research establishing the link between features and structural integrity is imperative.

Hence, not only must the most appropriate damage sensitive features for monitoring historic masonry be determined, but these features must be interpreted to determine the stability as well as the overall performance of the structure. Measuring these features through a continuous structural health monitoring process, could increase the availability of data collection for more accurate RUL predictions, providing advanced warning of unfavorable structural conditions.

2.6. Conclusion

Prognostic techniques stand as a potential framework in which knowledge of time-dependent degradations and their effects can be utilized in forecasting the future health and life-expectancy of an historic masonry structure. While currently unapplied to this form of structure, prognostic methods have been under development in other damage-sensing fields. Lessons learned there can help guide structural engineers evaluating historic masonry. Through the

application of prognostics, engineers might better understand when these structures are most vulnerable and enact condition based maintenance to avoid continuing damage and ultimate collapse.

In this report, the authors elucidated several masonry degradation schemes and inspection methods for their applicability within a prognostic approach. General concepts in prognostics were emphasized in the Introduction prior to a subsequent literature review covering masonry degradation, inspection and vibration-based SHM. The authors also presented model-based and data-driven prognostic approaches coupled with a discussion of specific methodologies that may be adaptable to masonry structures. Next, the authors reviewed the adaptation of pattern recognition techniques, namely machine learning algorithms, to prognosis. Depending on data availability and prior knowledge of the structure, an appropriate prognostic approach and algorithm should be selected for predicting the RUL of the particular historical masonry structure. Finally, challenges and future work in employing prognostic techniques to historic masonry were discussed.

Depending on the budget and desired accuracy, model-based prognostics implemented in combination with data-driven approaches, when sufficient historical data is available, may be the most effective prognostic approach to masonry. Once the future state of the structure is projected and RUL predictions are estimated, effective maintenance can be scheduled to protect historic masonry structures.

ACKNOWLEDGEMENTS

Sponsorship for this work was provided by the PTT Grants program of the National Center for Preservation Technology and Training (NCPTT) of the Department of Interior: the Grant Agreement Number MT-2210-11-NC-02.

CHAPTER THREE

ADAPTIVELY WEIGHTED SUPPORT VECTOR REGRESSION: PROGNOSTIC APPLICATION TO A HISTORIC MASONRY COASTAL FORTIFICATION

3.1. Introduction

In recent years, a significant amount of research has been directed towards the development of prognostic methodologies to forecast the future health state of an engineering system assisting condition based maintenance. However, applications of these potentially useful and informative techniques to historic masonry structures are rare, if any. Developing prognostic methodologies for deteriorating historic masonry monuments and infrastructure affords the possibility of ensuring structural safety, reducing maintenance costs, and preventing secondary damage of such cultural heritage.

Among available prognostic models, Support Vector Regression (SVR) shows a distinct potential for application to historic masonry construction as it offers high accuracy, provides good generalization, and handles nonlinearity (Müller et al. 1997; Samanta and Nataraj 2008; Haydock and Atamturktur 2013). The predictive performance of SVR however, relies on the complexity of the model determined by the tradeoff between fitting accuracy and flatness. The dual objective of SVR then seeks to find the flattest possible model while simultaneously minimizing fitting error (Smola and Schölkopf 2004). The theory of SVR recognizes that more complex models may have greater fitting accuracy but are less generalizable to other datasets of similar underlying processes (Myung 2000). The optimal *weight*, defining the relative importance of flatness to fitting accuracy, however is dependent upon the noise resulting from extraneous loading conditions, such as live, wind, or temperature loads that are time-variant. It must be noted that such extraneous loading conditions are different than causal effects of long

term deterioration. Therefore, it becomes important to adjust the *weight* as new measurements become available to obtain a model complex enough to provide a close fit to data but simple enough to predict global trends well.

The article begins with a review of established literature on prognostic evaluation in Section 2. Main concepts and governing equations for SVR are given in Section 3 followed by a discussion on the adaptively weighted SVR approach. Section 4 then presents the historic masonry case study structure and applies the adaptively weighted SVR to improve forecasting accuracy in the prognostic evaluation. A discussion of the results as well as a summary of the contributions of this study concludes the chapter in Sections 5 and 6.

3.2. Background on Prognostic Evaluation of Historic Masonry

Prognosis, in the context of structural health management of engineering systems, is the estimation of a system's remaining useful life, beyond which, corrective action is required (Saxena et al. 2009). Prognostic techniques are suitable for forecasting gradual degradation processes as opposed to damages caused by sudden unpredictable events. Thus, prognosis is an acausal problem, meaning that it requires knowledge of future loading and operating conditions to make accurate predictions. As future conditions are typically unknown and uncontrollable, conjectures of expected future loading environments must be made based on the history of the structure (Saxena et al. 2010).

The main objective in the implementation of prognostic techniques therefore is to enable educated planning of maintenance of the evaluated system (EI-Tawil et al., 2011). Such improvement in the management of engineering systems has been made possible by prognostic evaluation in many fields; however, prognostic evaluation of masonry heritage structures is in its infancy. With prognostic techniques fully developed and successfully applied to historic masonry

monuments, timely condition-based maintenance and restoration efforts can be planned and the life of such heritage structures can be prolonged.

Masonry construction is prone to experience gradual degradations affecting structural integrity in two forms: material degradations resulting mainly from environmental impacts, and structural degradations resulting mainly due to applied loads or movement of supports (Haydock and Atamturktur 2013). Of the latter, differential support settlements are common in masonry structures due to the heavy weight of the construction and are particularly detrimental to the integrity of the structure due to the low tensile capacity of unreinforced masonry.

Non-destructive inspection techniques with potential to be automated that provide an indication of the global (rather than local) structural integrity are desired for prognostic evaluation of historic masonry structures. Particularly, vibration responses that monitor damage sensitive features supply a viable solution to providing a diagnostic assessment of the structure.

3.3. Methodology

This section briefly discusses the theory behind support vector machines for regression (SVR) and introduces an approach for adaptively weighting the flatness to fitting accuracy in training SVR models to improve prediction accuracy.

3.3.1 Support Vector Regression

Motivated by results of the statistical learning theory (Vapnik 1998), Support Vector Machine (SVM) is a learning algorithm based on the structural risk-minimization principle, which finds a balance between model complexity and fitting error (Xu et al. 2012). In contrast to other machine learning approaches, such as neural networks, that are prone to overfitting the data and having poor generalization capabilities, SVM can allow a predetermined degree of flatness in the model to avoid overfitting (Burges 1998; Xu et al. 2012). Furthermore, most SVMs solve a

quadratic programming problem, which finds the optimal solution and assures that the obtained solution is the unique global solution

Originally created for cluster analysis of datasets belonging to separate classes or categories, SVM seeks to maximize the margin around the linear hyperplane dividing the linearly separable classes (Schölkopf et al. 1995; Xu et al. 2012). In cases where a linear hyperplane (i.e. model) is inappropriate for adequately separating data, a nonlinear model must be obtained by mapping the original data into a new high dimensional feature space through the use of kernels. With the use of kernel functions, the SVM operations are performed in the input space rather than the higher dimensional feature space, thereby reducing the computational demands of high dimensional problems (Gunn, 1998).

SVMs were extended to solve regression problems for model estimation with the addition of an appropriate cost function called the *loss function* (Vapnik 1998). Several types of loss functions have been offered (e.g. quadratic, ϵ -insensitive, Huber, etc.); thus, the user must select the loss function that best suits the problem (Smola and Schölkopf 2004).

The basic principles of SVM for regression, known as Support Vector Regression (SVR), can be illustrated for a training dataset $\{(x_1, y_1), (x_2, y_2), \dots, (x_n, y_n)\}$ of size n . Although more complex kernel functions are available and will be mentioned later, this discussion begins by using a linear kernel function (i.e. linear hyperplane) for simplicity. The linear kernel function, $f(x)$, can be used to solve the following regression problem,

$$f(x) = \langle w, x \rangle + b \quad w \in \mathbb{R}^n, b \in \mathbb{R}^n \quad (1)$$

where w is the coefficient and b is the constant offset known as bias. The model given in Eq. (1) is trained using a subset of the training dataset that constitutes the decision boundaries or margin bounds as shown in Figure 3.1 (Schölkopf et al. 1995). This subset of data points is

referred to as the *support vectors*. The complexity of the model depends on the number of support vectors by which it is represented and is independent of the dimensionality of the input space (i.e. size of input data) (Smola and Schölkopf 2004; Drucker et al. 1997). Generally, seeking a small $\|w\|$ in Eq. (1) decreases the percentage of data points utilized as support vectors thus, reducing model complexity and increasing model flatness (Smola and Schölkopf 2004).

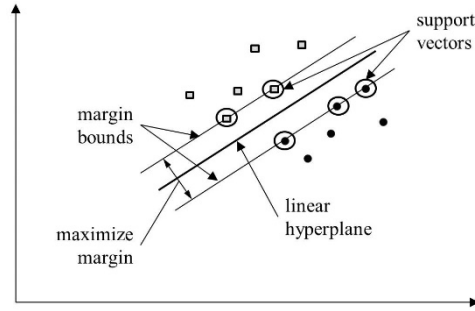


Figure 3.1. Support vectors and margin bounds.

The regression model is determined by the convex optimization problem:

$$\begin{aligned}
 &\text{minimize} && \frac{1}{2}\|w\|^2 + \frac{1}{\lambda} \sum_{i=1}^n (\xi_i + \xi_i^*). \\
 &\text{subject to} && \begin{cases} y_i - \langle w, x_i \rangle - b \leq \xi_i \\ \langle w, x_i \rangle + b - y_i \leq \xi_i^* \\ \xi_i, \xi_i^* \geq 0 \end{cases} \quad (2)
 \end{aligned}$$

in which the regularization parameter λ is traditionally a pre-specified constant that determines the effect of the slack parameters, ξ, ξ^* (i.e. the errors calculated by the loss function) on the objective function. When $\lambda \rightarrow 0$, maximizing fitting accuracy (i.e. minimizing fitting error) is the main objective of the optimization. Conversely, when $\lambda \rightarrow \text{infinity}$, maximizing model flatness (i.e. minimizing complexity) becomes the main objective of the optimization. Therefore, applying $\lambda > 0$ achieves a compromise between fitting accuracy and flatness is achieved.

By minimizing Eq. (2), a balance is found between complexity, $\frac{1}{2}\|w\|^2$, and overall fitting loss, $\frac{1}{\lambda}\sum_{i=1}^n(\xi_i + \xi_i^*)$. This balance ensures that the obtained model generalizes well preventing the model from fitting to noise, also known as overfitting. As a result, the model sensitivity to noise is reduced.

The loss function used in this study is the quadratic loss function, however other loss functions, such as ϵ -insensitive or Huber (Gunn 1998) are also available. The quadratic loss function can be written as follows:

$$L_{quad}(f(x) - y) = (f(x) - y)^2, \quad (3)$$

To measure the error between the observed and estimated outputs for a given input, Eq. (3) uses the conventional least squares error criterion as shown in Figure 3.2.

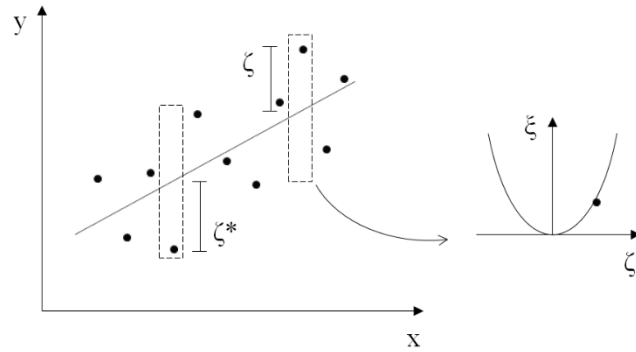


Figure 3.2. Quadratic loss function for a linear SVR.

The solution to Eq. (2) in the quadratic loss function formulation is given by,

$$\begin{aligned} \max_{\alpha, \alpha^*} W(\alpha, \alpha^*) = & \max_{\alpha, \alpha^*} -\frac{1}{2} \sum_{i=1}^l \sum_{j=1}^l (\alpha_i - \alpha_i^*)(\alpha_j - \alpha_j^*) \langle x_i, x_j \rangle + \sum_{i=1}^l (\alpha_i - \alpha_i^*) y_i \\ & - \lambda \sum_{i=1}^l (\alpha_i^2 - (\alpha_i^*)^2). \end{aligned} \quad (4)$$

By exploiting Karush-Kuhn-Tucker conditions,

$$\bar{\alpha}_i, \bar{\alpha}_i^* = 0, \quad i = 1, \dots, l, \quad (5)$$

the optimization problem can be simplified as,

$$\min_{\beta} \frac{1}{2} \sum_{i=1}^l \sum_{j=1}^l \beta_i \beta_j \langle x_i, x_j \rangle - \sum_{i=1}^l \beta_i y_i + \lambda \sum_{i=1}^l \beta_i^2. \quad (6)$$

with constraints,

$$\sum_{i=1}^l \beta_i = 0. \quad (7)$$

The regression model is given by Eq. (1) where

$$\begin{aligned} \bar{\omega} &= \sum_{i=1}^l \beta_i x_i \\ \bar{b} &= -\frac{1}{2} \langle \bar{\omega}, (x_r + x_s) \rangle. \end{aligned} \quad (8)$$

In Eqs. (4, 6 and 8), the dot product, $\langle x_i, x_j \rangle$, can be replaced by a kernel function to map the linear SVR formulation to solve a nonlinear problem, a process widely known as nonlinear mapping (Gunn 1998). Various kernel functions, such as polynomial, spline and radial basis functions are available for nonlinear mapping. Due to their flexibility and consistency of fitting and predicting with minimal residual error in comparison to other kernels, splines are a common kernel function of choice in SVR modeling (Gunn 1998; Mammen 1997; Rajasekaran et al. 2008); thus, the remainder of the chapter will focus on the spline kernel.

3.3.2 Adaptively Weighted Support Vector Regression

The trade-off between fitting accuracy and flatness of an SVR greatly affects the predictive performance of the prognostic evaluation. This principle is evident in Figure 3.3: models that are *too simple*, as shown by $\lambda=2$ on the left in Figure 3.3, may neither be able to fit the available data nor be able to generalize the trends well. Models that are *too complex* on the

other hand may accurately fit the available data, as shown by $\lambda \rightarrow 0$ on the left in Figure 3.3, but may not be able to generalize the trends well. Therefore, there is an optimal degree of flatness, as shown by $\lambda=0.01$ on the right in Figure 3.2 that finds a more suitable compromise between fitting error and flatness.

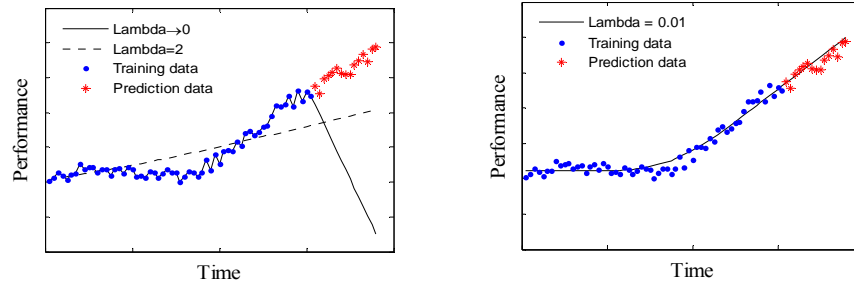


Figure 3.3. Trade-off between flatness and goodness of fit varying from (left) more extreme λ values to (right) more compromising λ value.

This optimal flatness depends on the extraneous noise present in the measurement. In measuring the structural responses of a system as in the case of the present study, extraneous noise may be incurred in the measurements due to the responses of the structure to sources other than those that cause long term degradation. For example, in using vibration measurements to monitor damage within a historic masonry structure caused by long term, gradual settlement of the foundation, wind and other external short term loading effects can influence the response of the structure, consequently adding noise to the data. Thus, the optimal λ is that which generalizes global trends in the presence of noise.

The dependency of optimal flatness to noise levels is demonstrated in Figure 3.4. In noise-free datasets, $\lambda \rightarrow 0$ (i.e. giving zero weight to flatness) may provide a suitable model as shown in Figure 3.4 (a). As noise increases, however, a larger λ is required, meaning that more weight is given to flatness than fitting accuracy, to achieve a similar trend as presented in Figures

3.4 (b) and (c). Therefore, λ must be correctly determined for a given dataset to ensure reliable predictions of the future health state of the system.

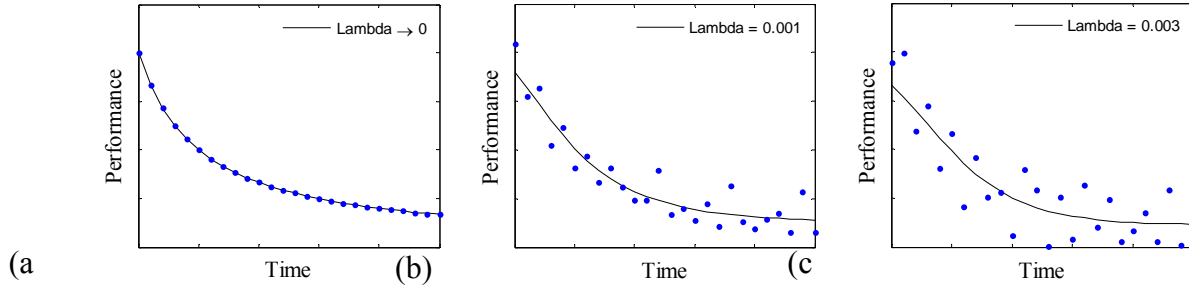


Figure 3.4. Magnitude of λ required to fit a given trend as noise is added.

Cross-validation has been used for selecting the λ by utilizing hold-out experiments; however, this technique focuses solely on fitting accuracy (in an interpolative manner) rather than prediction accuracy (in an extrapolative manner) (Stone 1974; Jaakkola and Haussler 1999; Smola and Schölkopf 2004). Because a prognostic evaluation requires accurate extrapolative projections of the future health of the structure, the focus in this chapter is to improve the forecasting accuracy of the model rather than its closeness of fit to available data. Hence, the optimal λ is selected by that which predicts with the least error a predetermined number of most recent measurements that are not used in training the SVR model. As the global trends and noise levels may change over time, a constant λ may not be the best approach to applying flatness. Here, the proposed method adaptively selects λ and thus that is referred to as adaptively weighted SVR.

The basic steps of this adaptively weighted prognostic approach can be demonstrated on an initial dataset of n points. In Figure 3.5, the dataset is divided into three parts: the *preliminary training set* consisting of the first m points, the *hold-out set* consisting of the following h points, and the *forecasting set* consisting of the next f points. During the preliminary stage, optimal λ is selected. For this, multiple candidate λ values (ten λ values for each multiple of 10 from 10^{-15} to

10^5) are tested in their ability to predict the hold-out set of h points from m to n , where $n = m + h$. The resulting L1 norm prediction error of the hold-out set is summed for each model trained by a different candidate λ , and, by comparison, the candidate λ producing the model with the least prediction error over the hold-out set is chosen as the optimal λ . During the forecasting stage, this optimal λ is then used to train a refined model using the total dataset that was used in the preliminary stage (i.e. up to n) to predict the forecasting set (i.e. from n to p). The adaptively weighted approach then repeats this process as additional measurements become available by adding these *new* data points to the training set and updating λ accordingly. The detailed steps of this process are shown in Algorithm 1.

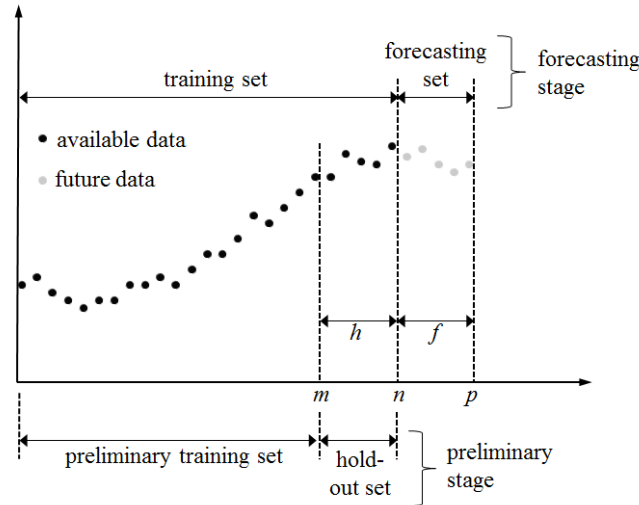


Figure 3.5. Dataset divisions for preliminary and forecasting stages of adaptively weighted SVR.

Table 3.1. Pseudocode for adaptively weighted SVR.

Algorithm 1. Basic structure of adaptively weighted SVR

Begin

Input SVR parameters

- $X = \text{independent variable}$
- $Y = \text{dependent variable}$
- $h = \text{number of hold-out points}$
- $f = \text{number of forecasting points}$
- $P = \text{total number of iterations}$
- $m = \text{index of final point in preliminary training set}$

- $n = \text{index of final point in hold-out set}$
- $p = \text{index of final point in forecasting set}$

For $i = 1$ to P

For $\lambda = 10^{-15}$ to 10^5

- *Train a support vector regression model (see Gunn 1998) using preliminary training set, X_1 to X_m , and forecast the hold-out set, X_m to X_n*
- *Compute the L1 norm residual error of the predicted hold-out set by comparison to the corresponding subset of Y*

End

- *Choose optimal λ as that which gave the least prediction error of the hold-out set*
- *Train a support vector regression model using training set, X_1 to X_n , and predict the forecasting set, X_n to X_p , where $X_p = X_{(n+f)}$*
- *Compute the residual error of the predicted forecasting set*
- *Define new input parameters:*
 - $X_m^{i+1} = X_n^i$
 - $X_n^{i+1} = X_p^i$

End

End

3.4. Case Study

Coastal fortifications built as defense mechanisms in protecting important seaports and harbors, were once the cornerstone of national defense in the United States (McGovern and Smith 2006). Today, these coastal fortifications, many of which are over 150 years old, are considered structures of national heritage. Over their lifetime, these structures are subject to harsh coastal environmental and operational conditions leading to material and structural degradations. To successfully preserve these important historic edifices for future generations, timely maintenance is imperative. Prognostic evaluation can assure such timely maintenance campaigns.

Fort Sumter, in Charleston, South Carolina, where the first shots of the American Civil War were fired in 1861 (National Park Service 1984) is one such historically important fort that is in need of accurate structural assessment and prognostic evaluation. There is evidence that differential settlement of the foundation has been occurring at Fort Sumter leading to extensive

cracks throughout the masonry casemates. Thus, this section demonstrates the weighted SVR prognostic technique as applied to one of the casemates of Fort Sumter considering gradual settlement of foundations.

3.4.1 Case Study Structure: Fort Sumter National Monument

The construction of the pentagonal-shaped clay masonry fort began in 1829 on a man-made island. In the years of the Civil War, Fort Sumter witnessed several battles that severely damaged the structure (National Park Service 1984). After several rounds of demolition and reconstruction, Fort Sumter was declared a national monument in 1948. The fort has since been maintained by the National Park Service and is currently accessible to visitors (see Figure 3.6).



Figure 3.6. Current aerial view of Fort Sumter (Courtesy: National Park Service).

3.4.2 Finite Element Model Development

The FE model of the single casemate used in this study as shown in Figure 3.7 is developed in Ansys 13.0 by incorporating data from on-site inspections and evaluations discussed in detail in (Atamturktur et al. 2013). Laboratory tests are conducted on core samples of the masonry and a masonry prism specimen from fallen debris in order to obtain the material properties. 3D laser scanning is performed to obtain the precise as-is geometry of the casemate with which the FE model geometry is constructed while preserving key geometrical features such as any permanent deformation, material deterioration, tilting of the walls. The FE model is developed using SOLID65 elements that are specialized for modeling concrete-like brittle

materials (Özen 2006; Mahini et al. 2007). The SOLID65 element uses a smeared crack analogy to account for deformations due to cracking and crushing of the material. The linear material properties of the model are calibrated to experimentally obtained modal parameters (i.e. first two natural frequencies and mode shapes).

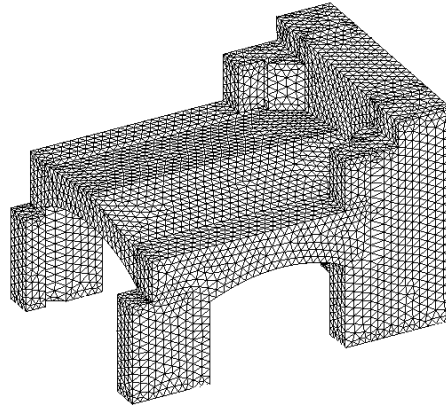


Figure 3.7. FE model of Fort Sumter casemate used in case study (refer to Atamturktur et al. 2013).

Because the barrel vaulted casemates are built adjacent to but detached from the scarp wall, the scarp wall and the casemate are two independent structural entities. Therefore, contact elements that allow sliding and separation (but do not allow penetration) of two adjacent components are used to model this interface. A dynamic hammer impact test was used to calibrate the friction coefficient accounting for the friction and cohesion (if any) at the interface to represent this possible sliding action in the FE model. To take into consideration the lateral interaction with the adjacent casemates, adjacent casemates are represented using substructuring techniques. To keep the size of the model to a manageable level, the foundations of the casemate are idealized as a series of linear springs having finite stiffness. Details of the model development process are provided in Atamturktur et al. (2013).

3.4.3 Simulations of Support Settlement

The FE model used to simulate support settlement is shown in Figure 3.8, where the casemate of interest is the center casemate with the adjacent casemates modeled as substructures. The ground below the casemates can be visualized as a rectangular plane as shown on the left of Figure 3.8. By tilting this rectangular plane in the direction perpendicular to the external wall as shown in Figure 3.8 (right), the settlement configuration is simulated. This configuration representing settlement of the external wall is used to obtain the structural response data for application of the proposed prognostic technique.

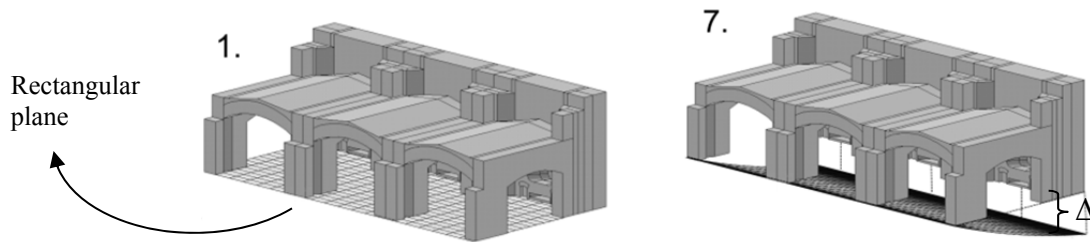


Figure 3.8. Initial model configuration on level surface (left) and settlement configuration (right).

In the simulations, the ground plane of the casemate is gradually settled with a maximum displacement (Δ) under the scarp wall of from 2.5 mm to 100 mm at increments of 2.5 mm. The first principal strain at the two control point locations, POINT 1 and Point 2, shown in Figure 3.9 are monitored during these settlement simulations. As shown in Figure 3.8, Point 1 is located at the base of the pier, and Point 2 is located at the springing of the arch. The resulting first principal strains at the two control points obtained from the simulated settlement are plotted in Figure 3.10 with randomly generated non-stationary noise added.

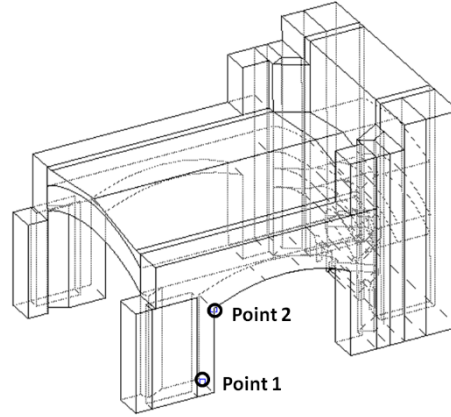


Figure 3.9. Locations Point 1 and Point 2 of monitored strains during settlement (circled).

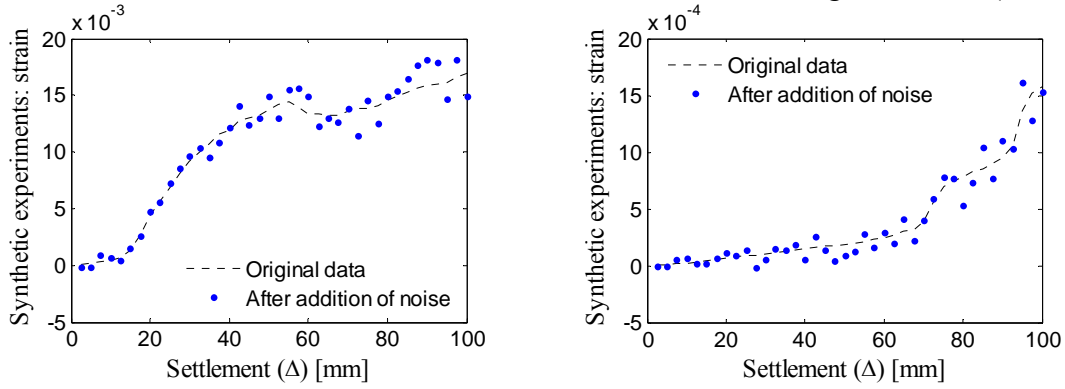


Figure 3.10. Settlement induced strains obtained from FE model of Point 1 (left) and Point 2 (right) with added noise.

3.4.4 Prognostic Evaluation using Weighted SVR

The algorithm presented in the methodology section is deployed on the simulated dataset shown in the previous section. 15 data points simulating the strain response of the casemate under settlement up to 40 mm are assumed to be available for the prognostic evaluation. To determine the initial λ value, the first ten of these data points are used in the preliminary training set (up to 27.5 mm settlement) and the next five data points are used as the hold-out set (from 27.5 mm to 40 mm settlement) (refer back to Figure 3.5). Multiple candidate λ values between 10^{-15} and 10^5 are tested to find the optimal λ that yields the minimal error in predicting the hold-out set. With the identified optimal λ , a refined SVR model is trained and is executed to forecast

the next five data points (from 40 mm to 52.5 mm settlement). This process is repeated as new measurement data become available, and the optimal λ is updated during each iteration. In this case study, a total of five iterations are completed to reach 100 mm settlement, thus the optimal λ is updated four times after it is initially determined in the first trial. The predicted response, prediction error, and adaptively refined optimal λ obtained as a result of this analysis are displayed in Figure 3.11 for Point 1 and Figure 3.12 for Point 2 (note that results shown after the vertical dashed line in Figures 3.11 and 3.12 (a) and (b) are the compiled results of the five forecasting iterations). For comparison, the predicted response and prediction error of an SVR model trained using a constant λ of $\lambda \rightarrow 0$, which gives all weight to fitting error and none to flatness, are also included in the figures.

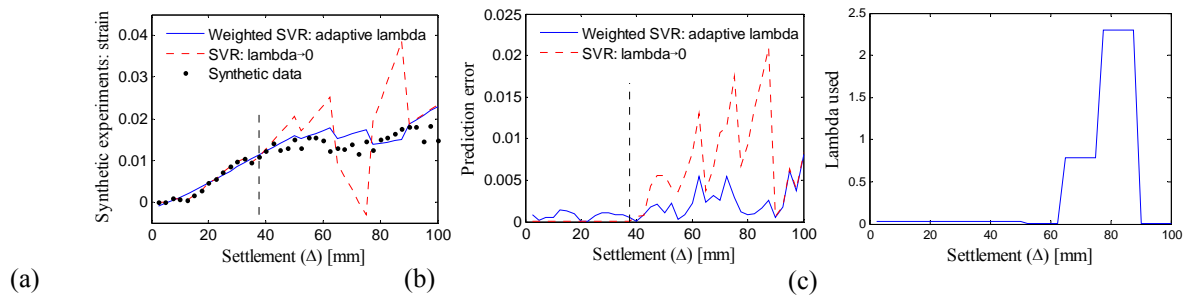


Figure 3.11. Comparison of adaptively weighted SVR to non-weighted SVR using Point 1 data with increasing noise: (a) predicted response, (b) prediction error, and (c) λ value used for prediction model.

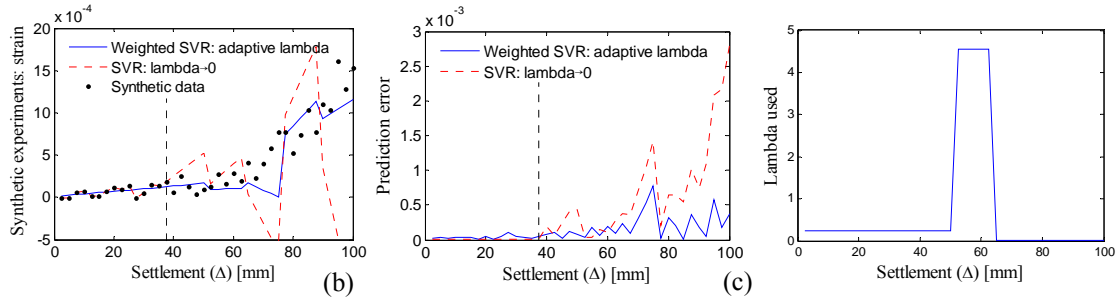


Figure 3.12. Comparison of adaptively weighted SVR to non-weighted SVR using Point 2 data with increasing noise: (a) predicted response, (b) prediction error, and (c) λ value used for prediction model.

As evidenced in Figures 3.11 and 3.12, the adaptively weighted SVR predicts the settlement induced strains with less than half as much error as the non-weighted approach (see Table 3.2). It must be noted that the noise added to the simulated data is non-stationary in nature. Therefore, the distinct advantage of the adaptive approach is its ability to recover the optimal λ as noise fluctuations occur over time, as is the case in practical *in situ* monitoring applications.

Table 3.2. Total prediction error for adaptively weighted SVR and non-weighted SVR.

SVR Approach	Point 1	Point 2
Adaptively weighted	0.0719	0.0057
Non-weighted	0.1898	0.0178

3.5. Conclusion

Although SVR is known for its superior prognostic abilities, the performance of this machine learning technique is reliant on the selection of an appropriate regularization parameter, λ , determining the tradeoff between fitting accuracy and model complexity (i.e. flatness). The optimal tradeoff is greatly affected by the presence of time-variant extraneous noise within measurements, which is common during *in situ* monitoring applications. Therefore, an ideal process for selecting optimal λ is one in which the model sensitivity to noise is decreased.

Within this chapter, an adaptive weighting approach for SVR is developed, which first determines the optimal λ based on forecasting accuracy, and then uses this optimal λ to develop a refined model for future predictions. As additional data becomes available in time, the optimal λ is updated allowing the new model to be adjusted for fluctuations in noise intensity. Thus, the most suitable model complexity for a given dataset is selected for each set of predictions. In testing the performance of this approach on the simulated settlement response of a historic masonry coastal fortification, the adaptively weighted SVR shows greatly increased forecasting accuracy over the non-weighted approach.

The developed adaptively weighted SVR has potential to be incorporated in a structural health monitoring process to ultimately assist in preserving the cultural heritage by predicting its future structural integrity. However, future direction in research should focus on determination of appropriate damage sensitive features and corresponding monitoring techniques for prognosis of historic masonry structures. Furthermore, a failure threshold indicating the structure's end of life must also be defined. Such a threshold can only be defined by developing a link between nondestructive measurements and the remaining load carrying capacity of the masonry monument as suggested in Atamturktur et al. (2012), which is the primary attribute of concern in prognostic evaluation.

CHAPTER FOUR

AN EMPIRICAL ASSESSMENT OF LOAD CARRYING CAPACITY OF A SCALED MASONRY DOME: SIMULATIONS VALIDATED WITH NON-DESTRUCTIVE AND DESTRUCTIVE MEASUREMENT

4.1 Introduction

Masonry, one of the oldest construction materials, exhibits high load-carrying capacity in compression but much lower capacity in tension, to the point that structural analysis of masonry often assumes a theoretical value of zero tensile capacity (Heyman, 1995). Large spans in structural masonry are possible using domes that allow forces to be transferred in compression. These masonry domes, found in many historic buildings across the world, typically stand in a state of structural distress appearing in the form of cracking. For example, the great dome of Florence stands with 493 symmetrically distributed cracks of various widths (Suro, 1987). The growth of these cracks due to natural aging or disastrous events can threaten the safety of these masonry domes regardless of the length of time they may have been safely standing. Furthermore, the sudden collapse of many historic masonry monuments over the last several decades has demonstrated the vulnerability of masonry systems to failure with no particular warning or structural indication of imminent failure; see for example, the Civic Tower of Pavia, Italy (Binda et al., 1992); the bell tower of St. Magdalena in Goch, Germany (Garntert Engineering Studio, 1993); Cathedral of Noto, Italy (Binda et al., 1999); the bell tower of the St. Willibrordus Church in Meldert, Belgium (Ignoul and Van Gemert, 2006); the Maagdentoren in Zichem, Belgium (Ignoul and Van Gemert, 2007); the Church of Kerksken, Belgium (Verstrynge et al., 2011).

Recently, vibration-based structural health monitoring (SHM) techniques have been increasingly used to help maintain safe and economic operation of aging masonry structures. The

purpose of vibration-based SHM is to exploit the sensitivity of the vibration signature of a system to the structural damage and has been successfully implemented to detect the onset of damage in published literature (Atamturktur et al., 2011). Detecting the onset of damage, while helpful for efficient and effective maintenance, is only part of the solution for safe and economic operation of heritage structures. What is ultimately needed is an assessment of the structural integrity of the damaged system; therefore estimating the reduction in load carrying capacity after the onset and progression of damage must be one of the goals of SHM. However, until recently, little effort has been made to decipher the indirect relationship between the changes in the vibration characteristics and the reduction in load carrying capacity due to damage.

A masonry domical structures under excessive loads or support movements develop meridional and parallel cracks, which cause a reduction in the stiffness of the structure. In turn, this reduction in stiffness can be detected experimentally through the reductions in the measured natural frequencies of the dome. Experimental modal analysis (EMA) and the companion operational modal analysis (OMA) techniques are nondestructive testing and evaluation methodologies for measuring the natural frequencies of a structure. These techniques can be conveniently employed to monitor the changes in the vibratory characteristics of a structure as damage progresses in a non-invasive manner. Aside from degrading the stiffness, development of meridional and parallel cracks due to distress also reduces the strength of the dome. However, the reduction in strength results in the reduction of the load-carrying capacity, which is a challenging property to quantify without destructive testing (Brown et al., 1995). As it is hard to imagine conducting destructive experiments on an existing structure, the central query then becomes one of estimating the reduction in the load carrying capacity due to damage (which we

cannot directly measure) by exploiting the changes in the natural frequencies (which we can directly measure with EMA and OMA).

The fundamental contribution of this manuscript is to exploit the sensitivity of the vibration characteristics to the structural integrity of the masonry dome and formulate an empirical relationship between the changes in the natural frequencies and reduction in load carrying capacity due to damage. Such empirical relationship is an intrinsic characteristic of particular type, material, and geometry of the structure and thus, must be treated in a case-specific manner. The proposed approach however presents itself to be useful for structures with many repetitive components, see for instance the structures studied in Atamturktur and Sevim (2011) and Atamturktur and Boothby (2010). The proposed empirical relationship, once successfully formulated for a specific structure type, can be used in practical applications to assess the remaining load carrying capacity of existing structures.

In the present study, this empirical relationship is developed based on a combined experimental and numerical study completed on a scaled masonry dome constructed in the laboratory with autoclaved aerated concrete (AAC) tiles and fast-setting gypsum mortar (plaster of Paris). The numerical model of the dome is built in ANSYS v. 13, a finite element (FE) analysis program. The uncertain linear elastic material properties of the model, such as the Young's modulus, are calibrated by comparing the model predictions against experimentally obtained natural frequencies which are paired according to mode shape correlations. Next, the nonlinear constitutive behavior is added to the model and the uncertain nonlinear properties, such as the tensile stress capacity, are calibrated by comparing the predicted load-displacement plots to those experimentally measured in the laboratory. Once a FE model that can accurately represent both linear (natural frequencies) and nonlinear (load carrying capacity) behavior of the

domes is obtained, the model is then used to simulate the effects of crack development on both the stiffness (and thus, natural frequency) and the strength (and thus, load carrying capacity). The gradual reduction in natural frequencies caused by cracks with increasing lengths up to 20 in. is documented and correlated with the corresponding reduction in the load carrying capacity of the dome. A mathematical function (i.e., an emulator or a surrogate model) is trained to represent this indirect relationship between natural frequencies and load carrying capacity. The established empirical relationship is conservative as an upper bound to the reduction in load carrying capacity is defined and is (to an extent) generally applicable since domes with various span-to-height ratios are considered.

4.2 Scaled dome model

The structure studied herein is a scaled masonry dome built in the laboratory with the traditional methods of tile vault construction, except for a material change to AAC tiles. These tiles are lightweight, fire resistant and composed of cement, lime, water, sand, and aluminum powder (Costa et al., 2011). The geometric properties of the tested dome are listed in Table 4.1 and the configuration is shown in Fig. 4.1.

Table 4.1 Geometric properties of the dome.

Properties	Values
Radius of curvature	1.52 m (60 in)
Span at base	2.13 m (84 in)
Rise above springing	0.44 m (17.4 in)
Angle of embrace	45°
Thickness	0.03 m (1.25 in)

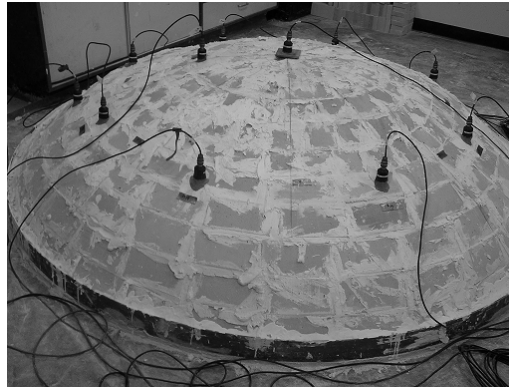


Fig. 4.1. The scaled dome constructed with AAC tile and fast-setting gypsum cement.

4.3 Finite element model development

Although the FE analysis is an efficient method to simulate the behavior of civil structures, developing an accurate numerical model is a challenging task due to the large number of assumptions that must be established and the parameters that must be defined. Masonry construction is a non-homogenous and non-isotropic composite, which in the dome studied here is composed of individual tile units and mortar joints. The complex and irregular nature of masonry construction is responsible for the difficulties in accurately predicting the structural behavior of such systems. Of course, the problem is further exacerbated by the degrading effects of aging, such as localized or diffused cracks and by poorly documented history of structural intervention and rehabilitation schemes. Although detailed micro-models that incorporate individual tile units and mortar joints and localized damage are capable of addressing some of the complexities, their application is primarily restricted to small-scale structures with simple geometric forms (Lourenço, 2002).

In this study, the macro-modeling approach is implemented using ANSYS v. 12, in which the tile units and mortar joints are smeared together as one continuum with homogenized

properties representative of the combined behavior of the two components in the masonry assembly (Lourenço, 2002). The first step of macro-modeling is to reproduce the geometry of the structure as precisely as possible. This is accomplished using the available geometric documentation from the original design of the dome (see Fig. 4.2). Even though in Lau (2006) construction imperfections have been reported to result in $\pm 1.7\%$ deviations between the designed and built dome, in the FE model, the dome is idealized to have perfectly symmetric geometry. Moreover, the dome is idealized to have symmetric boundary conditions where the boundaries of the dome along the bottom edge are kept restrained from translating in all three directions.

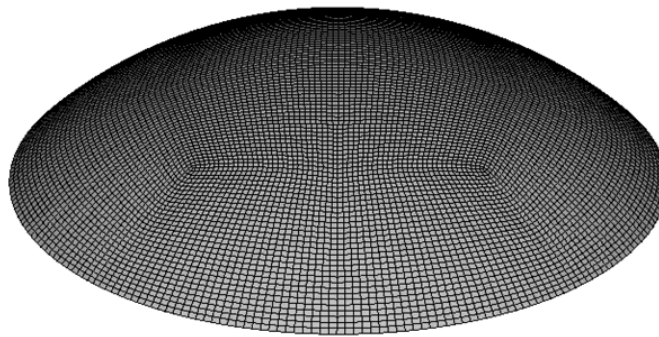


Fig. 4.2. FE model of the dome.

In FE analysis, obtaining a proper spatial discretization of the solid model, in which the geometric model is systematically discretized into finite elements, is a critical step. Indeed, the selected mesh size can drastically affect the accuracy of the numerical solution. Theoretically, with an infinite number of elements, a complete computational reproduction of the structure can be achieved; it is of course impractical to use such excessively large number of elements. Therefore, it becomes important to determine both the optimal element type and the optimal mesh size that result in converged solutions for the output of interest, which in this study is the modal and static responses of the tile dome.

The solution accuracy is monitored for the natural frequencies, static load-carrying capacity and stiffness as the number of finite elements in the model is gradually increased from 14520 to 49284 (i.e. the mesh size is gradually reduced and the number of elements gradually increased). Natural frequencies of the six modes of the dome, which are later presented in Section 4.4.2 during test-analysis correlation, are monitored. The asymptotic convergence of the predicted natural frequencies as the mesh is refined is shown in Fig. 4.3.

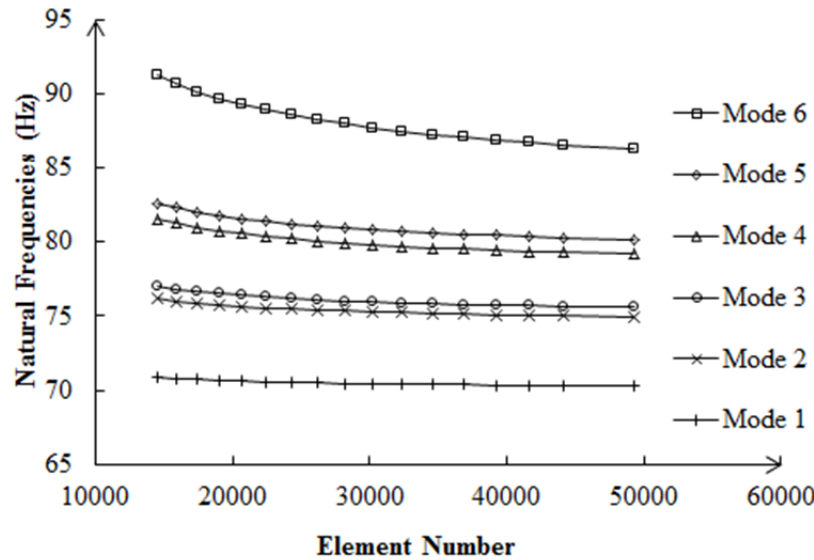


Fig. 4.3. Asymptotic convergence of the six natural frequencies as mesh is refined.

Similarly, for the nonlinear analysis, a vertical 5338 N (1200 lb) load is gradually applied within a radius of 30.48 cm (12 in) around the crown of the dome. This configuration generates force-displacement diagrams and mimics the actual destructive tests as explained later in Section 4.5.1. The mesh is refined to ensure that the predicted ultimate load carrying capacity and stiffness have converged. Similar to mesh convergence depicted in Fig. 4.3, beyond 30000 elements, further refinement of the mesh is observed to yield only minimal improvement in predictive capability. As a result, a mesh with a total number of 32400 elements is implemented to obtain the desired numerical accuracy for both the linear and nonlinear solutions.

To properly represent the constitutive behavior of the domical structure correctly, a suitable element type must be defined in the FE model. AAC materials share a similar stress-strain law with that of normal strength concrete (Costa et al., 2011). Developed specifically for concrete, SOLID65 is a three-dimensional, 8-node solid isotropic element readily available in ANSYS v. 12 to model the nonlinearity of brittle materials (ANSYS, 2010). The nonlinear behavior of SOLID65 element is based upon the Willam-Warnke yield criterion, a constitutive model for the failure and tri-axial behavior of concrete materials (William and Wamke, 1975) as seen in Fig. 4.4. Although Willam-Warnke yield criterion is developed for concrete material, it is also demonstrated to be suitable for masonry (Page). There has been several successful applications of the Willam-Warnke yield criterion to masonry structures; see for instance, Andreas et al. who evaluated the lateral load carrying capacity of unreinforced masonry structures (Andreas et al., 2002); Truong et al. who compared the different modeling strategies (micro vs. macro) for masonry underground movements (Linh and Debra, 2008); Aiello et al. who evaluated the bond behavior between masonry components (Aiello et al.); and Brencich et al. who adopted the criterion in the safety analysis of the masonry dome of Basilica of S. Maria of Carignano (Brencich et al., 2001).

The SOLID65 element is capable of accounting for cracking in tension with a smeared crack analogy and crushing in compression with a plasticity algorithm. The stress-strain relationship of SOLID65 has two phases: linear elastic behavior and nonlinear behavior after either of the specified tensile or compressive strengths is exceeded. Cracking or crushing occurs when any of the three principal stresses exceed the specified tensile or compressive strength of the concrete at any of the eight integration points. After the occurrence of cracking or crushing, a plane of

weakness is introduced in the requisite principle stress direction, thus decreasing the global stiffness and simulating the formation of a crack (Fanning, 2001).

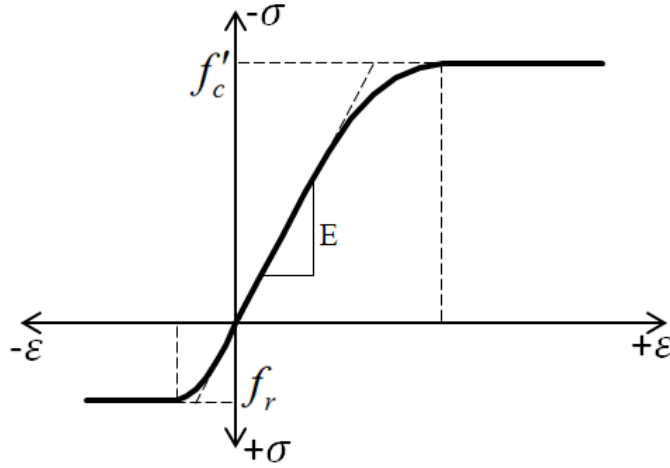


Fig. 4.4. Simplified Stress-Strain curve for concrete in ANSYS.

The AAC brick used in this study is mid-grade TruStone AAC TS 3, which has a compressive strength f'_b of 4.14 MPa (600 psi) (TruStone America, 2005). The modulus of elasticity of AAC brick is calculated using Eq. (1) according to ACI-530 Section 1.8.2.3.1 (MSJC, 2008):

$$E_b = 6500(f'_b)^{0.6} \quad (1)$$

where f'_b is the specified compressive strength (in psi) of AAC masonry.

The modulus of elasticity of the AAC tile is calculated using Eq. (1) as 2.08 GPa (3.02×10^5 psi). There are other recommended prediction equations for the modulus of elasticity of AAC, which are provided in Narayanan and Ramamurthy (2000). These alternative equations all yield values close to or a range containing the value calculated using Eq. 1. In the absence of experimental data, the elastic modulus of the wet gypsum mortar is initially assumed to be 25% that of the tile yielding 0.52 GPa (7.55×10^4 psi). The Uniform Building Code (UBC-1991) recommends Eq. (2) to calculate the modulus of elasticity of the homogenized material of brick

and mortar units (ICC, 1991). The equation considers the thickness and elastic modulus of both the AAC tile and the mortar to provide an approximate value of the homogenized modulus of elasticity, E_m which is given by

$$E_m = \frac{1 + \gamma_t}{1 + \gamma_t / \gamma_m} E_b \quad (2)$$

in which E_b is the modulus of elasticity of brick (2.08 GPa (3.02×10^5 psi)); γ_m is the modulus ratio given by $E_j / E_b = 0.25$ where E_j is the modulus of elasticity of mortar joints (0.52 GPa (7.55×10^4 psi)); and γ_t is thickness ratio given by $t_j / t_b = 0.125$ where t_j is the thickness of mortar joints, (0.01 m (0.5 in)) and t_b is the thickness of brick along the curvature (0.10 m (4 in)). Thus, with all required values known, the initial value of the elastic modulus for the homogenized tile and mortar assembly is calculated from Eq. (2) as 1.56 GPa (2.27×10^5 psi).

The AAC tile used in this study has an approximate dry density of 581.28 kg/m³ (0.02 lb/in³) (TruStone America, 2005). AAC, being quite porous, has a moisture content of approximately 15-25% (Narayanan and Ramamurthy, 2000), which of course leads to an increase in the density. For new construction, this value can be as high as 45% (RILEM Technical Committee, 1993). In this study, the experiments were conducted within 48 hours after the dome was constructed, therefore an approximate of 35% moisture content is adopted while calculating the density. The wet density of AAC tile is then calculated as 775.04 kg/m³ (0.03 lb/in³). According to the product manual, the wet density of the gypsum cement is 1762 kg/m³ (0.06 lb/in³) (USG [internet]). Therefore, assuming a composition of 60% bricks and 40% mortar, a homogenized density is calculated to be 1190 kg/m³ (0.04 lb/in³).

Lau (2006) reports the uniaxial tensile strength test results for the brick-mortar bond conducted for the scaled tile dome discussed herein. It is reported that the bond has a tensile

strength within a range of 0.07 MPa (10 psi) to 0.27 MPa (39 psi), and with an average value of 0.16 MPa (23 psi). Accordingly, in this study, the initial value for the tensile strength of the FE model is defined as 0.16 MPa (23 psi).

Table 4.2 FE model input parameters before and after calibration

(**fine-tuned parameter values*)

Parameter	Before	After
Young's Modulus*, E_m	1.56 GPa (227000 psi)	1.55 GPa (225000 psi)
Poisson's ratio, ν	0.25	0.25
Open shear transfer coefficient, β_t	0.2	0.2
Closed shear transfer coefficient, β_c	0.6	0.6
Ultimate uniaxial compressive strength, f'_c	4.14 MPa (600 psi)	4.14 MPa (600 psi)
Ultimate uniaxial tensile strength*, f_t	0.16 MPa (23 psi)	0.14Pa (20 psi)

4.4 Correlation of the FE model with nondestructive tests: linear properties

The natural frequencies of the structure which must be measured to establish the proposed empirical relationship can be obtained using either experimental modal analysis (EMA) or operational modal analysis (OMA) techniques. In published literature, both EMA and OMA have been successfully applied to masonry structures. For EMA, see for instance Armstrong et al. (1995) who studied a masonry arch vibrations to detect spandrel wall separation; Brown et al. (1995) who tested masonry arch bridge prototypes to determine the development of cracks and hinges under overloading; and Atamturktur and Boothby (2010) who exploited the vibrations of the cathedral vaults to validate the numerical models. For OMA, see for instance Gentile and Saisi (2007), who studied a masonry tower to determine the regions with diffused cracks; Ramos

et al. (2010), who evaluated a historic masonry cathedral and Bayraktar et al. (2011), who studied the vibration of a minaret to update the numerical the finite element model. Also see Atamturktur et al. (2011) for a comparison of practical and technical differences of EMA and OMA techniques as applied to large-scale masonry monuments.

4.4.1 Experimental campaign

EMA is adapted for the vibration evaluation of the scaled dome by collecting the acceleration response of the masonry tile dome due to a short-duration hammer impact. The objective of this dynamic test is to provide physical evidence for the calibration of the linear parameters entered into the FE model. For the impulse excitation, a 1.01 kg (2.42 lb) model 086D20 sledge-hammer manufactured by PCB, Inc. is used. This hammer is selected due to its capability to excite the frequency range of interest, which is 0-150Hz (to identify the first 20 modes of the dome). In an effort to maximize the number of modes that are successfully identified, seven distinct excitation locations are selected as shown in Fig. 4.5 (Left). PCB Model 393A03 uniaxial seismic accelerometers, with a frequency range of 0.3-4000 Hz and a sensitivity of 10 volts/g, are used during the test. The accelerometers are arranged at 20 locations over outer surface of the dome as shown in Fig. 5 (Right).

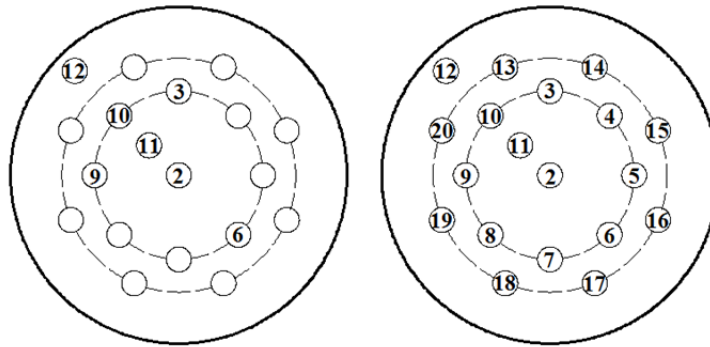


Fig. 4.5. (Left) Excitation points, (Right) Measurement points.

The data is processed and recorded by SigLab data acquisition system, manufactured by Spectral Dynamics, Inc. The time domain response measurements are obtained with a record length and sampling frequency of 2048 samples and 1000Hz, respectively. The responses are recorded within 4 seconds, which fully capture the response of the dome in a single time frame, thus preventing the leakage of higher-frequency energies over the lower frequencies. The short duration impact of the hammer excites the tile dome to vibrate at a wide range of its inherent natural frequencies until the response dies out exponentially. A typical time domain measurement of hammer impulse and acceleration response can be seen in Fig. 4.6. As seen in this figure, the measurements are collected over 4 seconds to allow the decay of the dome's vibratory response, which allows us to eliminate the need for window functions. The measurement duration is determined by the desired Frequency bandwidth and resolution. All variables of signal processing equipment are given in Table 3.

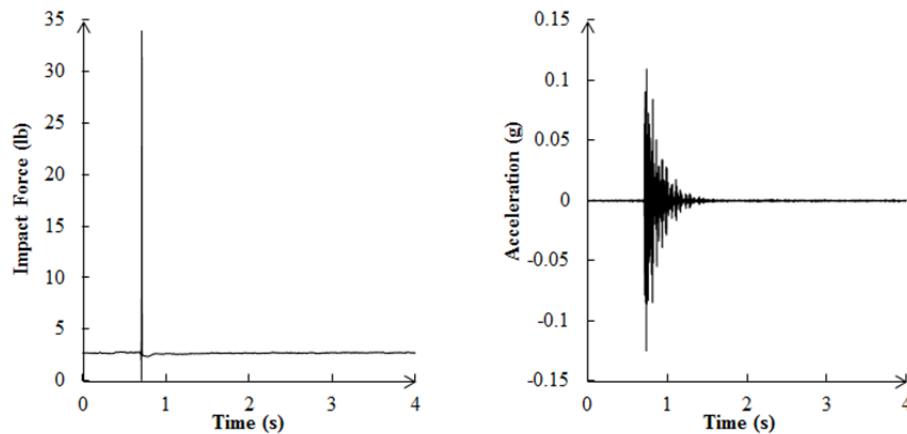


Fig.4.6. Typical response history measurements: (Left) hammer impact, (Right) vibration response.

Table 4.3 Variables of the digital signal-processing.

Parameter description	Parameter value
Data acquisition time	4.0 s

Frequency resolution	0.25 Hz
Frequency bandwidth	200 Hz
Frequency range of interest	60-200 Hz
Sampling frequency resolution	1000 Hz
Total number of samples	2048
Number of frequency lines	800
Number of averages	5
Window function	Boxcar (no window)

The frequency response functions (FRFs), which are the ratio of the output response of a structure to an applied force in the frequency domain are calculated. Assuming an accurate measurement of the excitation force, SigLab accounts for uncertainties and noise in the response signals, and thus uses an H_1 FRF estimator (Rocklin et al., 1985). As recommended by Atamturktur et al., FRFs obtained for five repeated tests are averaged to reduce the degrading effects of ambient vibrations (Atamturktur et al., 2009). Observing the coherence functions ensure the quality of the measurements as did reciprocity and linearity checks.

Reciprocity of the dome measurements is checked by comparing the response at Point 10 due to an excitation at Point 6, against the response at Point 6 due to an excitation at Point 10 (see Fig. 4.7). In reciprocity checks, the discrepancies may derive from many sources (e.g. test-to-test variability caused by the hammer excitation, accelerometer setups, ambient vibration from the environment, and testing equipment noise) (Atamturktur et al., 2009). In Fig. 4.7, over the frequency range of 0-200 Hz, the area between the two FRF curves is approximately 23% of the average area of the two FRFs. Despite this deviation, the peaks are closely adjacent with an average deviation of 3.9% for the six modes of interest. This limited variability indicates that the

modal parameter identification is minimally affected; thus the reciprocity between the two FRFs, and thus the linear behavior of the structure, is deemed acceptable.

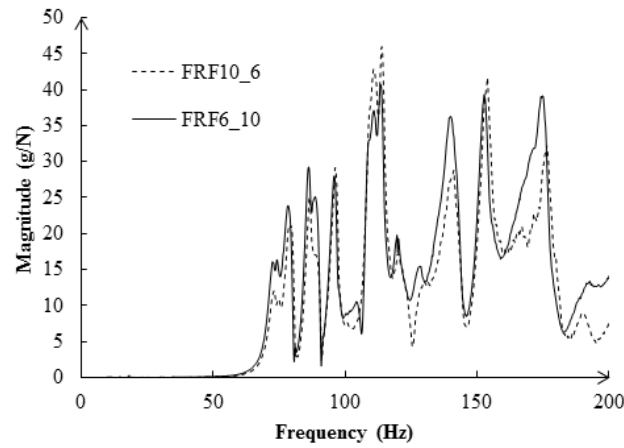


Fig. 4.7. Reciprocity check.

In theory, as a linear system should have identical FRFs at different magnitudes of hammer excitation, the linear response of the dome can also be checked by comparing the FRFs obtained at different excitation levels. Fig. 4.8 shows the linearity check through a comparison of the responses and the coherence functions of the driving point measurements¹ with two levels of excitations. Over the frequency range of 0-200 Hz, the area between the two FRF curves obtained with 27.22 kg (60 lb) and 45.36 kg (100 lb) excitations is approximately 13.00% of the average area of the two FRFs. The peaks in the FRFs are less influenced by the change in the excitation force with an average deviation of 2% in the natural frequencies.

¹ Driving point measurement indicates where one excites and measures at the same location.

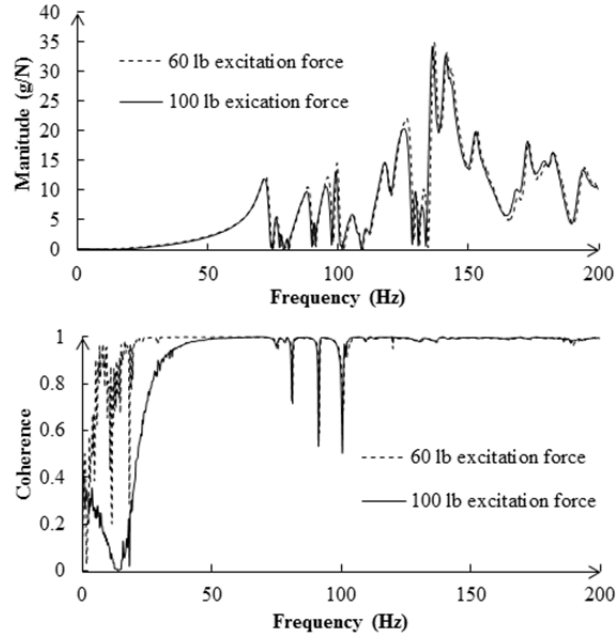


Fig. 4.8. Linearity check (Top) the driving point FRF for the crown of the dome, (Bottom) the corresponding coherence function.

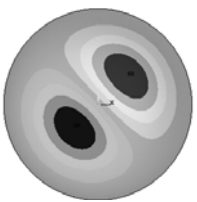



Using PULSE Reflex version 15.0.0, manufactured by B&K Company, system identification of the natural frequencies and mode shapes is conducted, the result of which are discussed in the next section.

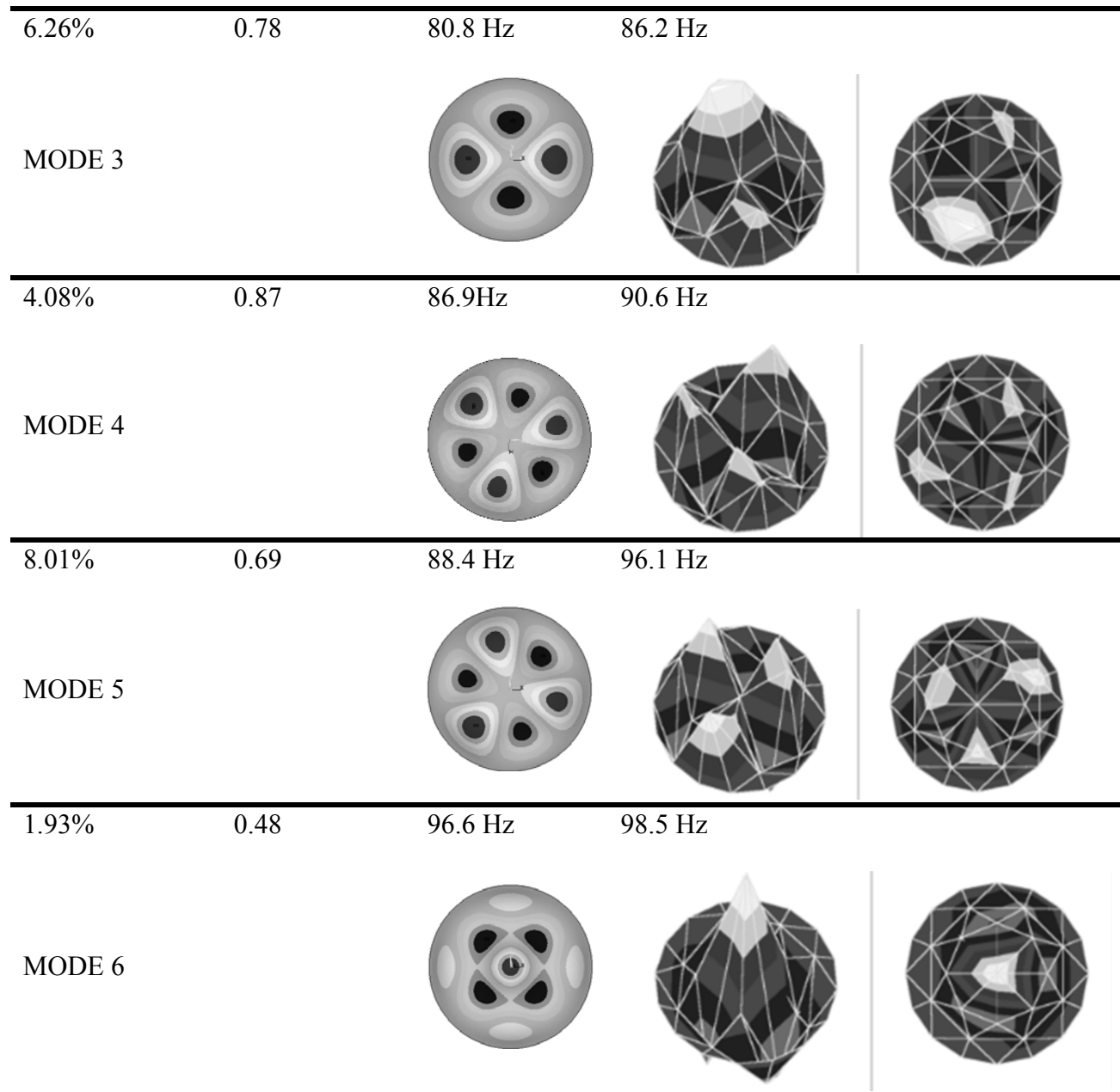
4.4.2 Test-analysis correlation

Since the FE model is used to predict the changes in the natural frequencies as a result of development and propagation of cracks, it is critical to ensure that it reproduces the natural frequencies of the actual tile dome accurately. However, while comparing measured and calculated natural frequencies, it is most important to ensure that the modes are paired in a correct sequence such that natural frequencies are correctly compared against each other, i.e., measured first bending mode is compared against the calculated first bending mode. Therefore, we first pair the measured and calculated natural frequencies according to their mode shape vectors. We verify each pair by both visually correlating the mode shapes and checking the Modal Assurance Criterion (MAC) values (see Table 4.4).

Table 4.4 presents this test-analysis correlation for the six modes of the dome, where the maximum deviation between the natural frequencies is approximately 8%. Table 4.4 also presents the visual comparison of mode shapes along with the MAC values between the measured and calculated modes with an average of 0.73. For the first four modes, the MAC values are above 0.7 indicating a sufficiently well correlated modes. The fifth and sixth modes however yield lower MAC correlations. Note that Brownjohn and Xia state that MAC statistics are imperfect indicators of modal correlation inferior to visual comparison (Brownjohn and Xia, 2000). Satisfactorily high MAC values for the first four modes and the clear visual agreement of the last two modes in combination enable us to verify the mode shape sequence.

Table 4.4 Comparison of the predicted and measured natural frequencies and corresponding mode shapes.

Frequency Disagreement	MAC Correlation	Analytical Mode Shape	Experimental Mode Shape
2.90%	0.81	74.5 Hz	72.4 Hz
MODE 1			
3.07%	0.76	80.6 Hz	78.2 Hz
MODE 2			



While obtaining the agreement presented in Table 4.4, one of the linear material property values listed in Table 4.2, the homogenized Young's modulus, E_m , is calibrated from 1.56 GPa (227000 psi) to 1.55 GPa (225000 psi).

4.5 Test analysis correlation with destructive tests: nonlinear properties of the FE model

In published literature, researchers have frequently resorted to destructive experiments to determine the load carrying capacity of masonry structures. Balaji and Sarangapani (2007) conducted a load-to-failure test on a scaled dome model built with brick and mud mortar. Deflections of the dome were measured as a function of the uniformly distributed load applied evenly on the dome and simultaneously, propagation of meridional cracks was recorded. In this study, a gradual reduction of stiffness was observed as the cracks develop. There has been a greater interest in conducting destructive experiments on masonry arches compared to domes, owing the need to assess the load carrying capacity of masonry arch bridges. Load-to-failure tests on arch bridges were completed in numerous studies (Page (1995), Boothby et al. (1995)) for field testing on in-service masonry arch bridges, (Gilbert and Melbourne, 1994) for full-scale destructive testing of an arch-bridge (Begimgil (1995), Søyland and Rosson (1995), Royles and Hendry (1991)) for destructive testing of scaled masonry arch bridge models.

Perhaps the most relevant earlier published work in the literature is Brown et al. (1995), through which a masonry arch bridge was incrementally loaded to failure in the laboratory with a vertical load at its quarter span. During this experiment, authors have conducted experimental modal analysis to observe the changes in the natural frequencies of the arch and observed a 10% reduction in the first natural frequency between the onset of damage and the formation of first hinge. As the damage in the arch bridge was further increased, progressive reduction in natural frequencies was observed. A novel “serviceability threshold criterion” to relate the load carrying capacity of the damaged arch bridge to its natural frequency was also proposed (Brown et al., 1995).

4.5.1 Experimental campaign

A load-to-failure test is conducted on the masonry tile dome studied herein to evaluate both the load-displacement behavior and failure pattern under a distributed load applied at the crown (see the test setup in Fig. 4.9). A vertical 5.338 N (1200 lb) load is gradually applied within a radius of 30.48 cm (12 in) around the crown of the dome. The applied load and the deflection of the dome are measured until the dome reached collapse.

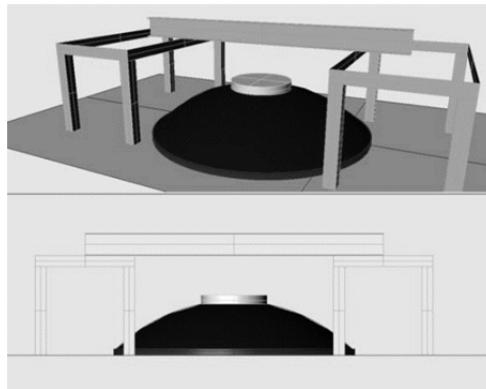


Fig. 4.9. Experimental setup for the destructive testing (Ramage (2006), with permission).

4.5.2 Test-analysis correlation

During the load-to-failure evaluation, the structure enters into the nonlinear range and therefore, the available destructive test data can be used to calibrate the nonlinear material properties entered into the FE model. Consistent with the experimental campaign, a 5.338 N (1200 lbf) vertical force is applied over a circular region with a 30.48 cm (12 in) radius at the top of the FE model. The comparison of the calculations with measurements given in Fig. 10 yields a good agreement, where the difference between the average stiffness is approximately 2.9% within the elastic range. The stiffness is calculated from measurements, as the average of 201 experimental data points and from calculations, according to the ultimate load carrying capacity and the corresponding displacement as shown in Fig. 4.10. The mean value of the maximum load

during the experiment is approximately as 3.98 kN (895.66 lbf), while the FE model has a load-carrying capacity of 3.96 kN (889.32 lbf), which yields a difference of 0.71%. To obtain such agreement as presented in Fig. 10, the ultimate uniaxial tensile strength, f_r , is fine-tuned and is reduced from 0.16 MPa to 0.14 MPa.

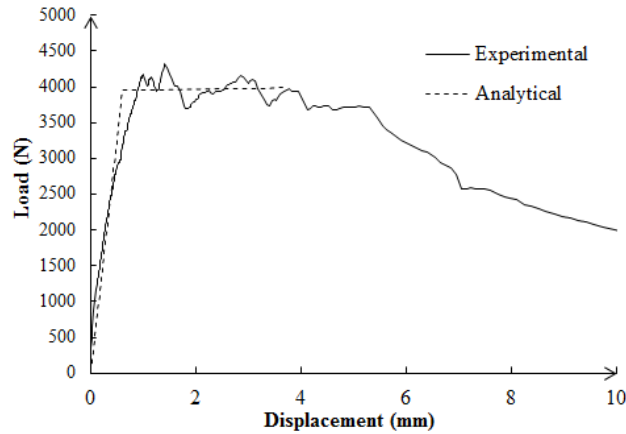


Fig. 4.10. Test and simulation correlation.

4.6 Simulation of damage via experimentally informed FE models

4.6.1 Crack patterns and modeling

A common feature of unreinforced masonry domes is that under vertical loads the lower portion of the dome tends to spread outward. The resulting hoop tension then causes longitudinal cracks at the base, ultimately resulting in the separation of the dome into a series of arches with the top portion acting as a common key stone (see Fig. 4.11 top) (Heyman (1995), Fraternali (2010)). Such behavior, which has been observed in many historic domes, was the primary motivation for the invention of the tension ring placed at the base of domes, see for instance the dome of Hagia Sophia where continuous iron clamps were used between bricks to resist the hoop forces (Mainstone, 2001). For domes with tension rings, although a similar crack pattern may be

observed, the cracks do not reach the base of the dome since the tension ring prevents opening of the cracks (Fig. 4.11 bottom).

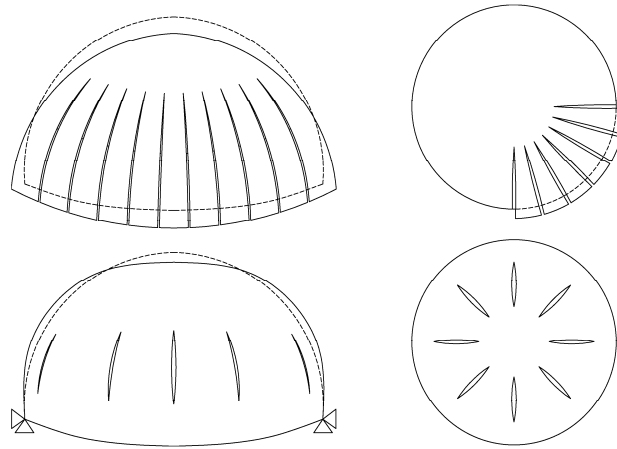


Fig. 4.11. (Top) Spherical masonry domes without hoop tension carrying mechanism: aerial and plan view of cracks (reproduced with permission, (Heyman, 1995)); (Bottom) Spherical masonry domes with a tension ring: aerial and plan view of cracks.

Although a dome may remain stable after the occurrence of cracks, owing to the inherent ductility of masonry construction (Abrams, 1992), the propagation of such cracks clearly degrades the strength of the dome. These cracks can threaten the structural integrity if they become too extensive, as with the unforeseen collapse of the domes of the Noto Cathedral in (Tringali et al., 2001). It is precisely this degradation in strength after the onset of damage (in this particular study, after the development of cracks) that must be determined for appropriate management and maintenance of masonry structures.

4.6.2 FE analysis of the crack distribution

To simulate a scenario in which cracks develop in the masonry tile dome due to overloading, the load applied at the crown of the dome is gradually increased. As the load

increases, the middle part of the dome bulges outward, thus resulting in hoop tension around the circumference of the dome. Fig. 4.12 shows the distribution of the first principal stress of the dome under the static load. The shaded area indicates regions where tensile stress levels exceed the tensile strength of the material, which initiates the crack formation. This simulation supplies a series of symmetrically distributed crack locations that are further discussed in Section 4.6.3.

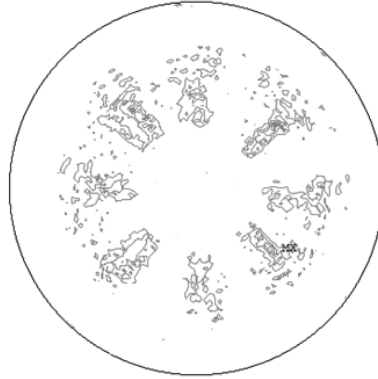


Fig. 4.12. 1st principal stress distribution above the tensile stress capacity (>0.14 MPa (20 psi)).

4.6.3 FE modeling of the damaged dome

For modeling cracks in FE analysis, two distinct methods are adopted: discrete crack models and smeared crack models. A smeared crack model is a suitable representation when an abundance of minor cracks are distributed across the structure, while discrete crack modeling is suitable to represent the actual discontinuity in the deformations if the problem only involves a few dominant cracks where the cracks are isolated and significant in size (Ngo and Scordelis, 1967).

Discrete crack modeling changes either the geometry or the mesh topology of the model to create a gap (or void) in the model that represents the crack (Fig. 4.13). Herein, initial four major cracks that represent the damage state of the dome are modeled by introducing a mesh discontinuity. However, during the nonlinear, load-to-failure analysis, as the applied loads are

gradually increased, minor, distributed cracks emerge, which are represented by the inherent smeared cracking capability of the SOLID65 elements readily available in ANSYS v.12.

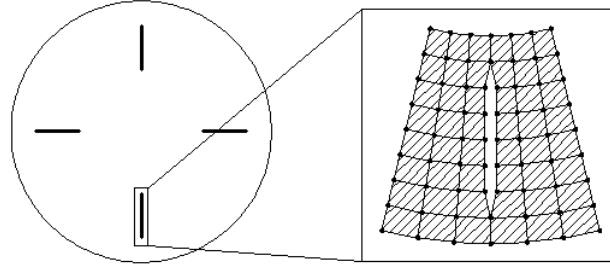


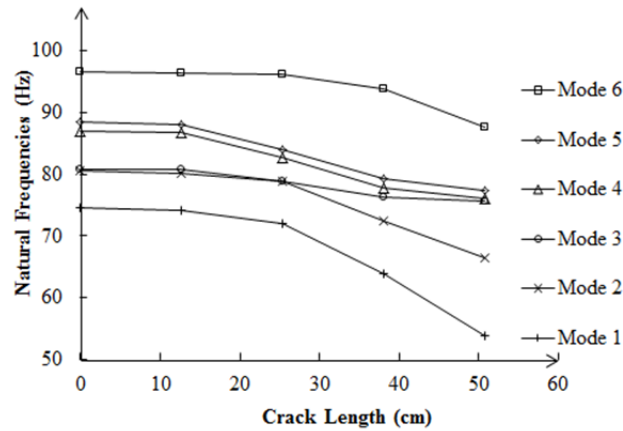
Fig. 4.13. Cracks introduced in the FE model.

When the mesh topology is being modified to introduce the meridional cracks into the FE model, it is important to automate the process in such a way that the mesh is kept identical for each model to avoid numerical uncertainties interfering in the comparisons. For increasing lengths of cracks from zero to 50.8 cm, the FE model is executed to predict the natural frequencies (see Table 4.5 and Fig. 4.14) and the load carrying capacity (see Table 4.6 and Fig. 4.15) to study the changes in the response of the increasingly damaged dome models.

The reductions in the natural frequencies due to the increasing levels of initial damage are presented in Fig. 4.14. Herein, the emphasis is on the same six modes presented earlier in Section 4.4.2 (recall Table 4.4). Fig. 4.14 illustrates that the decrease in natural frequencies caused by the progression of cracks is more evident for the first mode. This observation is also confirmed for cracks distributed in an unsymmetrical manner where the first mode is consistently observed to be the most sensitive mode to crack development.

Table 4.5 Modal analysis solutions, natural frequencies (Hz).

Health State	Mode 1	Mode 2	Mode 3	Mode 4	Mode 5	Mode 6
No Cracks (Healthy)	74.47	80.61	80.76	86.93	88.383	96.62
12.7 cm (5 in) Cracks (4 each)	74.15	80.20	80.68	86.66	88.11	96.32
25.4 cm (10 in) Cracks (4 each)	72.01	78.92	78.93	82.58	84.039	96.14
38.1 cm (15 in) Cracks (4 each)	63.88	72.40	76.23	77.82	79.277	93.77
50.8 cm (20 in) Cracks (4 each)	53.86	66.36	75.53	75.96	77.418	87.48

**Fig. 4.14.** Natural frequencies of the five health conditions.

Using the FE models developed with cracks of increasing length, static analysis is conducted as discussed in Section 4.5.2 with a distributed load applied at the crown. FE model is used to calculate the reduction in the load carrying capacity of the dome that is increasingly damaged with cracks. A comparison between the load-carrying capacities of the damaged and undamaged domes is plotted in Fig. 4.15.

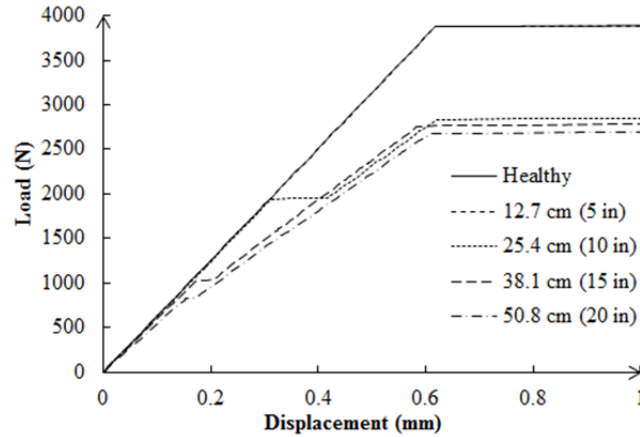


Fig. 4.15. Comparison of load-carrying capacity of damaged and undamaged models.

To evaluate the influence of the damage on the structural strength of the dome, ultimate load-carrying capacity, displacement at the ultimate load and stiffness are extracted from the load vs. displacement diagrams (Table 4.6). Ultimate load carrying capacity is determined by the yielding point, beyond which the dome further displaces without an increase in load. The stiffness is calculated as the slope of an imaginary line between the origin and this yielding point where ultimate load carrying capacity is reached. Table 6 shows that a 12.7 cm (5 in) crack has little influence on the load-carrying capacity and stiffness of the dome and causes only a 0.15% reduction in load carrying capacity and a 0.36% reduction in stiffness. After the length of the crack increases from 12.7 cm (5 in) to 25.4 cm (10 in), however, a clear drop in both the load-carrying capacity and stiffness of the structure becomes evident where the load carrying capacity is reduced by 26.4% and stiffness is reduced by 26.6%.

Table 4.6 Comparison of the simulated mechanical behavior of the dome.

Health State	Healthy	12.7 cm (5 in)	25.4 cm (10 in)	38.1 cm (15 in)	50.8 cm (20 in)
Capacity (N)	3960.16	3954.40	2913.21	2834.26	2750.42
Ultimate displacement (mm)	0.62	0.62	0.62	0.62	0.63
Stiffness (kN/m)	6397.15	6373.94	4690.48	4554.49	4365.74

4.6.4 Formalizing a semi-empirical relationship

Due to the unavoidable limitations in computational resources, the relationship between reduction in the first natural frequency and the load carrying capacity is simulated only at a limited number of discrete crack lengths. However, it is of interest to estimate this relationship for all levels of crack severity including the crack lengths for which simulations are not obtained. This relationship should of course be defined conservatively, meaning that the reduction in the load carrying capacity must not be underestimated.

The semi-empirical relationship trained using solely the data presented in Fig. 4.14 and 4.15 would of course be only valid for the tile dome studied herein, since such semi-empirical relationship is expected to vary depending on the material properties, boundary conditions and geometric characteristics. However, by incorporating material properties and geometric characteristics in the training process, this relationship can be made more generally applicable. To demonstrate the concept, here we study the spherical domes with varying span-to-rise ratios; however future study must be conducted to incorporate different material properties and boundary conditions.

Many mathematical functions can be implemented to define this relationship; preference of one over the other can be determined by the errors associated with the fit as well as the robustness of the fit. As stated by the Weierstrass' approximation theorem, any real-valued continuous function are approximated on a closed and bounded interval by polynomials given in a generic form in Eq. 3, to any desirable degree of accuracy by increasing the polynomial order, (Atkinson and Han (2009), Mastroianni and Milovanovic (2008)).

$$\phi = a_1 + \sum_{j=2}^p a_j \beta^j \quad (3)$$

Eq.3 presents a power function in which power of β can take any real value. In polynomials, these powers are non-negative integers.

$$\phi = a_1 + a_2 \beta^\alpha + a_3 \beta^{(\alpha+1)} + a_4 \beta^{(\alpha+2)} + a_5 \beta^{(\alpha+3)} \quad (4)$$

where ϕ is the reduction in load carrying capacity (a quantity that is hard to measure), β is the reduction in the natural frequency (a quantity that is convenient to measure), α is the height-to-span ratio. Recognizing that $\alpha > 0$ and $\beta > 0$, and enforcing $a > 0$ the polynomial given in Eq. (4) will be monotonic and strictly increasing in nature and therefore suitable for our application as higher reduction in natural frequencies should indicate a higher degradation in load carrying capacity.

To train an emulator representing the semi-empirical relationship, we seek for the coefficients a of the Eq.4. In doing so, we minimize the objective function defined as sum of the square of the differences between the emulator and available simulation data points as shown in the following optimization problem:

$$\begin{aligned} Obj(a_1, a_2, \dots, a_5) = & \sum_{j=1}^N ([a_1 + a_2 \beta_j^{\alpha_j} + a_3 \beta_j^{(\alpha_j+1)} + a_4 \beta_j^{(\alpha_j+2)} + a_5 \beta_j^{(\alpha_j+3)}] - \phi_j)^2 \\ & [a_1 + a_2 \beta_j^{\alpha_j} + a_3 \beta_j^{(\alpha_j+1)} + a_4 \beta_j^{(\alpha_j+2)} + a_5 \beta_j^{(\alpha_j+3)}] \geq \phi_j \quad j=1, \dots, N \quad \text{Constraints} \end{aligned} \quad (5)$$

where Obj is the objective function, a_1, a_2, \dots, a_5 are coefficients of the power function that are considered as optimization variables and N is the number of available simulation data points. Additional constraints are assigned to assure that the load carrying capacity reduction in the emulator is always higher than the simulated results such that the emulator is a conservative, upper-bound. We used MATLAB's *fminsearch* function for the optimization problem (Lagarias et al, 1998). For the dome studied herein, the coefficients are obtained to be $\alpha_1=3.78$, $\alpha_2=18.98$, $\alpha_3=6.45$, $\alpha_4=1.47$ and $\alpha_5=3.46$. The power function obtained with these coefficients supply a conservative, upper bound as depicted in Figure 16 (left).

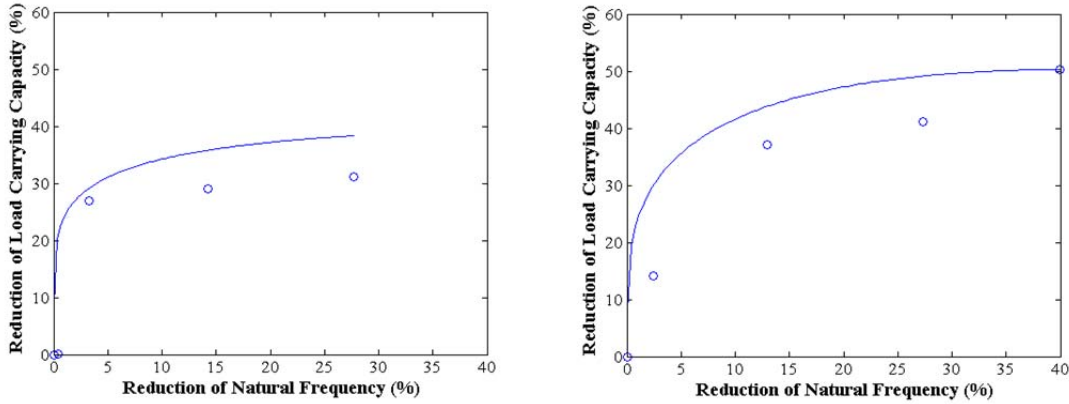


Fig. 4.16. (Left) Span-to-height ratio of 0.21; (Right) Span-to-height ratio of 0.35 representing the dome studied herein.

Fig. 4.17 demonstrates the three-dimensional plots of the functional relationship defined in Eq. (3) for domes of same thickness but with height-to-span ratios varying from 0.15 to 0.50. This functional form, given in Eq. (3) and demonstrated in Fig. 4.17 can be improved by increasing the number of simulation runs and can be made more generally applicable by considering the different thicknesses, boundary conditions and materials that can be used for masonry domes.

Therefore, the semi-empirical relationship presented herein should be considered to be for demonstration purposes only.

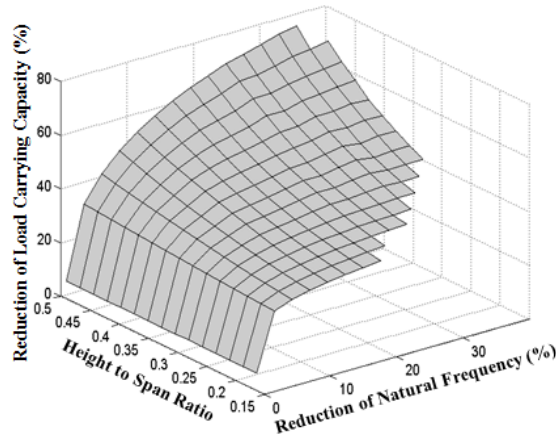


Fig. 4.17. The semi-empirical formulation.

4.7 Conclusions

Damage to a structural system causes degradation in not only the strength but also the stiffness of the structure. The degradation in strength manifests itself as reduced load carrying capacity; while degradation in stiffness influences the increased deformations. For instance, a damaged structure becomes less stiff compared to its healthy counterpart, and thus deforms more under the same loading condition. Similarly, a damaged structure can be expected to have lower natural frequencies compared to its healthy counterpart.

Measuring the reduction in load carrying capacity due to the presence of damage requires some form of destructive testing and thus in practical applications is not feasible. However, the vibration characteristics, which are also sensitive to the presence of damage, can be conveniently measured in a non-intrusive and non-invasive manner from an existing structure. If this indirect relationship between the reduction in load carrying capacity and changes in the vibration response can be determined for a structure, then by monitoring the vibration characteristics,

infrastructure managers can determine the remaining strength. Accordingly, the infrastructures can prescribe timely and efficient maintenance and rehabilitation campaigns preventing potentially unforeseen catastrophic failures of historic masonry monuments.

In this manuscript first, considerable efforts are made to develop a FE model that is a sufficiently accurate representation of both the vibration characteristics (i.e. natural frequencies) and the load carrying capacity of a scaled laboratory dome built with AAC tile and plaster of Paris. For these purposes, natural frequencies measured during nondestructive tests and load-displacement curves obtained during destructive tests are used to fine-tune the imprecise material properties of the FE model. The first natural frequency of the dome is determined to be the most sensitive mode to crack propagation. Next, the calibrated FE model is used to predict the reduction in the load carrying capacity and in the first natural frequency of the dome as the dome is progressively damaged. The simulated damage pattern is in the form of four, symmetrically distributed discrete cracks. The damage severity is gradually varied from no cracks to four 50.8 cm (20 in) cracks.

The obtained simulation based results are used to train an emulator representing a conservative upper bound for the indirect relationship between the changes in vibration response and the reduction in load carrying capacity. This semi-empirical relationship is of course only valid for the tile dome studied herein and would vary depending on the material properties, geometric characteristics and type of the damage. In an attempt to make the obtained empirical relationship more generally-applicable, the relationship between strength and stiffness is studied for domes with varying span-to-rise ratios. An emulator is trained that contains a variable for the span-to-rise ratios and the plotted for various geometric configurations. Future studies must

however follow to seek for generally applicable trends and relationships for varying material properties and damage types as well.

In this study, the first mode frequency exhibited the greatest sensitivity to the development of cracks and therefore used as the basis for the development of the aforementioned empirical relationship. However, even for domes with similar geometric properties, the most sensitive mode may vary depending on the cause and type of damage, i.e. differential support settlements may cause a different damage scenario than a distributed load on the crown to which a mode other than the first mode might be more sensitive. One approach to ensuring sensitivity to a wide range of damage scenarios that the domes studied herein may experience is to develop the empirical relationship considering all six modes as proposed (Prabhu and Atamturktur, 2011), where assimilation techniques are utilized to increase the sensitivity to damage.

This manuscript introduces a novel concept that can ultimately be applied to a wide range of structures. Of course, such empirical relationship between strength and stiffness will need to be defined for various structure types in future applications. When successfully developed and validated, such empirical relationship has the potential to improve the serviceability assessment of existing structures.

CHAPTER FIVE

LONG TERM MONITORING OF HISTORIC MASONRY MONUMENTS: DEVELOPMENT AND DEPLOYMENT OF WIRELESS SENSOR NETWORK

5.1 Introduction

Vibration based structural health monitoring (SHM) is widely applied for non-destructive assessment of civil infrastructure systems including historic monuments. The applications of SHM range from short-term deployment for condition assessment after an extreme event, such as an earthquake, to long-term deployment for the assessment of gradual structural degradation. The advantage of long-term deployment is twofold in that it serves to monitor gradual incremental degradation as well as to instantly assess the structural condition after an event such as an earthquake or a hurricane.

The foremost goal of SHM is *human safety*. By providing early warning of damage, SHM can prevent sudden catastrophic failures. A potential advantage of SHM is the ability to detect damage that can be missed during a routine visual inspection especially when the damage or its extent is not manifested on the exterior. Another benefit of deploying a long-term SHM system is that SHM can detect anomalies that occur in between routine visual inspections. In addition, the visual inspections tend to be subjective in that the results may vary drastically between inspectors. SHM provides a means for effectively evaluating the condition of the structure without objective interpretation of the inspectors.

The governing theory behind vibration-based SHM is that modifications to a structure, in the form of damage or retrofit, cause changes in the structure's stiffness, mass and damping, which in turn modifies the vibration characteristics of the structure. In SHM applications, typically a network of sensors is deployed on the structure that monitors the structural vibrations in terms of

displacement, velocity or acceleration. The high-dimensional raw time-series data from the sensors are then post-processed to yield low-dimensional features that are indicative to onset and development of damage. Traditional SHM campaigns have consisted of wired systems to allow for the sensors to communicate with the data-acquisition system. However, the coaxial cables used not only require expensive and labor-intensive installation, but also pose problems in term of maintenance (Lynch and Loh 2008; Kottapalli et al. 2003). In recent years, wireless sensor systems have gained the attention of the SHM community due to their relatively inexpensive cost of installation and autonomous operation, which can minimize the need for human interference. Recent studies have investigated the use of wireless sensors for such systems as civil infrastructure (Lynch 2006), aircrafts (Gause et al. 1999), and offshore structures (Li et al. 2003; Ou and Li 2003).

Developing a wireless sensor network and data pipe requires a close integration of expertise from computing science and civil engineering. Specifically, platform developers must balance the needs of the vibration data processing algorithms with the energy constraints of the system, the limitations of radio propagation, and inherent hardware restrictions. In this report, the authors present the development and deployment of a wireless sensor network designed to monitor ambient vibrations in a casement of historic Fort Sumter, an unreinforced masonry coastal fortification.

This document begins with a brief overview of Fort Sumter National Monument in Section 2 followed by a literature review of wireless sensor networks in Section 3. Section 4 discusses the wireless sensor system developed by the Clemson research team and further details regarding how the system remotely transfers data and performs online monitoring is presented in Section 5.

Next, Section 6 investigates the use of wireless sensors by comparing their measurements with wired sensors. Finally, concluding remarks are provided in Section 7.

5.2 Fort Sumter National Monument

Fort Sumter is a pre-Civil War Era sea fort located in Charleston Harbor, South Carolina. This historic monument is best known for the Battle of Fort Sumter, the event which began the American Civil War in 1861. The fort is a five-sided masonry structure built on a man-made sand-bar. 119 years after the initial construction of the fort began Fort Sumter was declared a national monument (National Park Service 1984). For more information regarding Fort Sumter, the reader is invited to visit Section 3.4.1.

5.3 Background

Typical wireless sensor networks consist of a sensing interface, a computational core, wireless receivers and occasionally an actuation interface (Lynch and Loh 2008). The sensing interface is responsible for collecting measurement data while the computational core stores, processes, and prepares the data for analysis. The wireless receiver is arguably one of the most important aspects of the wireless sensor network, as it not only enables the sensors to communicate but also allows the system to remotely transfer the collected data. The actuation interface, which includes a digital-to-analog converter, controls the sensors.

The three most widely used types of wireless network topologies for SHM are (a) star, (b) peer-to-peer, and (c) two-tier. (Figure 5.1). The wireless sensor system developed at Clemson University is of a star network (Figure 5.1.a). In this configuration, the sensors are able to communicate with the base station at the central node but are unable to communicate with each other. In a peer-to-peer configuration (Figure 5.1.b), all sensors share equal responsibilities – the networking is distributed evenly in the application. For a two-tier network (Figure 5.1.b), two

different carrier frequencies are present – one for short range, low data rate and a second for far range, high data rate.

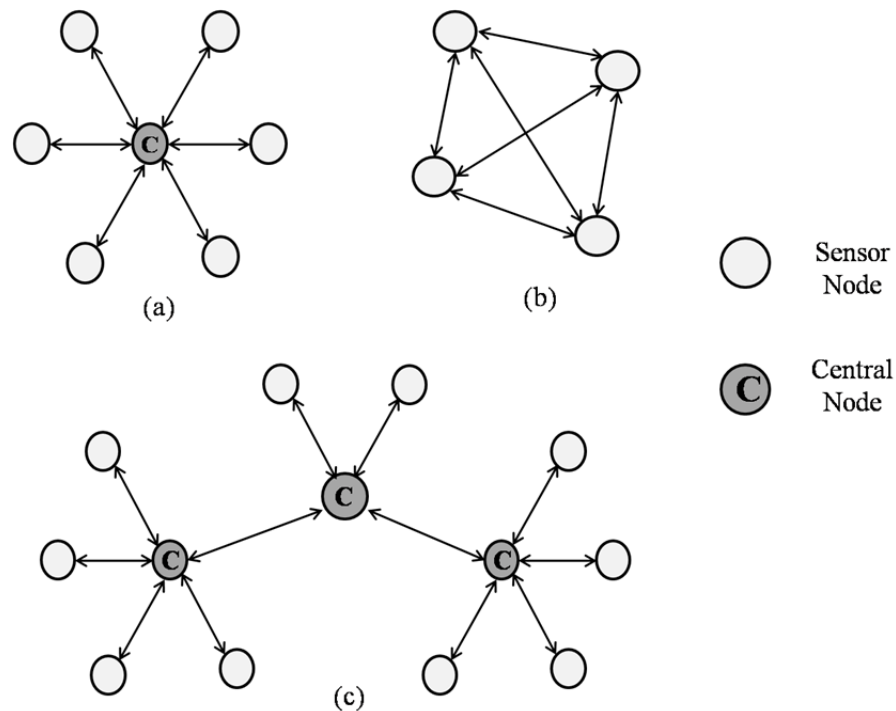


Fig. 5.1. Wireless network topologies

One main concern for wireless sensing networks is power consumption. Most remote sensing units are powered by batteries and as such, are unable to effectively transmit data over long ranges for extended periods of time. Because of this limitation, researchers have investigated alternative power supplies for wireless sensors including solar power and battery-free radio-frequency identification (RFID) sensors with promising results (Lynch and Loh 2008).

5.4 Wireless Sensor System

As a first step toward lower cost, long-term monitoring of historic masonry structures, the project team has developed a network of wireless vibration sensors for use at Fort Sumter National Monument.

5.4.1 System Configuration

The network consists of two different types of devices:

1) Vibration sensors that measure the magnitude of the attached masonry structure's accelerations,

2) A base station that receives gathered measurements and delivers the data, over the Internet, to a server on Clemson University's campus, where it is made available for analysis.

The following paragraphs describe the design of the hardware and software components of these devices.

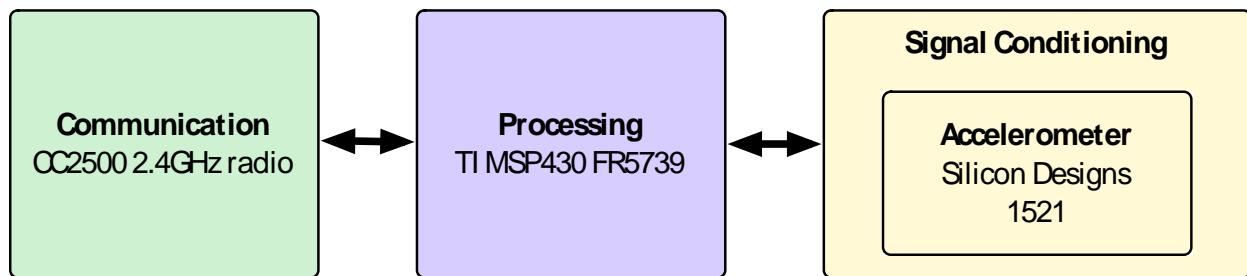


Fig. 5.2. Key components of the wireless sensor nodes

The vibration sensors consist of three core components, shown in Figure 5.2. The processing core—based on the ultra-low power MSP430 processors provided by Texas Instruments—serves as the central processor, which manages both the gathering and delivery of acceleration data. Data is sampled using a sensing board that consists of a Silicon Designs model 1521 accelerometer, along with additional circuitry for signal filtering and amplification, and for converting analog measurements to digital values. Finally, data is transmitted wirelessly using a short-range low-power CC2500 2.4GHz radio (also produced by Texas Instruments). These three components are connected using a standard SPI bus.

The wireless sensors are powered from a solar panel that provides up to 6V (open circuit voltage) and 70mA (closed circuit current), and a 1.75AHr Lithium Ion rechargeable battery that allows operation to continue at night and other times when solar energy isn't prevalent.

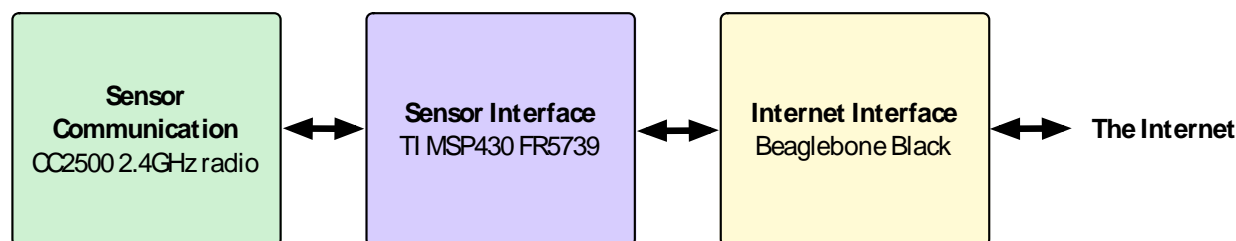


Fig. 5.3. Key functional components of the base station

The base station, as shown in Figure 5.3, shares many of the same components as the sensor nodes. Specifically, it includes the same CC2500 radio and MSP430FR5739 processor to simplify communication with the wireless sensors. A Beaglebone Black—an open source single-board computer—is used to connect the data gathered from the sensors to the Internet, over which data is delivered to our server, which is located at the following domain: ftsumter.cs.clemson.edu. The base station currently relies on wired power and a wired connection (Ethernet) to the NPS network; however, the base station could easily be made wireless, as well—requiring an additional solar panel, battery, and battery charging circuitry, and WiFi access to the NPS network. The Beaglebone Black is also configured to be accessible remotely via SSH, which allows us to reconfigure the network remotely. Appropriate system security is provided to prevent unauthorized access. Figure 5.4 shows the system.

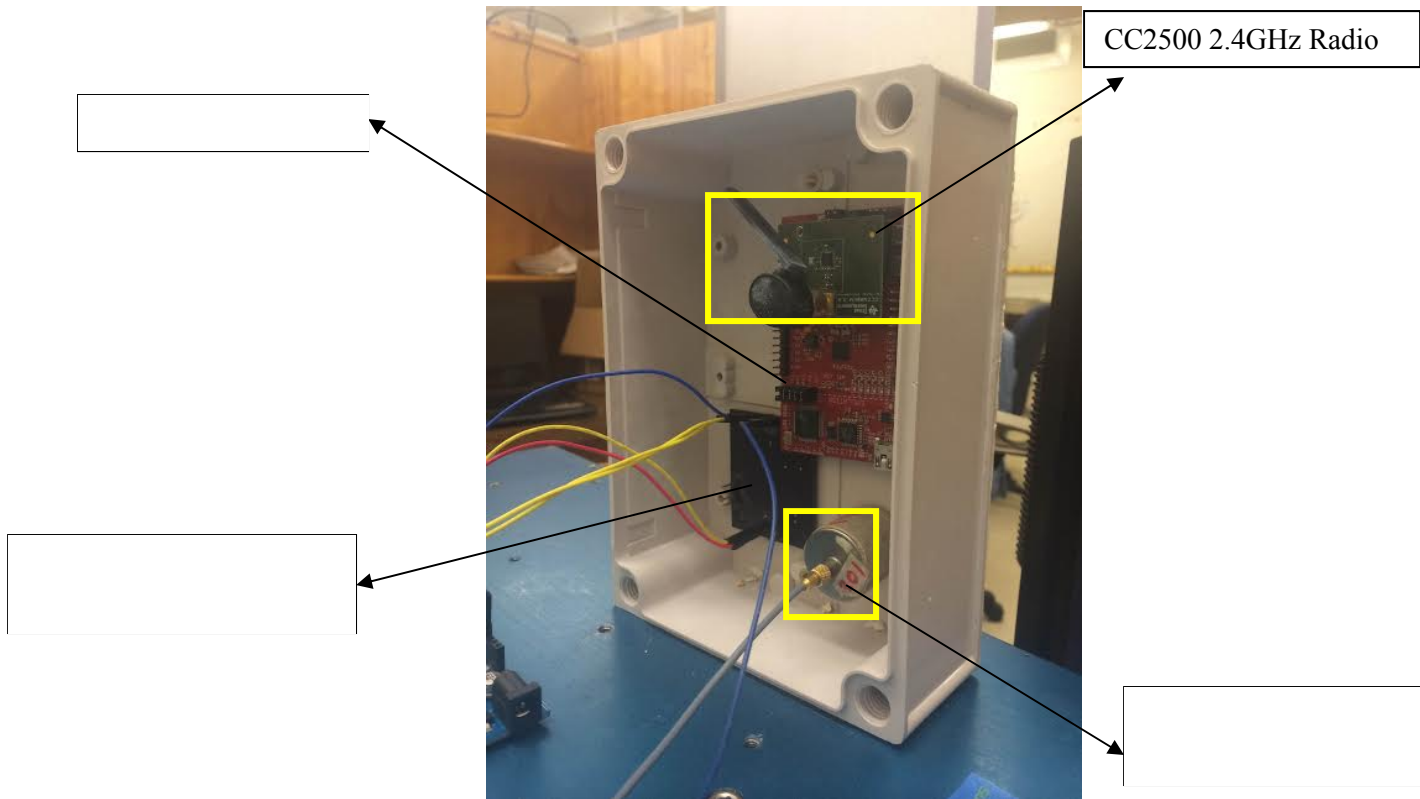


Fig. 5.4. Wireless sensor system. Note that the solar panel and Lithium Ion rechargeable batteries are not shown.

As seen in the figure, an additional part, the reference accelerometer, is shown. This device is used in laboratory testing to compare and verify the data acquired by the Silicon Design model 1521 accelerometer. Since reprogramming a wireless sensor node requires physical access, the project team designed the software to allow important parameters such as sensitivity and sampling frequency to be configured wirelessly by the base station. To reduce the complexity and improve the battery life of the wireless sensor nodes, the scheduling of data collection is controlled by the base station.

To conserve energy, the sensor nodes remain in sleep mode the majority of the time, while periodically exiting sleep mode to query the base station for new instructions and synchronization information. The sensor nodes then go back to sleep mode until they are

required (by the base station) to collect data. When the time to gather a series of sensor readings arises, the sensor nodes exit sleep mode, turn on the sensor board and accelerometer, and begin storing readings. When the sensor has gathered the requested number of readings, the sensor waits for its time slot (determined by the base station) at which time it transmits the gathered data to the base station using the CC2500 radio. The base station's algorithm determines ideal time slots for each sensor node based how much vibration data is acquired. These time slots are fine-tuned to reduce data loss due to radio interference.

5.4.2 System Validations

A validation test set-up was developed at Clemson University to investigate the reliability of the wireless sensor system. To validate the design, an experimental campaign was performed in which the wireless sensors were evaluated in comparison to wired sensors. The wired sensors were PCB seismic model 393B04. Table 5.1 gives the appropriate specifications of the sensors.

Table 5.1: Wired Sensor Specifications

Model	PCB 393B04 Seismic, miniature, ceramic flexural accelerometer
Sensitivity ($\pm 10\%$)	102 mV/(m/s ²) (1000mV/g)
Measurement Range	± 49 m/s ² pk (± 5 g pk)
Frequency Range ($\pm 5\%$)	0.06 to 450 Hz
Frequency Range (± 3 dB)	0.02 to 1700 Hz
Overload Limit (Shock)	± 300 g pk
Temperature Range	-18 to +80 °C (0 to +176 °F)

Two different tests were performed: (a) ambient testing and (b) shaker table testing. For both tests, two wired sensors and one wireless sensor were evaluated. One wired sensor was mounted to the side of the wireless sensor while the second wired sensor was mounted behind

the wireless sensor. This setup, which is shown in Figure 5.5, was to eliminate the measurement error caused by the different locations of the sensors.

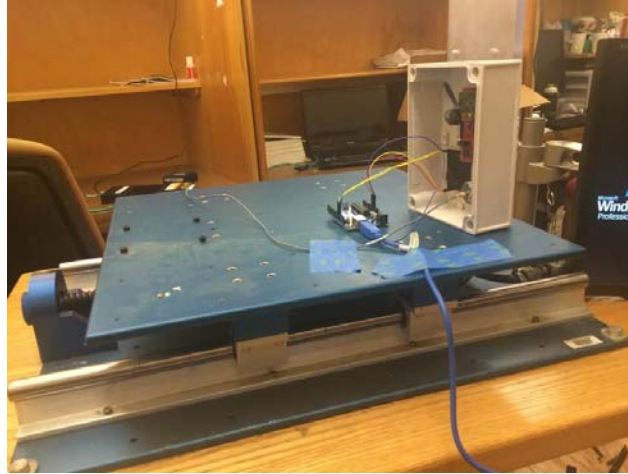


Fig. 5.5. Shaker Table Experimental Setup

For the ambient testing, data was recorded for a period of five seconds without any external excitation. Figure 5.6 shows a comparison time history plot for the two types of sensors.

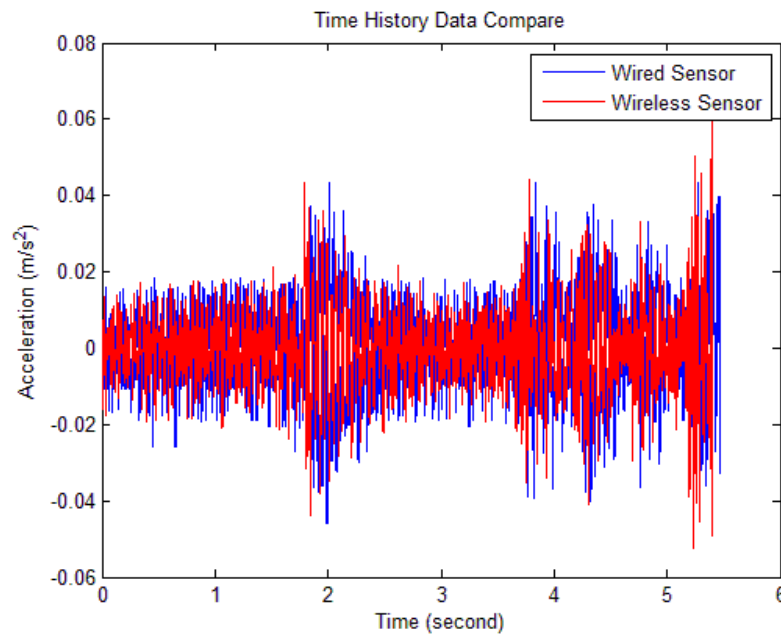


Fig. 5.6. Time History Plot for Wired (Blue) and Wireless (Red) Sensors for Ambient Testing

For the shaker table testing, a random vibration input signal was applied to the sensors for one minute and the data was recorded.

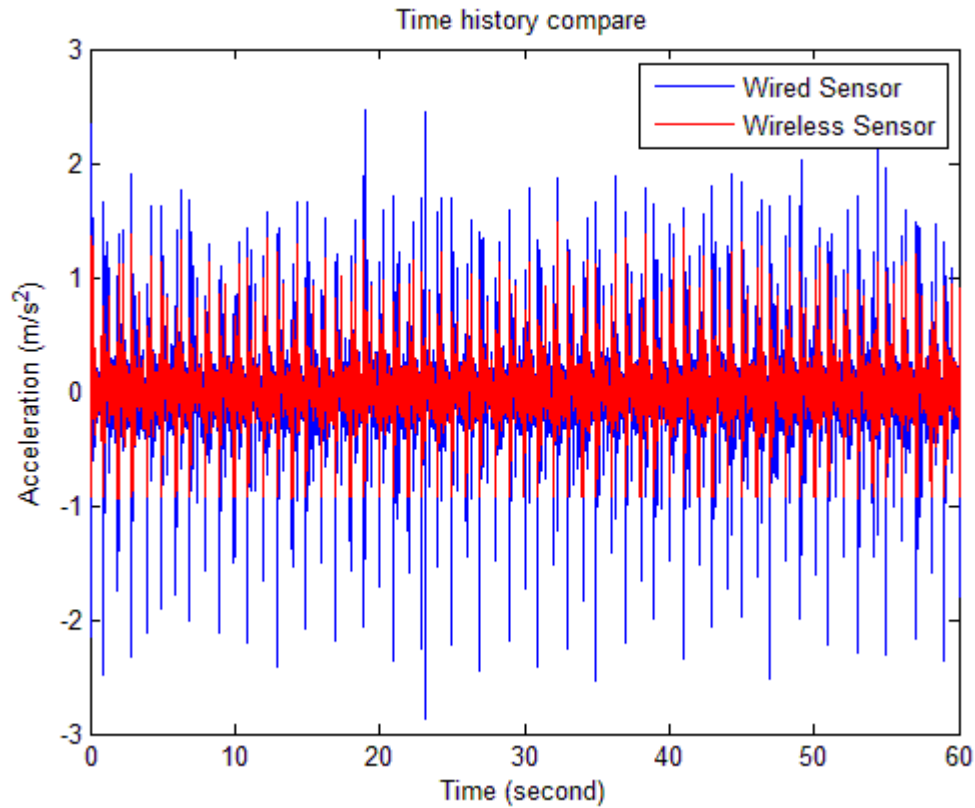


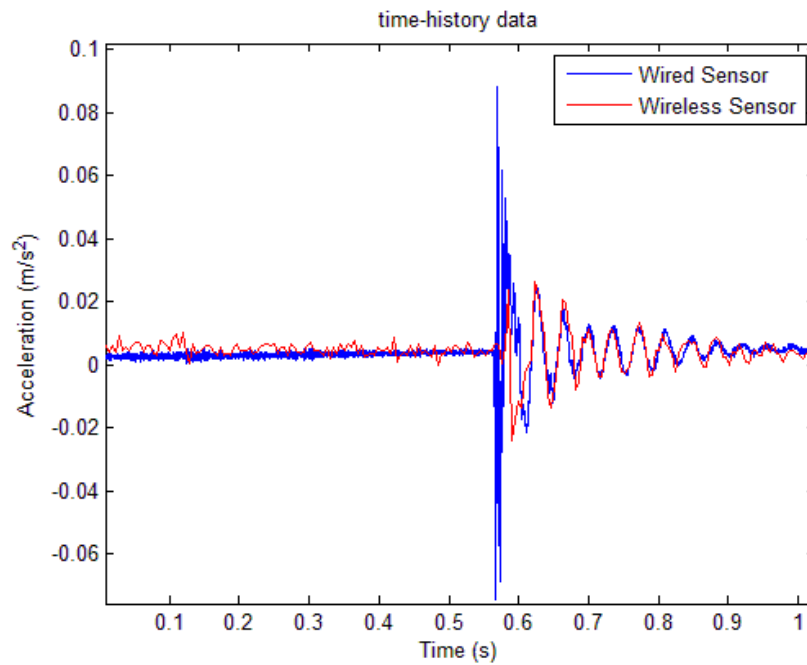
Fig. 5.7. Time History Plot for Wired (Blue) and Wireless (Red) Sensors for Shaker Table Testing

To help the reader better understand the information presented in Figure 5.7, Table 5.2 represents statistical values to show how well the sensors data agreed. As one can see the maximum acceleration for the wireless sensor does not match that of the wired sensor. It is believed that the wireless sensors have a better filter than the wired ones and therefore they smooth out the extreme values that the wired sensors are capturing.

Table 5.2. Comparison of Sensor Statistical Values

Sensor	Wireless (Red)	Wired (Blue)
Maximum Acceleration (m/s^2)	1.4806	2.8757
Mean Acceleration (m/s^2)	0.0000	0.0000
Standard Deviation	0.2218	0.2681

In addition to the shaker table testing, the ability of the wireless sensors to accurately under impact was evaluated as well. Figure 5.8 represents the findings from impact testing. As seen from the figure, the wireless sensors performed exceptionally well.

**Fig. 5.8** Time History Plot for Wired (Blue) and Wireless (Red) Sensors for Impact Testing

5.5 Remote Data Transferring and Online Monitoring

The base station runs services to maintain a persistent connection and periodically transfer data to the on-campus server. These services use tried and tested Linux utilities (Rsync,

AutoSSH) to ensure that connectivity is maintained and data is transferred reliably in the case of random network or power failures. A web service running on the campus server graphs the data and provides important information to provide a bird's eye view of overall system health. Figure 5.9 shows a sample of the website that is maintained for remote data transferring.

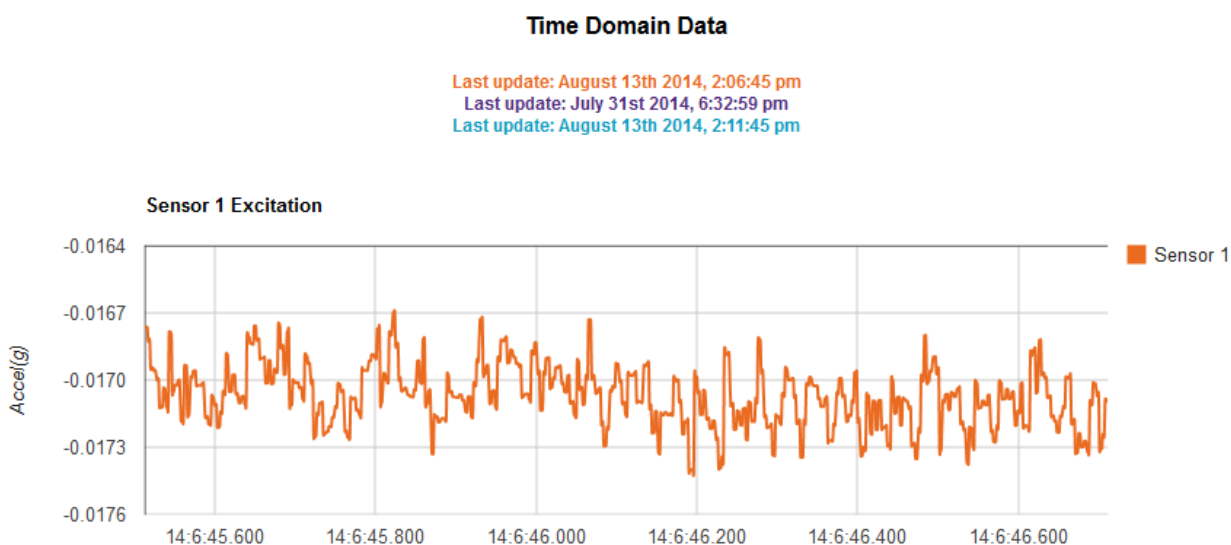


Fig. 5.9. Sample of Remote Data Transferring

5.6 Fort Sumter Measurement Data

Currently, a long term SHM system is being deployed on the Salient Angle casemates of Fort Sumter. This region is chosen because apparent settlement between the exterior wall and the arch pedestals has been reported. Also, due to the removal of the vaults on the left-face, a portion of the thrust from the right-face is believed to remain unresisted, resulting in stresses in the masonry that may be detrimental in the long-term. Severe cracking of the vaults is also observed in this region. The casemates covered under the SHM deployment are shown in Figure 5.9.

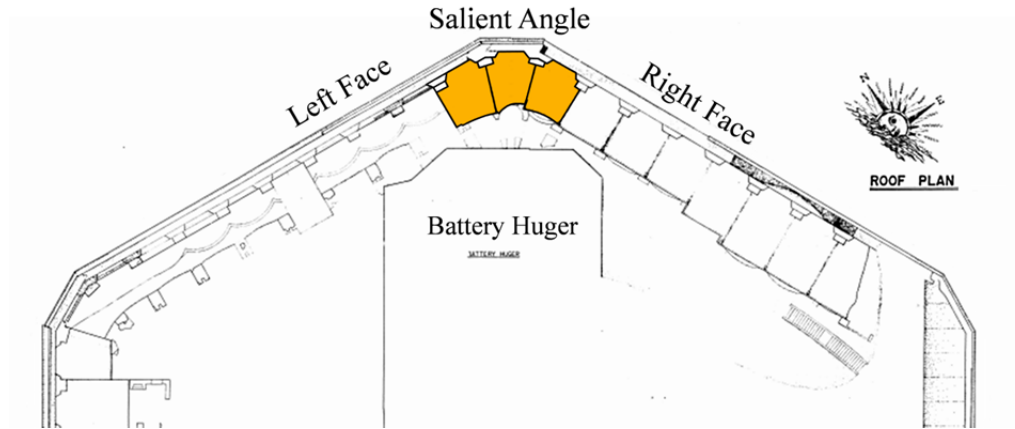
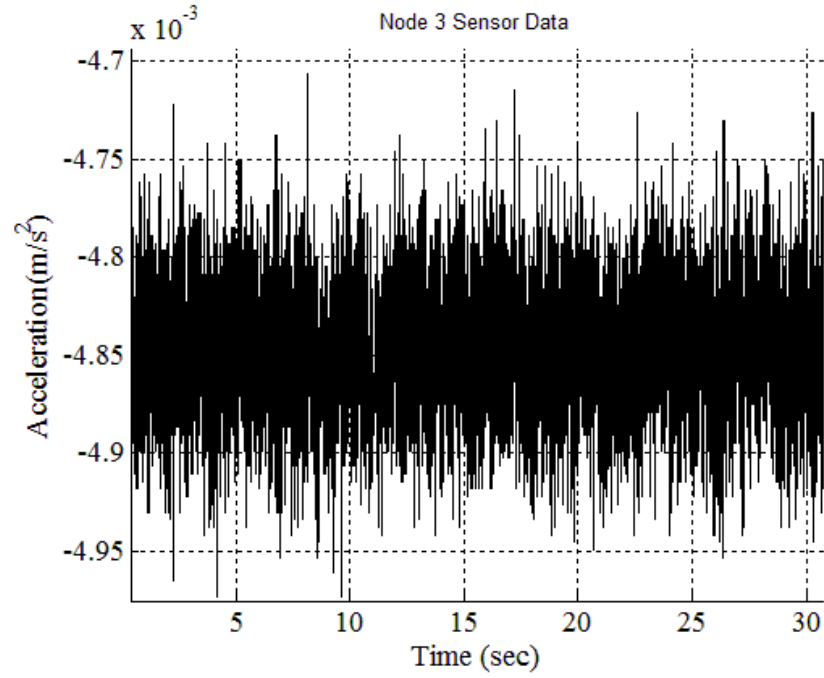


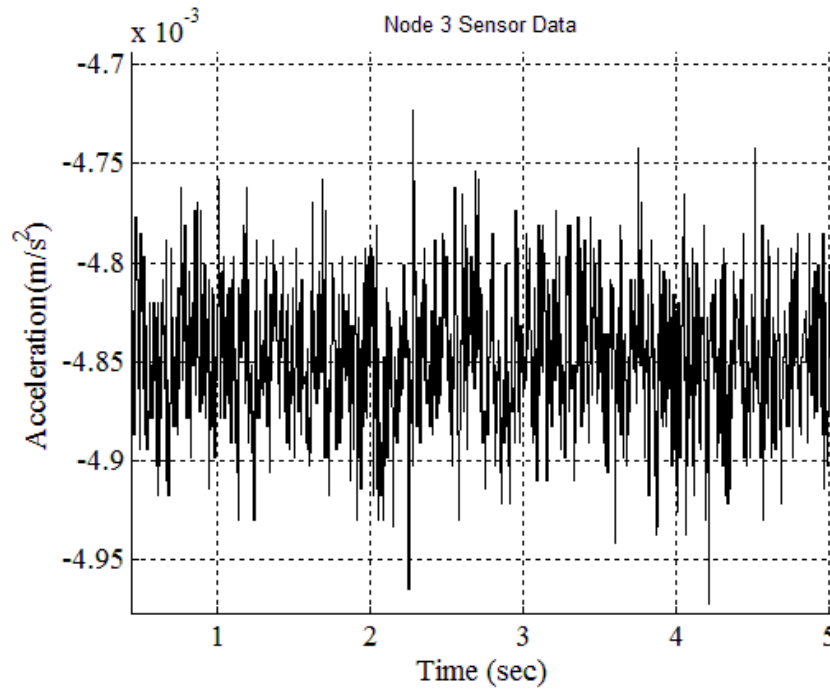
Fig 5.10. Roof plan of Fort Sumter highlighting the casemates on which the SHM system is deployed.

To preserve the aesthetics of the fort, it is important that the SHM hardware is as non-intrusive as possible to public view as well as non-obstructive for people walking through the casemates. The 3 sensors installed are out of the reach of tourists to avoid accidental damage or vandalism. Also, the hardware is protected from the elements and resistant to extreme events such as flooding. The sensors are mounted using a removable adhesive that will not harm the masonry surface in any manner. In addition, the mounting plates that go between the sensor and the masonry surface match the color of the masonry to make the system more non-intrusive to view.

To date, the 3 sensors are working well. Data that has been collected is not only remotely transferred to a real-time website, but is also stored and processed in Matlab. Figure 5.11 shows a reading from sensor 3, taken on July 31, 2014 at Fort Sumter.



(a)



(b)

Fig. 5.11. Collected Data from Sensor 3 at Fort Sumter for (a) 30 second window and (b) 5 second window

5.7 Conclusion

A long-term SHM Traditional SHM campaigns with wired cables can be expensive, time consuming, and distracting. Wireless sensor networks have quickly become an attractive solution for such problems since they have a relatively inexpensive cost of installation, are non-invasive, and allow for minimal human interference through their autonomous operation.

This manuscript investigates the use of wireless sensors in a long-term SHM deployment on Fort Sumter. The development of the wireless sensor network built at Clemson University is first described. To validate the system, initial testing was performed in the lab to compare the wireless sensors with wired sensors. After the system was confirmed to provide desirable results, the system was installed on Fort Sumter. Currently, tests are being executed on the fort to study the behavior of the structure.

The wireless sensor system developed is proving to be a valuable endeavor. The automated system of data collection and transmission requires minimal human intervention and allows for remote viewing of the collected data and extracted features over the internet. To date, this long-term SHM deployment on Fort Sumter has provided satisfactory results. Further monitoring of the coastal fort will continue to produce needed information about the condition of the structure so that preservation and rehabilitation campaigns can be successfully implemented.

CONCLUSIONS

This report has first examined the necessary considerations in applying prognostic methodologies to forecast the future health state of historic masonry monuments. An evaluation of common masonry degradation schemes and the capabilities of existing prognostic frameworks suggests that forms of degradation appropriate for prognosis of historic masonry must be gradual in nature. One example of such degradation, which is studied in this report, is settlement induced damage resulting from differential support settlement. Such foundation settlement is common in masonry structures due to the heaviness of masonry materials. Periodic inspection techniques assessing these damages, to be applicable to prognosis, must provide quantitative measurements, be as sensitive as possible to the damage of interest, and reflect the global (rather than local) behavior of the structure eliminating the need for *a priori* knowledge of damage location. To be incorporated in a monitoring process, these inspection techniques must be conducted in an automated manner. However, these *in situ* measurements are often susceptible to detecting the responses of the structure to extraneous load conditions other than the primary loads of interest, thus corrupting the measurements with noise. Therefore, the prognostic technique chosen should attempt to eliminate the effect of this noise on predictions.

A prognostic technique known as Support Vector Regression (SVR) is particularly suitable for *in situ* prognostic evaluation of masonry not only because of its ability to handle nonlinearity in measurements, but because of its ability to avoid overfitting to noise when training a prediction model. In SVR, the introduction of flatness in the prediction model decreases the model sensitivity to noise, thereby making the model more generalizable. In this report, SVR, which traditionally trains a prediction model with a predetermined constant degree of model complexity (or flatness), is enhanced to determine the optimal complexity of the model

and allow the optimal complexity to be updated over time. In contrast to existing approaches that focus on improving the fitting accuracy, the approach proposed herein calculates the optimal complexity of the model based on forecasting accuracy. The adaptive selection of optimal flatness also increases the model robustness to variations in noise levels that might occur over time. When implemented in prognostic evaluation of a historic masonry coastal fortification, Fort Sumter, the adaptively weighted approach outperformed the non-weighted approach in forecasting accuracy.

As the application of this adaptively weighted Support Vector Regression technique for prognostic evaluation of Fort Sumter is among first efforts in applying prognostics to historic masonry, future research is necessary to further the potential of such prognostic evaluations. In this report, simulated strain measurements are exploited for development of the prediction model. In the future, studies should be conducted to determine the most sensitive features to the damage type of interest for implementation in a prognostic framework. Moreover, a link between these non-destructively measured features and the remaining load carrying capacity of the structure, an aspect that can be measured only through destructive measurements, should also be identified. This link is necessary to develop a *failure threshold* defining the level of damage at which the structure reaches the end of its remaining useful life. With such information, timely maintenance campaigns can be planned. These important aspects, left out of the scope of this report, are essential for the future success of prognostic evaluation as applied to masonry construction.

With the prognostic methodologies for application to historic masonry structures matured, prognostic evaluation of the remaining structural integrity of masonry monuments and

infrastructure can be implemented in a structural health monitoring process to provide early detection of damage and enable effective maintenance strategies of such cultural heritage.

REFERENCES

- Abrams DP. Strength and behavior of unreinforced masonry elements. In: Proceedings of 10th World Conference on Earthquake Engineering; 1992 Jul 19-24; Madrid, Spain. 1992; p. 3475-80.
- Abu-Hanna, A., Lucas, P.J.F., (2001), Prognostic models in medicine, *Methods of Information in Medicine-Methodik der Information in der Medizin* 40 no.1, pp.1-5.
- Adams, D.E., Jata, K.V., (2010), Damage prognosis for metal and composite aerospace structures, *Encyclopedia of Aerospace Engineering*.
- Aguilar, R., Ramos, L.F., and Lourenco, P., “Wireless Sensor Technology for Structural Health Monitoring of Historic Masonry Structures,” *3rd International Operational Model Analysis Conference (IOMAC’09)*, Portonovo, Italy, pp.230-238, 2009.
- Aiello MA, Corvaglia P, Fortunato A, Manni O, Pedone F. Testing and modeling of the bond behavior between CFRP sheet and curved masonry substrate.
- Andreas JK, Gregory GP, Christos GD. Evaluation of simplified models for lateral load analysis of unreinforced masonry buildings. *J Struct. Eng.* 2002; 128(7): 890-7.
- ANSYS® Academic Research. Release 13.0, Help System, Mechanical APDL element reference. ANSYS, Inc; 2010.
- Anzani, A., Binda, L., Carpinteri, A., Invernizzi, S., Lacidogna, G., (2010), A multilevel approach for the damage assessment of historic masonry towers, *Journal of Cultural Heritage* 11 no.4, pp.459-470.

Anzani, A., Garavaglia, E., and Binda, L., “Long-term damage of historic masonry: a probabilistic model.” *Construction and Building Materials*, 23(2), pp.713-724, 2009.

Armstrong DM, Sibbald A, Forde MC. Integrity assessment of masonry arch bridges using the dynamic stiffness technique. *NDT&E International*. 1995;28(6):367-75.

Atamturktur S, Bornn L, Hemez F. Damage detection in masonry vaults by time-domain vibration measurements. *J. Eng. Struct.* Forthcoming 2011.

Atamturktur, S. and Sevim, B., (accepted 2011, in print), “Seismic Performance Assessment of Masonry Tile Domes through Non-linear Finite Element Analysis,” *ASCE Journal of Performance of Constructed Facilities*.

Atamturktur, S., and Boothby, T., (2010), “Calibration of Finite Element Models of Masonry Vaults”, *Journal of Masonry Society*, Vol. 28, No. 2, pp. 77-93.

Atamturktur S., and Prabhu S., “Selection of optimal sensor locations based on modified effective independence method: a case study on a gothic revival cathedral,” *Journal of Architectural Engineering*, 19(4), pp.288-301, 2012.

Atamturktur, S., and Laman, J.A., “Finite element model correlation and calibration of historic masonry monuments: a review,” *The Structural Design of Tall and Special Buildings*, 21(2), pp.96-113, 2012.

Atamturktur, S., Bornn, L., Hemez, F., (2011), Vibration characteristics of vaulted masonry monuments undergoing differential support settlement, *Journal of Engineering Structures* 33 no.9, pp. 2472–84.

Atamturktur, S., Farajpour, I., Prabhu, S., and Haydock, A., “Adaptively weighted support vector regression: prognostic application to a historic masonry coastal fortification,” *Journal of Performance in Constructed Facilities*, 2013a

Atamturktur, S., Gilligan, C., and Salyards, K., (accepted 2012, in print), “Detection of internal defects in concrete members using global vibration characteristics.” *ACI Structural Journal*.

Atamturktur, S., Hemez, F., Laman, J., (in review), “Verification and Validation Applied to Finite Element Models of Historic Masonry Monuments,” *Journal of Probabilistic Mechanics*.

Atamturktur, S., Li, T., Ramage, M., Farajpour, I., (2012), Remaining load carrying capacity assessment through vibration based health monitoring of a masonry dome, *Construction and Building Materials* 34, pp. 418–429.

Atamturktur, S., Pavic, A., Reynolds, P. and Boothby, T., (2009), “Full-Scale Modal Testing of Vaulted Gothic Churches: Lessons Learned,” *Journal of Experimental Techniques*, Vol. 33, No. 4, pp. 65-74.

Atamturktur, S., Prabhu, S., Brosnan, D., and Dorrance, R. (submitted 2013). "Foundation settlement analysis of Fort Sumter national monument: Model development and predictive assessment." *Engineering Structures*.

- Atamturktur, S., Prabhu, S., and Dorrance, R., “Structural assessment of Fort Sumter masonry coastal fortification subject to foundation settlements,” *Topics in Dynamics of Civil Structures*, 4, pp.471-483, 2013
- Atkinson K, Han W. Theoretical numerical analysis: a functional analysis framework. Third Edition, Springer-Verlag; 2009, p. 116-118.
- Avdelidis, N.P., Moropoulou, A., (2004), Applications of infrared thermography for the investigation of historic structures, *Journal of Cultural Heritage* 5 no.1, pp.119-127.
- Balaji NC, Sarangapani G. Load carrying capacity of brick masonry dome in mud mortar. In: International Symposium on Earthen Structures; 2007 Aug 22-24; Indian Institute of Science, Bangalore.
- Bayraktar A, Altrunışık AC, Sevim B, Türker T. Seismic response of a historical masonry minaret using a finite element model updated with operational modal testing. *J Vib Control*. 2011;17(1):129-49.
- Beck, J., Vanik, M., Katafigiotis, L., (1994), Determination of stiffness changes from modal parameter changes for structural health monitoring, in: *Proceedings of First World Conference on Structural Control* 2, pp. 13-22.
- Begimgil M. Behavior of restrained 1.25m span model masonry arch bridge. In: *Proceedings of the 1st International Conference on Arch Bridges*; 1995 Sept 3-6; Bolton, UK. Thomas Telford; 1995. p. 321-5.

Binda L, Baronio G, Gavarini C, De Benedictis R, Tringali S. Investigation on materials and structures for the reconstruction of the partially collapsed cathedral of Noto (Sicily). In: 6th International Conference on Structural Studies, Repairs and Maintenance of Historical Buildings; 1999; Dresden, Germany; 1999. p. 323-32.

Binda, L., Falco, M., Poggi, C., Zasso, A., Mirabella-Roberti, G., Corradi, R., and Tongini-Folli, R., "Static and dynamic studies on the Torrazzo in Cremona (Italy): the highest bell tower in Europe," *International Symposium on Bridging Large Spans (BLS) from Antiquity to the Present*, Istanbul, Turkey, 2000.

Binda L, Gatti G, Mangano G, Poggi C, Landriani GS. Collapse of the civic tower of Pavia: A survey of the materials and structure. *Masonry Int.* 1992;6(1):11-20.

Binda, L., Saisi, A., (2009), Application of NDTs to the diagnosis of historic structures, NDTCE, 06-03.

Boothby T, Domalik D, Dalal V. Assessment of masonry arch bridges by service load testing. In: Proceedings of the 1st International Conference on Arch Bridges; 1995 Sept 3-6; Bolton, UK. Thomas Telford; 1995. p. 345-54.

Bosiljkov, V., Uranjek, M., Žarnić, R., Bokan-Bosiljkov, V., (2010), An integrated diagnostic approach for the assessment of historic masonry structures, *Journal of Cultural Heritage* 11 no.3, pp. 239-49.

- Brenchich A, Gambarotta L, Ghia A, Structural models for the assessment of the masonry dome of the Basilica of S. Maria of Carignano in Genoa. In: 3rd International Seminar on Historical Constructions, Guimarães, Portugal, 2001.
- Brownjohn, J. M., De Stefano, A., Xu, Y. L., Wenzel, H., & Aktan, A. E. (2011). Vibration-based monitoring of civil infrastructure: challenges and successes. *Journal of Civil Structural Health Monitoring*, 1(3-4), 79-95.
- Brown G, Pretlove AJ, Ellick JCA, Hogg V, Choo BS, Changes in the dynamic characteristics of a masonry arch bridge subjected to monotonic loading to failure. In: Proceedings of the 1st International Conference on Arch Bridges, Bolton, UK; 1995. p. 375-83.
- Brownjohn, J.M.W., Xia, P.-Q., Dynamic assessment of curved cable-stayed bridge by model updating, *Journal of Structural Engineering* 126 (2000) (2), pp. 252–26
- Burges, C. (1998). "A tutorial on support vector machines for pattern recognition." *Data Mining and Knowledge Discovery*, 2(2), 121-67.
- Brownjohn, J.M.W., "Structural health monitoring of civil infrastructure," *Philosophical Transactions of the Royal Society: Mathematical, Physical and Engineering Sciences*, 365(1851), pp589-622, 2007.
- Burges, C.J.C., "A tutorial on support vector machines for pattern recognition," *Data Mining and Knowledge Discovery*, 2(2), pp.121-167, 1998.
- Capozucca, R., (2011), Shear behaviour of historic masonry made of clay bricks, *Open Construction and Building Technology Journal* 5 no.1-M6, pp. 89-96.

Carson, J.G., (2010), Rapid rise in US export orders supports ‘new mix’ prognosis for economic recovery, US Perspectives.

Chang, P.C., Flatau, A., and Liu, S.C., “Review paper: health monitoring of civil infrastructure,” *Structural Health Monitoring*, 2(3), pp.257-267, 2003.

Chiorino, M.A., Ceravolo, R., Spadafor, A., Fragonara, L.Z., Abbiati, G., (2011), Dynamic characterization of complex masonry structures: the sanctuary of Vicoforte, *International Journal of Architectural Heritage* 5 no.3, pp. 296-314.

Chiostrini, S., Foraboschi, P., Vignoli, A., (1992), Structural analysis and damage evaluation of existing masonry buildings by dynamic experimentation and numerical modeling, in: *Proceedings of the 10th World Conference on Earthquake Engineering*, pp. 3481-86.

Colleparidi, M., (1990), Degradation and restoration of masonry walls of historical buildings, *Materials and Structures* 23 no.2, pp.81-102.

Connelly, W., Kerr, L., Martino, A.P., Woodland, R., Secor, D., (2007), Climate and Saltwater Sport Fisheries: Prognosis for Change, Technical Report Series No. TS-537-07 of the University of Maryland Center for Environmental Science, no. UMCES CBL 07-119.

Costa AA, Penna A, Magenes G. Seismic performance of autoclaved aerated concrete (AAC) masonry: from experimental testing of the in-plane capacity of walls to building responses simulation. *J. Earthquake Eng.* 2011;15(1):4-10.

Daigle, M., Goebel, K., (2011), A model-based prognostics approach applied to pneumatic valves, *International Journal of Prognostics and Health Management* 2 no.2, pp.1-16.

- De Lautour, O.R., and Omenzetter, P., “Damage classification and estimation in experimental structures using time series analysis and pattern recognition,” *Mechanical Systems and Signal Processing*, 24(5), pp.1556-1569, 2010.
- De Stefano, A., “SHM actions on the holy shroud chapel in Torino,” *Encyclopedia of Structural Health Monitoring*, 2009.
- De Stefano, A., Clemente, P., (2006), SHM on historical heritage: robust methods to face large uncertainties, SAMCO Final Report, F11 Selected Papers.
- Deng, J., (1982), The control problems of grey systems, *Journal of Systems and Control Letters* 1 no.5, pp.288-294.
- Doebbling, S., Farrar, C. R., Prime, M. B., (1998), “A Summary Review of Vibration-Based Damage Identification Methods,” *Shock and Vibration Digest*, Vol. 30, No. 2, pp. 91-105.
- Duran, A., Robador, M. D., and Perez-Rodriguez, J.L., “Degradation of two historic building in northern Spain by formation of oxalate and sulphate-based compounds,” *International Journal of Architectural Heritage: Conservation, Analysis and Restoration*, 6(3), pp.342-358, 2010.
- El-Fouly, T.H.M., El-Saadany, E.F., Salama, M.M.A., (2006), Grey predictor for wind energy conversion systems output power prediction, *IEEE Transactions on Power Systems* 21 no.3, pp.1450-52.

- Elpek, G.O., Karaveli, S., Özgür, M.A., Saka, O., (2001), Stereologic estimation of mean nuclear volume in invasive ductal carcinoma of the breast: It's impact on prognosis, Turkish Journal of Cancer 31 no.2, pp.47-56.
- El-Tawil, K., Kadry, S., Jaoude, A., Noura, H., Ouladsine, M., (2011), Analytic prognostic for petrochemical pipelines, Journal of Mechanical Engineering Research 3, pp. 64-74.
- Ewins D.J., Ho, Y.K., (2000), "On the Structural Damage Identification with Mode Shapes," in Proceedings of the Conference held in E.T.S.I. Aeronauticos, Universidad Politecnica de Madrid, Spain, June 2000, pp. 677- 683.
- Fanning P. Nonlinear models of reinforced and post-tensioned concrete beams. Electron J Struct Eng. 2001;2:111- 9.
- Farrar, C.R., and Lieven, N.A., "Damage prognosis: the future of structural health monitoring," *Philosophical Transactions of the Royal Society A: Mathematical, Physical and Engineering Sciences*, 365, pp.623-632, 2007.
- Farrar, C.R., Worden, K., (1992), "An introduction to structural health monitoring," Phil. Trans. R. Soc., Fox, C.H.J., "The Location of Defects in Structures: A Comparison of the use of Natural Frequency and Mode Shape Data," in Proceedings of the 10th International Modal Analysis Conference, pp. 522- 528.
- Fraternali F., (2010), "A thrust network approach to the equilibrium problem of unreinforced masonry vaults via polyhedral stress functions," *Mechanics Research Communications*, 37, 198–204.

- Gantert Engineering Studio. Technical opinion about the collapse of the Bell Tower of St. Maria Magdalena in Goch, Germany. 1993.
- Gause, L. W., Krantz, D. G., Biermann, P. J., & Belk, J. H. (1999, July). Early demonstration of remotely queried microsensors. In *1999 Symposium on Smart Structures and Materials* (pp. 190-194). International Society for Optics and Photonics.
- Gentile C, Saisi A, Ambient vibration testing of historic masonry towers for structural identification and damage assessment. *Constr Build Mater.* 2007;21(6):1311-21.
- Gilbert M, Melbourne C. Rigid-block analysis of masonry structures. *The Struct. Eng.* 1994;72(21):256-61.
- Goebel, K., Saha, B., and Saxena, A., “A comparison of three data-driven techniques for prognostics.” *62nd Meeting of the Society for Machinery Failure Prevention Technology*, pp.119-131, 2008.
- Grimm, C.T., “Masonry cracks: a review of the literature,” *Masonry: Materials, Design, Construction and Maintenance*, 992, 1988.
- Grimm, C.T., “Water permeance of masonry walls: a review of the literature,” *Masonry: Materials, Properties, and Performance, ASTM STP*, pp.178-199, 1982.
- Groot, C.J.W.P., and Gunneweg, J., “Water permeance problems in single wythe masonry walls: the case of wind mills,” *Construction Building and Materials*, 18(5), pp.325-329, 2004.

- Gu, J., Azarian, M.H., Pecht, M.G., (2008), Failure prognostics of multilayer ceramic capacitors in temperature-humidity-bias conditions, in: Proceedings of IEEE International Conference on Prognostics and Health Management, pp. 1-7.
- Gu, J., Barker, D., Pecht, M., (2007), Prognostics implementation of electronics under vibration loading, *Microelectronics Reliability* 47 no.12, pp.1849-56.
- Gu, J., Pecht, M., (2008), Prognostics and health management using physics-of-failure, in: Proceedings of IEEE Reliability and Maintainability Symposium, pp. 481-487.
- Gunn, S. R. (1998). "Support Vector Machines for Classification and Regression." ISIS technical report, 14.
- Haydock, A. and Atamturktur, S. (submitted 2013). "A review on prognostic evaluation of historic masonry structures: present challenges and future direction." *Journal of Cultural Heritage*.
- Heyman J. The stone skeleton. 1st ed. New York: Cambridge University Press; 1995.
- Ignoul S, Van Gemert D. Bell Tower of Church of St. Willibrordus. NA: Triconsult; 2006. Internal Report, Report No.: D00466.
- Ignoul S, Van Gemert D. Maagdentoren at Zichem. NA: Triconsult; 2007. Internal Report, Report No.: D00394.
- Jaakkola, T. and Haussler, D. (1999). "Probabilistic kernel regression models." *Proc., 1999 Conference on AI and Statistics*, (126), pp. 0-4.

- Jardine, A.K., Lin, D., Banjevic, D., (2006), A review on machinery diagnostics and prognostics implementing condition-based maintenance, *Mechanical systems and signal processing* 20 no.7, pp.1483-1510.
- Kammer, D. C. (1991). Sensor placement for on-orbit modal identification and correlation of large space structures. *Journal of Guidance, Control, and Dynamics*, 14(2), 251-259.
- Ko, J.M., and Ni, Y.Q., “Technology developments in structural health monitoring of large-scale bridges,” *Engineering Structures*, 27(12), pp.1715-1725, 2005.
- Kotsiantis, S.B., “Supervised Machine Learning: A Review of Classification Techniques,” *Informatica*, 31, pp.249-268, 2007.
- Lagarias, J.C., J. A. Reeds, M. H. Wright, and P. E. Wright, (1998), “Convergence properties of the Nelder-Mead simplex method in low dimensions,” *SIAM Journal of Optimization*, 9(1), 112–147.
- Lall, P., Islam, N., Suhling, J., (2005), Prognostication and health monitoring of leaded and lead free electronic and MEMS packages in harsh environments, in: *Proceedings of IEEE 55th Electronic Components and Technology Conference*, pp. 1305-1313.
- Lanas, J., and Alvarez, J.I., “Masonry repair lime based mortars: factors affecting the mechanical behavior,” *Cement and Concrete Research*, 33(11), pp.1867-1876, 2003.
- Lau W. Equilibrium analysis of masonry domes. Cambridge, Massachusetts Institute of Technology, 2006. MS Thesis.

- Li, H. W., Zhou, Z., and Ou, J. P. 2003, “Offshore Platform Health Monitoring Applications of Wireless Sensor,” in Proceedings of the 21st International Modal Analysis Conference (IMAC XXI), Orlando, FL, February 3–6.
- Linh TH, Debra FL. Micro vs. macro models for predicting building damage underground movements. In: The international Conference on Computational Solid Mechanics; 2008 Nov 27-30; Hochiminh City, Vietnam, 2008.
- Lourenço PB. Computations on historic masonry structures. *Prog Struct Mater Eng*. 2002;4:301–19.
- Luo, J.H., Namburu, M., Pattipati, K., Qiao, L., Kawamoto, M., Chigusa, S., (2003), Model-based prognostic techniques, in: Proceedings of AUTOTESTCON, IEEE Systems Readiness Technology Conference, pp. 330-340.
- Lynch, J.P., “An overview of wireless structural health monitoring for civil structures,” *Philosophical Transactions of the Royal Society: Mathematical, Physical and Engineering Sciences*, 365(1851), pp.345-372, 2006.
- Lynch, J. P., & Loh, K. J. (2008). A summary review of wireless sensors and sensor networks for structural health monitoring. *Shock and Vibration Digest*, 38(2), 91-130.
- Mack, R.C., and Grimmer, A., “Assessing cleaning and water-repellent treatments for historic masonry buildings,” *National Park Service Cultural Resources*, 1, Government Printing Office, 2000.

- Mahini, S. S., Ronagh, H. R., and Eslami, A. (2007). "Seismic rehabilitation of historical masonry vaults using FRPs. A case study." Proc., 1st Asia-Pacific Conference on FRP in Structures, International Institute for FRP in Construction, Winnipeg, MB, Canada, 565-570.
- Mainstone R. Development in structural form. Oxford, England: Architectural Press; 2001.
- Mammen, E. (1997). "Locally adaptive regression splines." *The Annals of Statistics*, 25(1), 387-413.
- Masonry Standards Joint Committee (MSJC). ACI 530-08/ASCE 5-08/TMS 402-08. Section 1.8.2.3.1. Building Code Requirements for Masonry Structures, Farmington Hills (MI), Reston (VA), Boulder (CO). 2008; C-17.
- Mastroianni G, Milovanovic GV. Interpolation processes: basic theory and applications. Springer-Verlag; 2008. p. 3-4.
- McGovern, T. (2012). *American Coastal Defenses 1885-1950*. Osprey Publishing.
- Mishra, A.K., Jain, K.K., and Garg, K.L., "Role of higher plants in the deterioration of historic buildings," *The Science of the Total Environment*, 167(1), pp.375-392, 1995.
- Müller, K.R., Smola, A., Rätsch, G., Schölkopf, B., Kohlmorgen, J., Vapnik, V., (1997), Predicting time series with support vector machines, In: W. Gerstner, A. Germond, M. Hasler, J.D. Nicoud (Eds.), *Proceedings of ICANN'97*, Springer Lecture Notes in Computer Science no.1327, Berlin, pp. 999–1004.

- Myung, I. J. (2000). "The importance of complexity in model selection." *Journal of Mathematical Psychology*, 44(1), 190-204.
- Na, W.B., Kundu, T., Ehsani, M.R., (2002), Ultrasonic guided waves for steel bar concrete interface testing, *ARIEL* 129, pp. 31-248.
- Nagy, H., Watanabe, K., and Hirano, M., "Prediction of sediment load concentration in river using artificial neural network model," *Journal of Hydraulic Engineering*, 128(6), pp.588-595, 2002.
- NAHB Research Center Inc., (2002), U.S. Department of Housing and Urban Development, Office of Policy Development and Research, *Durability by Design: A Guide for Residential Builders and Designers*.
- Narayanan N, Ramamurthy K. Structure and properties of aerated concrete: a review. *Cement & Concrete Composites*. 2000; 22:325-6.
- National Park Service. Division of Publications. (1984). Fort Sumter: Anvil of War: Fort Sumter National Monument, South Carolina (No. 127). Government Printing Office.
- Ngo D, Scordelis AC. Finite element analysis of reinforced concrete beams. *ACI Journal*, 1967;64(3):152-163.
- Orban, Z., and Gutemann, M., "Assessment of masonry arch railway bridges using non-destructive in-situ testing methods," *Engineering Structures* 31(10), pp.2287-2298, 2009.

- Ou, J., & Li, H. (2003, April). Wireless sensor information fusion for structural health monitoring. In *AeroSense 2003* (pp. 356-362). International Society for Optics and Photonics.
- Ozaeta, R., Antonio, J., (2006), Improving assessment, optimization of maintenance and development of database for masonry arch bridges, Catalogue of Damages for Masonry Arch Bridges, International Union of Railways, Web. September 17, 2012.
- Page AW. The biaxial compressive strength of brick masonry. *Proc. Inst. Civ. Eng.rs*, 71(3): 893-906.
- Page J. Load tests to collapse on masonry arch bridges. *Arch Bridges: In: Proceedings of the 1st International Conference on Arch Bridges; 1995 Sept 3-6; Bolton, UK. Thomas Telford; 1995. p. 289-98.*
- Page J. Load tests to collapse on two bridges oat Strathmashie and Barlae. Department of Transport TRRL, Crowthorne, Research Report 201.
- Pecht, M., Jaai,R., (2010), A prognostics and health management roadmap for information and electronics-rich systems, *Microelectronics Reliability* 50 no.3, pp.317-23.
- Prabhu, S., and Atamturktur, S., “Selection of optimal sensor locations based on modified effective independence method: a case study on a gothic revival cathedral,” *ASCE Journal of Architectural Engineering*, 2012.
- Prabhu, S., Supler, J., and Atamturktur, S, “Feature Assimilation in Structural Health Monitoring Applications,” *Civil Engineering Topics*, 4, pp.285-295, 2011.

- Prabhu, S., Atamturktur, S., (2012), Vibration testing of gothic cathedrals: optimal sensor locations based on modified effective information method, *ASCE Journal of Architectural Engineering*.
- Radhika, Y., and Shashi, M. (2009). "Atmospheric temperature prediction using support vector machines." *International Journal of Computer Theory and Engineering*, 1(1), 1793-8201.
- Rajasekaran, S., Gayathri, S., and Lee, T. (2008). "Support vector regression methodology for storm surge predictions." *Ocean Engineering*, 35(16), 1578-1587.
- Ramage, M. Catalan vaulting in advanced material: new approaches to contemporary compressive form. Cambridge: Massachusetts Institute of Technology; 2006. MS Thesis.
- Ramos L, Marques L, Lourenço P, De Roeck G, Campos-Costa A, Roque J. Monitoring historical masonry structures with operational modal analysis: two case studies. *Mech Syst Signal Process*. 2010;24(5):1291-305.
- Ramos, L.F., (2007), "Damage Identification on Masonry Structures Based on Vibration Signatures," Ph.D. Thesis, University of Minho, Portugal.
- RILEM Technical Committee 78-MCA and 51-ALC. RILEM recommended practice, Autoclaved aerated concrete: properties, testing and design. Aroni S, de Groot GJ, Robinson MJ, Svanholm G, Wittman FS, editors. London (England): E&FN SPON. 1993. p. 246-9.

- Rocklin GT, Crowley J, Vold H. A comparison of H1, H2, and Hv frequency response functions. 3rd International Modal Analysis Conference, 1985 Jan, Orlando FL.
- Royles R, Hendry AW. Model tests on masonry arches. In: Proceedings of Institute of Civil Engineers; 1991; (Pt 2),91(6):299-321.
- Rytter, A. (1993). Vibrational based inspection of civil engineering structures. Ph.D. thesis, Department of Building Technology and Structural Engineering, University of Aalborg, Denmark.
- Samanta, B., Nataraj, C., (2008), Prognostics of machine condition using soft computing, Robotics and Computer-Integrated Manufacturing 24 no.6 816-23.
- Samaras, V. A., Fasl, J., Reichenbach, M., Helwig, T., Wood, S., and Frank, K., “Long-term gage reliability for structural health monitoring of steel bridges,” *SPIE Smart Structures and Materials+ Nondestructive Evaluation and Health Monitoring*, International Society for Optics and Phototronics, pp.83471Q, 2012
- Sankavaram, C., Pattipati, B., Kodali, A., Pattipati, K., Azam, M., Kumar, S., Pecht, M., (2009), Model-based and data-driven prognosis of automotive and electronic systems, in: Proceedings of IEEE International Conference on Automation Science and Engineering, pp. 96-101.
- Sansalone, M., Carino, N.J., (1986), Impact-echo: a method for flaw detection in concrete using transient stress waves, U.S. Department of Commerce, National Bureau of Standards, Gaithersburg, MD.

- Saxena, A., Celaya, J., Saha, B., Saha, S., and Goebel, K. (2009). "Evaluating algorithm performance metrics tailored for prognostics." *Aerospace Conference, IEEE*, 7, 1-13.
- Saxena, A., Celaya, J., Saha, B., Saha, S., Goebel, K., (2010), Metrics for offline evaluation of prognostic performance, *International Journal of Prognostics and Health Management*, pp. 1-20.
- Schölkopf, B., Burges, C., and Vapnik, V. (1995). "Extracting support data for a given task." *Proc., First International Conference on Knowledge Discovery and Data Mining, AAAI Press. Menlo Park, CA*, 252-257.
- Scholkopf, B., Sung, K.K., Burges, C.J.C., Girosi, F., Niyogi, P., Poggio, T. and Vapnik, V. (1997) "Comparing support vector machines with Gaussian kernels to radial basis function classifiers." *IEEE Transactions on Signal Processing*. Vol. 45, pp. 2758- 2765.
- Schuller, M.P., Atkinson, R.H., and Noland, J.L., "Structural evaluation of historic masonry buildings," *APT Bulletin*, 26, pp.51-61, 1995.
- Schwabacher, M.A., "A survey of data-driven prognostics," *Proceedings of the AIAA Infotech@Aerospace Conference*, 2005
- Schwarz, J., Maiwald, H., (2008), Damage and loss prediction model based on the vulnerability of building types, in: *Proceedings of 4th International Symposium on Flood Defence: Managing Flood Risk, Reliability and Vulnerability*, Toronto.

- Shah, A.A., Alsayed, S.H., Abbas, H., and Al-Salloum, Y.A., “Predicting residual strength of non-linear ultrasonically evaluated damaged concrete using artificial neural network,” *Construction and Building Materials*, 29, pp.42-50, 2012.
- Si, X.S., Wang, W., Hu, C.H., and Zhou, D.H., “Remaining useful life estimation – a review of statistical data driven approaches,” *European Journal of Operational Research*, 213(1), pp.1-14, 2011.
- Smola, A. and Schölkopf, B. (2004). "A tutorial on support vector regression." *Statistics and Computing*, 14(3), 199-222.
- Sohn, H., and Farrar, C.R., “Damage diagnosis using time series analysis of vibration signals,” *Smart Materials and Structures*, 10(3), pp.446-451, 2001.
- Sohn, H., Farrar, C.R., Hemez, F.M., Park, G., Robertson, A.N., Williams, T.O., (2003), A coupled approach to developing damage prognosis solutions, *Key Engineering Materials* 245-246 no.3, pp.289-306.
- Solla, M., Lorenzo, H., Riveiro, B., and Rial, F.I., “Non-destructive methodologies in the assessment of the masonry arch bridge of Traba, Spain,” *Engineering Failure Analysis* 18(3), pp.828-835, 2011.
- Søyland K, Rosson BT. The influence of mortar properties on the system behavior of masonry arch bridges. In: *Proceedings of the 1st International Conference on Arch Bridges*; 1995 Sept 3-6; Bolton, UK. Thomas Telford; 1995. p. 355-64.

- Stone, M. (1974). "Cross-validators choice and assessment of statistical predictors (with discussion)." *Journal of the Royal Statistical Society*, (B36), 111-147.
- Strickland, K., (1991), The school finance reform movement, a history and prognosis: will massachusetts join the third wave of reform, *B.C.L.* 32 no.5, pp.1105-77.
- Suro R. Cracks in a great dome in Florence may point to impending disaster. *New York Times*. July 28, 1987.
- Suykens, J. A., De Brabanter, J., Lukas, L., and Vandewalle, J. (2002). "Weighted least squares support vector machines: robustness and sparse approximation." *Neurocomputing*, 48(1), 85-105.
- Thissen, U., Van Brakel, R., De Weijer, A., Melssen, W., Buydens, L., (2003), Using support vector machines for time series prediction, *Chemometrics and Intelligent Laboratory Systems* 69 no.1-2, pp. 35-49.
- Tringali S, De Benedictis R, Gavarini C, La Rosa R. The cathadral of Noto: from the analysis of the collapse to the restoration and reconstruction project. In: *Proceedings of the UNESCO/ICOMOS International Millennium Congress Archi 2000*; 2001 Sept 10-12. Paris, France.
- TruStone America, Physical properties. 2005.
- Twelmeier, H., Sperbeck, S., Budelmann, H., (2006), Durability prognosis model of historical natural stone masonry regarding joint repairing measures, in: *Proceedings of 5th*

International Conference on Structural Analysis of Historical Constructions, New Delhi, India, pp. 1051-1058.

Uniform Building Code Standards (1991 Edition). International Code Council; 1991.

USG [internet]: Industrial Plasters and Gypsum Cements: Versatile Products for Countless

Industrial Applications. [Accessed: 2011 Sept 29].

<http://www.usg.com/rc/brochures/industrial-plasters-cements/industrial-plasters-gypsum-cements-brochure-en-IG504.pdf>

Van Hees, R. P. J., Binda, L., Papayianni, I., and Toumbakari, E., “Characterization and damage analysis of old mortars,” *Materials and Structures* 37(9), pp.644-648, 2004.

Vapnik, V. (1998). Statistical Learning Theory. Springer, NY.

Verstrynghe E, Schueremans L, Van Gemert D, Hendriks MAN. Modeling and analysis of time-dependent behavior of historical masonry under high stress levels. *Eng Struct.* 2011;33(1):210-7.

West, G., *Alkali-Aggregate Reaction in Concrete Roads and Bridges*, Thomas Telford, 1996.

Willam KJ, Warnke EP. Constitutive model for the triaxial behavior of concrete. In: Proceedings of the International Association for Bridge and Structural Engineering, ISMES, Bergamo, Italy, 1975. p. 1-30.

Witten, I., Frank, E., (2005), Data mining: practical machine learning tools and techniques, 2nd ed., Amsterdam, Morgan Kaufman.

Worden, K., & Duijvelde, J. M. (2004). Damage identification in systems and structures. *International Journal of Structural Health Monitoring*, 3, 85-98.

Xu, Y., Lv, X., and Xi, W. (2012). "A weighted multi-output support vector regression and its application." *Journal of Computational Information Systems*, 8(9), 3807-814.